Pertanika Journal of

SCIENCE & TECHNOLOGY

JST

VOLUME 16 NO.1 • JANUARY 2008

A scientific journal published by Universiti Putra Malaysia Press

About the Journal

Pertanika is an international peer-reviewed journal devoted to the publication of original papers, and it serves as a forum for practical approaches to improving quality in issues pertaining to tropical agriculture and its related fields. Pertanika Journal of Tropical Agricultural Science began publication in 1978. In 1992, a decision was made to streamline Pertanika into three journals to meet the need for specialised journals in areas of study aligned with the interdisciplinary strengths of the university. The revamped, Pertanika Journal of Science and Technology (JST) is now focusing on research in science and engineering, and its related fields. Other Pertanika series include Pertanika Journal of Tropical Agricultural Science (JTAS); and Pertanika Journal of Social Sciences and Humanities (JSSH).

JST is published in English and it is open to authors around the world regardless of the nationality. It is currently published two times a year i.e. in **January** and **July**.

Goal of Pertanika

Our goal is to bring the highest quality research to the widest possible audience.

Quality

We aim for excellence, sustained by a responsible and professional approach to journal publishing.

Future vision

We are continuously improving access to our journal archives, content, and research services. We have the drive to realise exciting new horizons that will benefit not only the academic community, but society itself.

We also have views on the future of our journals. The emergence of the online medium as the predominant vehicle for the 'consumption' and distribution of much academic research will be the ultimate instrument in the dissemination of the research news to our scientists and readers.

Aims and scope

Pertanika Journal of Science and Technology aims to provide a forum for high quality research related to science and engineering research. Areas relevant to the scope of the journal include: *bioinformatics, bioscience, biotechnology and bio-molecular sciences, chemistry, computer science, ecology, engineering, engineering design, environmental control and management, mathematics and statistics, medicine and health sciences, nanotechnology, physics, safety and emergency management,* and related fields of study.

JST accepts submission of mainly four types: original articles, short communications, reviews, and proposals for special issues.

Editorial Statement

Pertanika is the official journal of Universiti Putra Malaysia. The abbreviation for Pertanika Journal of Science & Technology is *Pertanika J. Sci. Technol.*

Editorial Office

Pertanika, Research Management Centre (RMC), 4th Floor, Administration Building
Universiti Putra Malaysia, 43400 Serdang, Selangor, Malaysia
Tel: +603 8946 6185, 8946 6192 • Fax: +603 8947 2075
E-mail: ndeeps@admin.upm.edu.my
www.rmc.upm.edu.my/pertanika

Publisher

The UPM Press
Universiti Putra Malaysia
43400 UPM, Serdang, Selangor, Malaysia
Tel: +603 8946 8855, 8946 8854 • Fax: +603 8941 6172
penerbit@putra.upm.edu.my
URL : http://penerbit.upm.edu.my

Pertanika Journal of Science & Technology
Vol. 16 (1) Jan. 2008

ISSN: 0128-7680
Pertanika J. Sci. & Technol. **16 (1)**: 1 - 13 (2008)

Comparison on Optimization of Star Fruit Juice Using RSM between Two Malaysian Star Fruit Varieties (B11 and B10)

M.K. Siti Mazlina[*1], L.A. Abdul Ghani [2], A.R. Nur 'Aliaa[1], H. Siti Aslina[2] and O. Rozita[2]

[1]Department of Process and Food Engineering, Faculty of Engineering, Universiti Putra Malaysia, 43400 UPM, Serdang, Selangor, Malaysia

[2]Department of Chemical and Environmental Engineering, Faculty of Engineering, Universiti Putra Malaysia, 43400 UPM, Serdang, Selangor, Malaysia

**E-mail: siti@eng.upm.edu.my*

ABSTRACT

In Malaysia, two star fruit varieties, B11 and B10, are planted for commercial purposes. These types of star fruits are suitable for making juices. However, the fresh star fruit juice is cloudy, viscous and green in colour, necessitating the use of enzymes to clarify the juice. Thus, the aim of this study was to establish the optimum conditions for enzymatic treatment of star fruit (B11) juice using response surface methodology (RSM) and to compare the optimum conditions of this variety (B11) with the B10. Star fruit juice (B11) was treated with pectinase enzyme at different enzyme concentrations, incubation times, and temperatures. The effect of this enzymatic treatment was analyzed based on turbidity, clarity, and viscosity. The regression models describing the changes of turbidity, clarity and viscosity were established with the coefficient of determination, R^2, which were greater than 0.8. The optimum operating conditions for clarifying star fruit juice (B11) was found to be at 0.01% enzyme concentration at 30 min of incubation time and 30ºC of temperature using response surface methodology. The method of treatments for B10 was similar to that of B11. The two varieties of star fruit (B11 and B10) showed different optimum conditions on enzyme concentration and incubation time, however there was no difference in terms of incubation temperature at optimum conditions.

Keywords: B10, B11, enzymatic clarification, response surface methodology, star fruit juice, clarity, turbidity, viscosity

INTRODUCTION

Nowadays, tropical fruit juices have become popular, and the positive trend is more people like to drink juices especially in the morning replacing the traditional caffeinated drinks. This positive trend is mainly due to the wholesomeness that the fruit juices offer in terms of nutritional benefits, all enriched with vitamin, fibres or other ingredients. Fruit juices have potentially open up new market opportunities tailoring fruit products to consumer demands.

One of the most popular tropical fruit juices is star fruit or Carambola. Star fruit is sweet and slightly acidic, succulent and juicy with attractive flesh and distinctive flavour. Star fruit can be found in different shapes ranging from oblong to ellipsoid. The fruit when cross-sectionally cut, produces beautiful star shapes, from which the name 'starfruit' is derived. The skin is translucent, smooth and waxy with yellowish green colour skin when ripe. The flavour is variable and ranges from light sour to sweet. These fruits are relatively inexpensive as well as extremely rich in vitamins C, low fat and cholesterol free.

* Corresponding Author

Star fruit has been planted commercially in some countries such as Malaysia, China, India and Taiwan. Star fruit has approximately seventeen different cultivars (varieties), and each has its own origin, flavour and production levels (Vaillant *et al.*, 1999). In Malaysia, varieties B10 and B11 are planted for commercial purposes. Star fruit is easy to process and transform to juices, and the juice could be used in tropical drinks and smoothies. Recently, many countries have been involved in big scale star fruit juice processing especially manufacturers in Malaysia, Hawaii and China. Star fruit juices are usually cloudy, contain colloidal suspension, and green in colour, and this is associated with the quality of the juice which may influence consumer's acceptability. A clear juice is usually more acceptable by the consumer and tends to be easily marketed.

The cloudiness of the juices is mainly due to the presence of pectin. Pectin can be associated with plant polymers and the cell debris which are fibrous-like molecular structure. The cloudiness could be removed by enzymatic depectinization. Several studies have been reported on depectinization using enzymatic treatment such as pectinases that could effectively clarify the fruit juices (Alvarez *et al.*, 1998; Ceci and Lozano, 1998; Isabella *et al.*, 1995; Lee *et al.*, 2006; Rai *et al.*, 2004; Sin *et al.*, 2006; Yusof and Ibrahim, 1994). The pectinase hydrolyzes pectin and causes pectin-protein complexes to flocculate. The resulting juice from this pectinase treatment contains much lower amount of pectin and reduces its viscosity, which is advantageous in facilitating the subsequent filtration processes.

The enzymatic hydrolysis of pectin depends on several physicochemical factors such as incubation time, incubation temperature and enzyme concentration (Isabella *et al.*, 1995; Lee *et al.*, 2006; Rai *et al.*, 2004; Sin *et al.*, 2006; Sreenath and Santhanam, 1992). Enzymes are expensive biocatalysts and clearly, juice manufacturers want to minimize their operating costs by using enzymes at optimum conditions. It is desirable to obtain the optimum conditions which will maximize the effectiveness of juice clarification.

Optimization of different parameters that influence the depectinization rate was the main reason for this work. Response Surface Methodology (RSM) is an effective method to carry out optimization studies. RSM is a statistical tool that uses quantitative data from appropriate experimental design to determine and simultaneously solve multivariate equations (Giovanni, 1983). RSM can reduce the number of experimental trials needed to evaluate multiple parameters and their interactions, thus, less time consuming compared to other approaches. RSM has been widely applied in optimization processes in food industries (Lee *et al.*, 2006; Sin *et al.*, 2006; Wong *et al.*, 2003; Yusof *et al.*, 1988).

Liew Abdullah *et al.* (2007) and Liew Abdullah (2007) studied the optimization conditions for clarification of B10 star fruit juice using a commercial enzyme. The objectives of this work were to establish the optimum process conditions (incubation time, temperature and enzyme concentration) for enzymatic clarification of star fruit juice using Response Surface Methodology for B11 and compare that to a previous study with variety B10 (Liew Abdullah *et al.*, 2007; Liew Abdullah, 2007).

MATERIALS AND METHODS

Fruit

Fresh star fruits (*Carambola averrhoa* L.) of variety B11 were purchased from a local market in Serdang, Malaysia. Colour index 3 (25% to 75% yellow) was chosen for the ripeness of the fruit for this study (Colour index according to the FAMA[1] Standards grade for starfruit).

Enzyme

Pectinex Ultra SP-L from *Aspergillus niger* obtained from Novozymes Switzerland AG, Dittengen, Switzerland, was used for enzymatic treatment of star fruit juice and stored at 4ºC. The activity of pectinex ultra SP-L enzyme was 26,000 PG per ml.

Juice Extraction Process

Star fruits were washed, peeled, deseeded and the star fruits were blended using a food blender (Panasonic, Malaysia) for 2 – 3 min until a homogenous solution was obtained. The juice was filtered out using a cheese cloth to separate the pulp from the juice. *Fig. 1* shows the extraction steps and subsequent clarification using enzymatic treatment of star fruit juice.

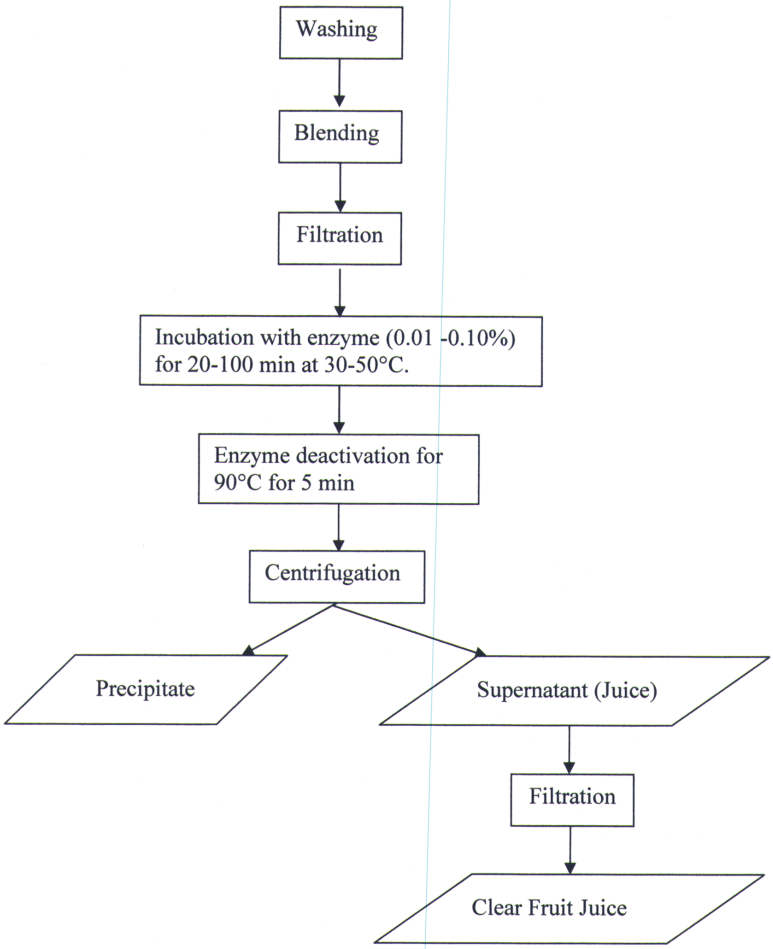

Fig. 1: Steps for extraction and subsequent clarification by enzymatic treatment of star fruit juice

[1]FAMA is Malaysia Federal Agriculture Marketing Authority.

Enzyme Treatment

The juice was strained using a muslin cloth. For each experiment, about 150 ml juice was treated with different enzyme conditions as shown in Table 1. The independent variables for enzymatic treatments were incubation time, X_1 (30 – 100), incubation temperature, X_2 (30 – 50) and concentration of enzyme used, X_3 (0.01 – 0.1). The temperature of enzymatic treatment was adjusted to the desired level using a water bath (Model 903, Protech Electronic, Malaysia, ± 0.5ºC). At the end of enzymatic treatment, the enzyme in the sample was inactivated by heating the suspension at 90ºC for 5 minutes in a water bath. The treated star fruit juices were centrifuged at 3000g for 10 min (Avanti J-25, Beckman Coulter, USA) and the supernatant was collected. Then, the juice was filtered through a filter paper (Whatman No.1, Whatman International Ltd., England) using Eyela vacuum aspirator. The filtrate was collected for further analysis.

TABLE 1
Effect of incubation time, incubation temperature and enzyme concentration on three responses

	Independent variables			Dependent variables		
	Incubation time (min)	Incubation temperature (ºC)	Enzyme Concentration (%)	Turbidity (NTU)	Clarity (abs)	Viscosity (cps)
Trial	$X_1(x_1)$	$X_2(x_2)$	$X_3(x_3)$	y_1	y_2	y_3
1	65(0)	40(0)	0.01(-1)	56.5	0.059	1.4
2	65(0)	40(0)	0.1(+1)	11.9	0.025	1.4
3	65(0)	30(-1)	0.055(0)	14.8	0.039	1.4
4	65(0)	50(+1)	0.055(0)	15.0	0.020	1.4
5	30(-1)	40(0)	0.055(0)	19.4	0.030	1.3
6	100(+1)	40(0)	0.055(0)	15.3	0.020	1.3
7	100(+1)	50(+1)	0.1(+1)	23.0	0.027	1.4
8	100(+1)	50(+1)	0.01(-1)	24.3	0.058	1.2
9	100(+1)	30(-1)	0.1(+1)	24.0	0.031	1.2
10	100(+1)	30(-1)	0.01(-1)	22.0	0.056	1.4
11	30(-1)	50(+1)	0.1(+1)	21.5	0.031	1.3
12	30(-1)	50(+1)	0.01(-1)	12.7	0.043	1.3
13	30(-1)	30(-1)	0.1(-1)	16.5	0.060	1.3
14	30(-1)	30(-1)	0.01(-1)	32.2	0.019	1.3
15	65(0)	40(0)	0.055(0)	32.2	0.019	1.4
16	65(0)	40(0)	0.055(0)	33.9	0.021	1.4
17	65(0)	40(0)	0.055(0)	34.1	0.021	1.3
18	65(0)	40(0)	0.055(0)	34.3	0.020	1.4
19	65(0)	40(0)	0.055(0)	34.7	0.020	1.3

Turbidity Analysis

Turbidity was determined using a portable Turbidimeter (Model 2100P, Hach Company, Loveland, Colorado,USA) and the results were reported as Nephelometric Turbidity Units (NTU).

Clarity Analysis

Clarity was determined by measuring the absorbance at 660nm using a UV-VIS spectrophotometer (Model UV-1201, Shimadzu Corporation, Japan). Distilled water was used as a reference.

Viscosity Analysis

The viscosity of the juice was determined using a Brookfield viscometer (Model LVDV-II+, Brookfield Engineering Laboratory, Inc., Middleboro, USA) at 100 rpm with spindle SC4-18 at room temperature ± 27ºC.

Experimental Design

Response Surface Methodology (RSM) was used in this study to determine the optimum conditions for the enzymatic clarification of star fruit juice. The experimental design and statistical analysis were performed using ECHIP Software Version 6 (Echip Inc., Hockessin, Delaware, USA).

The experiments were based on a central composite rotational design (Cochran and Cox, 1957) with a quadratic model in order to study the combined effect of the three independent variables (incubation time, temperature and enzyme concentration). These three independent variables were represented as X_1, X_2 and X_3, respectively. Each independent variable had 3 levels which were -1, 0, and +1. Based on Baumann (1981), these three chosen variables were responsible for the mechanism of enzyme activity in the juice. A total of 19 combinations including five replicates of the center point were carried out in random order according to a central composite design configuration for the three chosen variables. The experimental design in the coded (x) and actual (X) levels of variables is shown in Table 1. The dependent variables (y) measured were turbidity (y_1), clarity (y_2), and viscosity (y_3) of the star fruit juice. These dependent variables were expressed individually as a function of the independent variables known as response function. The variance for each factor assessed was partitioned into linear, quadratic and interactive components and were represented using the following second order polynomial function.

$$y = b_0 + b_1x_1 + b_2x_2 + b_3x_3 + b_{12}x_1x_2 + b_{13}x_1x_3 + b_{23}x_2x_3 + b_{11}x_1^2 + b_{22}x_2^2 + b_{33}x_3^2 \quad (1)$$

The coefficients of the polynomial were represented by b_0 (constant term), b_1, b_2 and b_3 (linear coefficient), b_{11}, b_{22} and b_{33} (quadratic coefficient), and b_{12}, b_{13} and b_{23} (interactive coefficient). The significance of all terms in the polynomial functions were assessed statistically using F-value at a probability (p) of 0.001, 0.01 or 0.05. The regression coefficients were then used to generate contour maps from the regression models. The three-dimensional plots were generated by keeping one variable constant at the center point and varying the other variables within the experimental range.

Method for B10

The treatment and experimental methods for B10 (Liew Abdullah *et al.*, 2007; Liew Abdullah, 2007) was similar to that for B11.

RESULTS AND DISCUSSION

Statistical Analysis

The experimental values for all responses (independent variables) under different conditions are presented in Table 2 (B11). The independent variables and dependent variables (responses) were fitted to the second order polynomial function and examined for the goodness of fit. The R^2 or coefficient of determination which is defined as the ratio of explained variation to the total variation is a measure of the degree of fit (Haber and Runyon, 1977). The R^2 values for turbidity, viscosity and clarity were 0.996, 0.829 and 0.964, respectively. The closer the value of R^2 approaches unity, the better the empirical model fits the actual data. The smaller the value of R^2, the less relevant was the dependent variables in the model in explaining the variation of behavior (Little and Hills, 1978; Mendenhall, 1975). The result for this study was above 0.8. The values of R^2 for turbidity, viscosity and clarity for B10 were slightly less than B11 which were 0.880, 0.779 and 0.864 respectively (Liew Abdullah *et al.*, 2007).

Turbidity

Turbidity is considered as 'muddy' for a juice, thus, indicating the turbidity should be minimal for marketing purposes. Therefore, clear and sparkling star fruit is required. The response surfaces for turbidity can be visualized in *Fig. 2a*, which shows the contour map for the effect of the independent variables on turbidity of B11.

TABLE 2
Regression coefficient, R^2, values for four dependent variables for enzymatic clarification of star fruit juice

Regression coefficient	Turbidity (NTU)	Viscosity (cps)	Clarity (abs)
b_0	16.4495	1.37773	0.0231278
b_1	-393.333 ***	-1.24444 ***	-0.416 ***
b_2	-0.171429 ***	-0.000857143 *	-0.000159143 **
b_3	-0.084	-0.000699999	-0.000315
b_{12}	6809.21 ***	-9.82561	6.12957 **
b_{22}	0.0086438 ***	-2.44056e-005	2.49989e-006
b_{32}	-0.0071134	0.000451031	3.06237e-005
b_{12}	2.46825 ***	-0.0079365	0.00254762 *
b_{13}	5.52778 **	0.0388889	0.000305556
b_{23}	-0.00703571 **	5.71429e-005	-4.89286e-006
R^2	0.996	0.829	0.964
p	0.000 ***	0.0138 *	0.000 ***

Subscripts: 1 = enzyme concentration; 2 = incubation time; 3 = temperature.
* Significant at 0.05 level.
** Significant at 0.01 level.
*** Significant at 0.001 level.

By referring to Table 2, the turbidity (B11) was significantly affected by incubation time and enzyme concentration for both the linear and quadratic cases. Both independent variables showed a negative effect on the linear terms and a positive effect on the quadratic terms. It was a significant interaction effect between enzyme concentration and incubation time with a positive effect on turbidity. This means that the action of the enzyme was dependent on the incubation time during the enzymatic treatment of the star fruit juice.

The turbidity of the fruit juice is mainly caused by the polysaccharides in the juice such as pectin (Grassin and Fauquembergue, 1999). Thus, increase in enzyme concentration and incubation time might decrease the turbidity of the juice. *Fig. 2a* shows the effect of enzymatic treatment at a fixed temperature (40ºC). The turbidity of the juice decreased drastically when enzyme concentration increased. These results strongly agree with those reported by Alvarez *et al.* (1998); as the enzymatic treatment process took place, the amount of pectin in the juice decreases and hence, reducing the turbidity of the juice. Similar trends were observed by Liew Abdullah *et al.* (2007) for variety B10 juice, at a fixed temperature (30ºC), turbidity decreased with an increase in enzyme concentration (*Fig. 2b*).

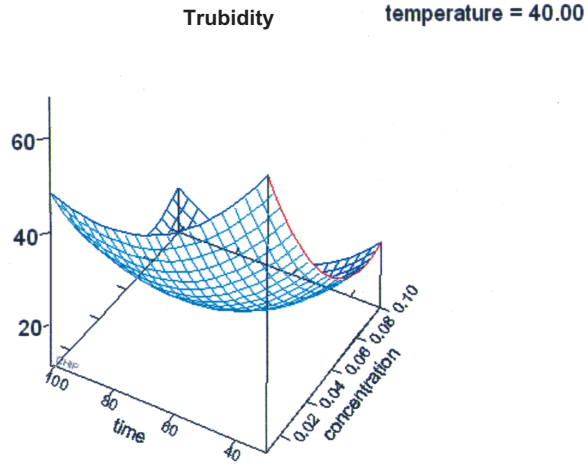

Fig. 2a: Response surface for turbidity of star fruit juice (B11) as a function of time and enzyme concentration (at 40ºC)

Clarity

Clarity is another important index of clarified juice (Sin *et al.*, 2006). Clarified juice is a natural juice that is pulpless and clear in appearance. It is observed from Table 2 that clarity mainly depends on the enzyme concentration as its quadratic effect was positive and significant at $p<0.001$. The incubation time also significantly affects the clarity in the linear case. There are also significant interaction effects between incubation time and enzyme concentration at $p< 0.05$ with a positive effect, which indicates that the incubation time was dependent on enzyme concentration.

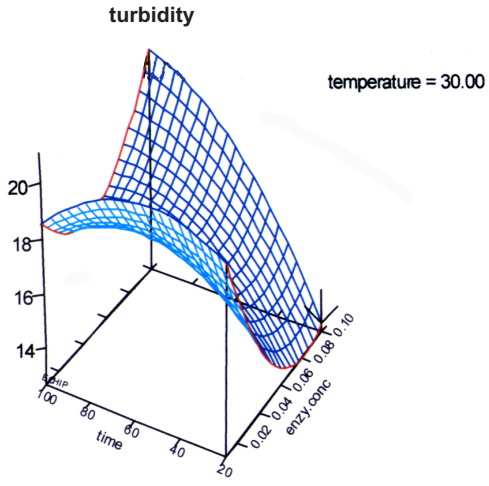

Fig. 2b: Response surface for turbidity of star fruit juice (B10) as a function of time and enzyme concentration (at 30°C) (Adapted from Liew Abdullah et al., 2007)

Fig. 3a shows a 3D plot for juice clarity with enzyme concentration and incubation time at a fixed temperature of 40°C for variety B11. It was evident that the absorbance value decreased with an increase in enzyme concentration. Low absorbance values indicate a clearer juice is being produced. It was also observed that the absorbance values decreased with increased the incubation time. The time required to obtain a clear juice is inversely proportional to the concentration of enzyme used at constant temperature (Kilara, 1982). *Fig. 3b* (Liew Abdullah *et al.*, 2007) shows the plot for variety B10 juice clarity. From the figure, it can also be observed that the absorbance value decreased with increasing enzyme concentration and incubation time at fixed temperature.

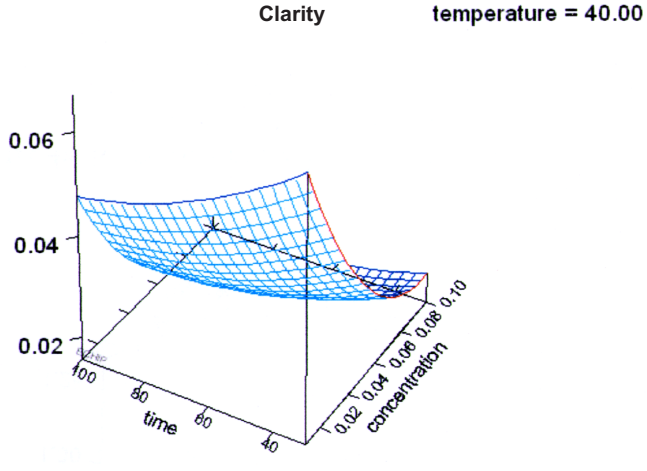

Fig. 3a: Response surface for clarity of star fruit juice (B11) as a function of time and enzyme concentration (at 40°C)

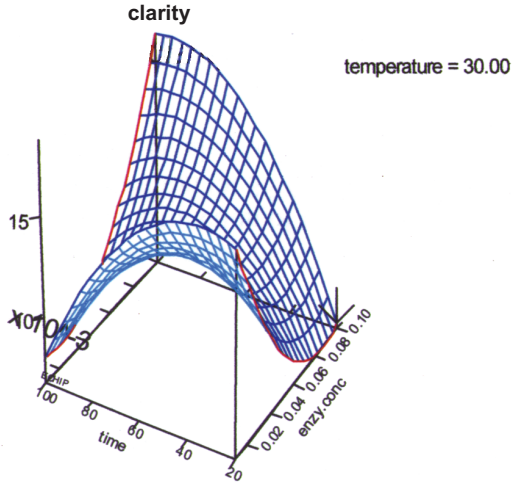

Fig. 3b: Response surface for clarity of star fruit juice (B10) as a function of time and enzyme concentration (at 30°C) (Adapted from Liew Abdullah et al., 2007)

Viscosity

The viscosity of the star fruit juice decreased as the enzyme concentration increasing as shown in *Fig. 4a* for variety B11. Enzyme concentration had a negative effect on viscosity for the linear case, showing a highly significant level at $p<0.001$. Upon enzymatic treatment, the degradation of pectin leads to a reduction of water holding capacity. Free water was released to the juice and its viscosity was reduced.

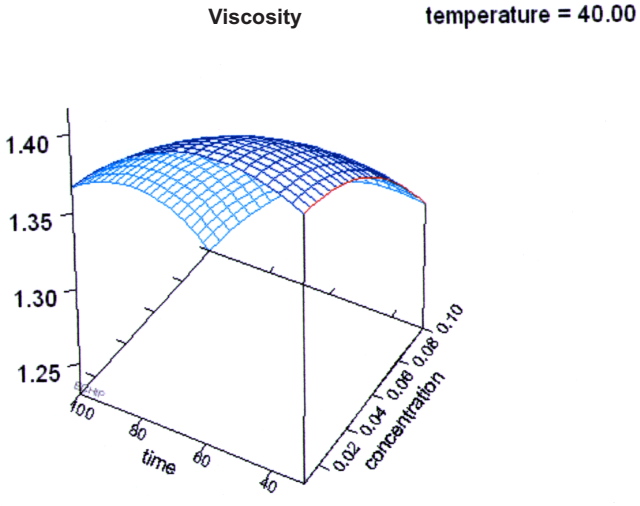

Fig. 4a: Response surface for viscosity of star fruit juice (B11) as a function of time and enzyme concentration (at 40°C)

Fruit juice with high viscosity may lead to a few problems during the filtration process (Vaillant *et al.*, 1999). To get a better filtration performance, it is recommended that fruit juices be enzymatically treated before filtration for the purpose of hydrolyzing soluble polysaccharides responsible for its high viscosity (Cheryan and Alvarez, 1995). Urlaub (1996) reported that the viscosity of fruit juice could be reduced via enzymatic hydrolysis of pectin. Thus, juice with lower viscosity is preferable in the enzymatic clarification (Sin *et al.*, 2006). *Fig. 4b* (Liew Abdullah *et al.*, 2007) shows the plot for viscosity for variety B10. It can be observed that the viscosity was significantly reduced at a higher enzyme concentration.

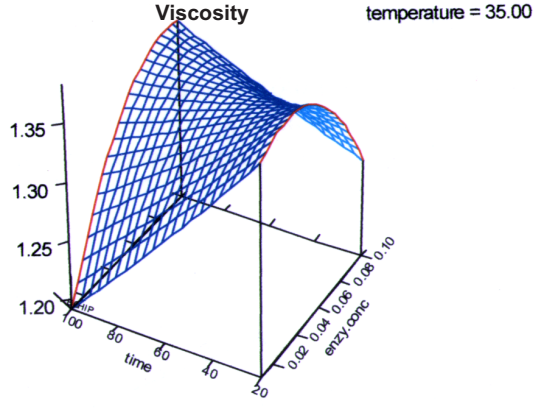

Fig. 4b: Response surface for viscosity of star fruit juice (B10) as a function of time and enzyme concentration (at 35°C) (Adapted from Liew Abdullah et al., 2007)

Optimization

During juice clarification, the cost of pre-treatment using enzyme is very important. Therefore, the best combination of process variables for response functions (turbidity, clarity, viscosity) need to be determined by taking into account the cost of enzyme used. The optimum conditions for the clarification of star fruit juice using enzymatic treatment were determined by superimposing the contour plots of all responses. The condition would be considered optimum if the turbidity, absorbance value, and viscosity were at a minimum. The criteria applied for graphical optimization were: (a) minimum turbidity, (b) minimum absorbance value, and (c) minimum viscosity. The computer generated plots for turbidity, clarity and viscosity for the variety B11 (*Figs. 2a–4a*), and with the criteria being set previously, produced an optimum region in the superimposed plot as shown in *Fig. 5a.* These criteria were selected as they are important parameters of the physical characteristics of the clarified juice. *Figs. 2a–4a* show the optimum conditions for each response, while *Fig. 5a* (variety B11) shows the optimum combined conditions that was found to be at 0.01% enzyme concentration at 30°C for 30 min. *Fig. 5b* from the work of Liew Abdullah *et al.* (2007) shows the superimposed plot for the optimum conditions for each response for variety B10. Liew Abdullah *et al.* (2007) concluded that the optimum combined conditions for B10 was 0.1% enzyme concentration at 30°C for 20 min. Table 3 shows the differences in characteristics between B10 and B11 in terms of turbidity, clarity, viscosity and optimum conditions for enzymatic treatment.

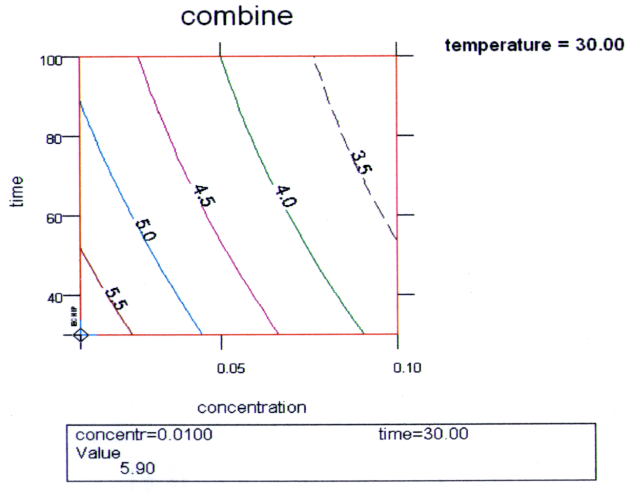

Fig. 5a: Contour plots for optimum combined condition (B11) as a function of enzyme concentration and incubation time at 30°C

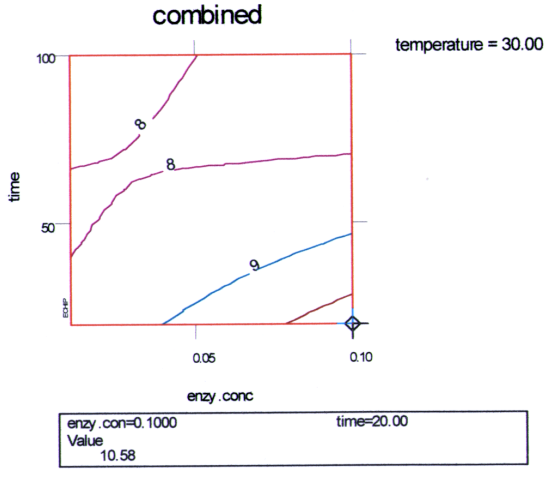

Fig. 5b: Contour plots for optimum combined condition (B10) as a function of enzyme concentration and incubation time at 30°C (Adapted from Liew Abdullah et al., 2007)

TABLE 3
Comparison on characteristics between B10 and B11 varieties

Characteristics	B10	B11
R^2 (Turbidity)	0.880	0.996
R^2 (Viscosity)	0.779	0.829
R^2 (Clarity)	0.864	0.964
Optimum incubation temperature (°C)	30	30
Optimum incubation time (min)	20	30
Optimum enzyme concentration (%)	0.10	0.01

CONCLUSIONS

Different conditions for enzymatic treatment affect the turbidity, clarity and viscosity of the star fruit juice. Therefore, statistical analysis using RSM could be used to establish the optimum process variables for enzymatic clarification of star fruit juice. By using response surface and contour plots, the optimum set of operating variables could be obtained graphically in order to achieve the desired pre-treatment levels for the star fruit juice for clarification processes. It is recommended that the enzymatic treatment clarification conditions for variety B11 of the star fruit juice was 0.01% enzyme concentration at temperature 30ºC and 30 min incubation time. These values are different from the optimum conditions for B10 variety which was 0.1% enzyme concentration at 30ºC for 20 min. It can be concluded that different varieties of star fruit need different optimum conditions of enzymatic treatment for the clarification of the juice. It may be due to the structural difference between these two varieties and also their properties and composition which influence the susceptibility of the fruit to enzyme.

ACKNOWLEDGEMENTS

Thanks to Mr. Abdul Ghani Liew Abdullah of the Department of Chemical and Environmental Engineering, Universiti Putra Malaysia for his assistance in making this study possible.

REFERENCES

ALVAREZ, S., ALVAREZ, R., RIERA, F.A. and COCA, J. (1998). Influence of depectinization on apple juice ultrafiltration. *Colloids and Surfaces A: Physichochemical and Engineering Aspects, 138*, 377-382.

BAUMANN, J.W. (1981). Application of enzymes in fruit juice technology. In G.G. Birch, N. Blakebrough and K.J. Parker (Eds.), *Enzymes and food processing* (p. 129-147). London: Applied Science Publication.

CECI, L. and LOZANO, J. (1998). Determination of enzymatic activities of commercial pectinases for the clarification of apple juice. *Food Chemistry, 61*, 237-241.

CHERYAN, M. and ALVAREZ, J.R. (1995). Food and beverage industry application. In R.D. Noble and S.A. Stern (Eds.), *Membrane separation technology principles and applications* (p. 443-465). London: Elsevier.

COCHRAN, W.G. and COX, G.M. (1957). Some methods for the study of response surfaces. In *Experimental designs* (2nd ed.) (p. 12-20). New York: John Wiley and Sons Inc.

GIOVANNI, M. (1983). Response surface methodology and product optimization. *Food Technology, 37*, 41-45.

GRASSIN, C. and FAUQUEMBERGUE, P. (1999). Enzymes, fruit juice processing. In M.C. Flickinger and S.W. Drew (Eds.), *Encyclopedia of bioprocess technology: Fermentation, biocatalysis, bioseparation* (p. 1030-1061). New York: John Wiley and Sons, Inc.

HABER, A. and RUNYON, R. (1977). *General Statistics* (3rd ed.). Reading, MA: Addison Wesley Publishing Company.

ISABELLA, M.B., GERALDO, A.M. and RAIMUNDO, W.F. (1995). Physical-chemical changes during extraction and clarification of guava juice. *Food Chemistry, 54*(4), 388-386.

KILARA, A. (1982). Enzymes and their uses in the processed apple industry: A review. *Process Biochemistry, 23*, 35-41.

LEE, W.C, YUSOF, S., HAMID, N.S.A. and BAHARIN, B.S. (2006). Optimizing conditions for enzymatic clarification of banana juice using response surface methodology (RSM). *Journal of Food Engineering, 73*, 55-63.

LIEW ABDULLAH, A.G., SULAIMAN, N.M., AROUA, M.K., MEGAT MOHD NOOR, M.J. (2007). Response surface optimization of conditions for clarification of carambola fruit juice using a commercial enzyme. *Journal of Food Engineering, 81*, 65-71.

LITTLE, T.M. and HILLS, F.J. (1978). *Agricultural experimentation design and analysis* (p. 170). New York: John Wiley.

MENDENHALL, W. (1975). *Introduction to probability and statistics* (4th ed.) (p. 273). North Settuate, MA: Duxbury Press.

RAI, P., MAJUMDAR, G.C., DASGUPTA, S. and DE, S. (2004). Optimizing pectinase usage in pretreatment of mosambi juice for clarification by response surface methodology. *Journal of Food Engineering, 64*, 397-403.

SIN., H.N., YUSOF, S., HAMID, N.S.A. and RAHMAN, R.A. (2006). Optimization of enzymatic clarification of sapodilla juice using response surface methodology. *Journal of Food Engineering, 73*, 313-319.

SREENATH, H.K. and SANTHANAM, K. (1992). The use of commercial enzymes in white grape juice clarification. *Journal of Fermentation and Bioengineering, 73*(3), 241-243.

URLAUB, R. (1996). Advantages of enzymatic apple mash treatment and pomace liquefaction. *Fruit Processing, 6*(10), 339-406.

VAILLANT, F., MILLAN, P., O'BRIEN, G., DORNIER, M., DECLOUX, M. and REYNES, M. (1999). Crossflow microfiltration of passion fruit juice after partial enzymatic liquefaction. *Journal of Food Engineering, 42*, 215-224.

WIKIPEDIA. (2006). Carambola. Access on June 2006 through website: en.wikipedia.org/wiki/carambola

WONG, P.K., YUSOF, S., GHAZALI, H.M. and CHE MAN, Y. (2003). Optimization of hot water extraction of Roselle juice by using response surface methodology: a comparative study with other extraction methods. *Journal of the Science of Food and Agriculture, 83*, 1273-1278.

YUSOF, S. and IBRAHIM, N. (1994). Quality of soursop juice after pectinase enzyme treatment. *Food Chemistry, 51*, 83-88.

YUSOF, S., TALIB, Z., MOHAMED, S. and BAKAR, A. (1988). Use of response surface methodology in the development of guava concentrate. *Journal of Science and Food Agricultural, 43*, 173-186.

ISSN: 0128-7680
Pertanika J. Sci. & Technol. **16 (1)**: 15 - 22 (2008)

Understanding the Tabletting Behaviour of *Ficus deltoidea* Herb

Yus Aniza Yusof*, Rohaiza Abdullah, Chin Nyuk Ling and Russly Abd. Rahman
Department of Process and Food Engineering, Faculty of Engineering,
Universiti Putra Malaysia, 43400 UPM, Serdang, Selangor, Malaysia
**E-mail: niza@eng.upm.edu.my*

ABSTRACT

This paper presents a study on tabletting of *Ficus deltoidea*, a herb known as "Emas Cotek" in Malaysia and traditionally used for treating gout, hypertension and diabetes as well as to improve blood circulation and to reduce cholesterol and toxins levels in the body. Research has shown that this herb contains active compounds such as flavonoid, tetripenoids, tannins and phenols. For centuries, it was consumed at home through infusion and recently the herb was marketed in the form of tea sachet, capsules and tablets. The tablet is a universal form of delivery in modern medicine due to its ability to provide uniform product composition, particle size and density distributions, and to eliminate dust formation; and most importantly, it has a longer shelf life compared to the other forms of delivery. It is achieved by pressing a blend of ingredients into a tablet. In this study, a 13-mm-diameter cylindrical uniaxial die was used for tabletting. Pressures ranging from 7.5 to 75 MPa were applied to the herb powder. The effect of binder was investigated using Avicel, with compositions ranging from 10 to 60 % of the blend. The strength of the tabletted herb was then tested using an indirect tensile strength test, called diametrical compression test. The results were presented in the form of pressure-volume relationship and tensile strength. The experimental data was then compared to that of the prediction using a first order model. The results indicated that this simple approach can be used to understand the tabletting behaviour of the herb.

Keywords: *Ficus deltoidea*, pressure-volume, tabletting, tensile strength

INTRODUCTION

Ficus deltoidea or well known as "emas cotek" is a plant that is becoming popular amongst modern Malaysian community. This herb is usually cultivated as a houseplant or as an ornamental shrub and it quite unique as there are two types; the male and female. For the male species, the leaves are small and light weight, with one red spot at the back of the leaves, while for female species the leaves are bigger, round and thicker with a few black spots at the back of the leaves.

The chemical contents analysis carried out by researchers in Universiti Malaya and MARDI showed that *Ficus deltoidea* contains flavonoids, tannins, triterpenoids, and phenols compounds. Traditionally, *Ficus deltoidea* was used for treating gout, hypertension and diabetes as well as to improve blood circulation, to reduce cholesterol and toxins levels in the body and to strengthen the uterus after childbirth (Ismail, 2006).

For centuries, it was consumed at home through infusion and recently the herb has been marketed in the form of tea sachet, capsules and tablets. The tablets are generally in high demand due to several advantages such as convenience during consumption, and sweeteners or coatings can be used to mask any unpleasant taste of *Ficus deltoidea*. Tablets are defined as solid mixtures of active substances and binders, usually in powder form,

* Corresponding Author

and compressed into solid. The binders represent the materials that provide the necessary bonding in order to hold the powders together to form granules under compaction. A compactor is a device that performs compaction and in this study, the uniaxial die compaction was used for tabletting of grounded *Ficus deltoidea* leaves.

The main objectives of this study were to investigate the compactibility and compressibility of *Ficus deltoidea* powder and the effect of addition of binder such as Avicel, or also known as microcrystalline cellulose upon tabletting. Compactibility is the ability of two or more substances combined with each other to form a homogeneous composition of useful plastic properties, with negligible reactivity between materials in contact. Compressibility is defined as the ability of a powder to decrease in volume under pressure.

VALIDATION OF THE EXPERIMENTAL DATA

Pressure-volume relationship from the uniaxial die compaction is used for the analysis of the interactions between the particles and the particles as well as the particles and the wall, and the study of the microstructure of compact. There are many equations to describe the powder compaction processes (Heckel, 1961; Cooper and Eaton, 1962; Kawakita and Lüdde, 1970/71). The Kawakita and Lüdde (1970/71) equation is probably the most widely used model in both powder metallurgy and pharmaceutical industries particularly for soft medical powders, and was adopted for this study. Kawakita and Lüdde (1970/71) equation is shown below.

$$\frac{\sigma_a}{C} = \frac{1}{ab} + \frac{\sigma_a}{a} \tag{1}$$

where s_a is the pressure applied, C is the degree of volume reduction (defined as $C = (V_o - V)/V_o$, with V_o is the powder volume before pressure is applied, and V is the powder volume after pressure is applied), and a and b are the constants characteristics of the powder. The constant value a represents the initial porosity in the case of piston compression. The value of the constant b is related to the resisting force, or the cohesiveness, of powdery particles in the case of tapping and vibrating.

MATERIALS AND METHODS

Materials

Ficus deltoidea powder (Ya'acob Berkat Enterprise, Melaka) and microcrystalline cellulose, trade name Avicel PH-101 (Sigma – Aldrich Chemil GmbH, Ireland) were used in this study. The particle size of the powders was estimated based on the Scanning Electron Microscopy (SEM) images. SEM was used to capture images of *Ficus deltoidea* and Avicel powders at 500 magnifications as shown in *Fig. 1.* The material properties before the uniaxial die compaction process are shown in Table 1. The moisture content of the powders was measured using a digital moisture analyzer (OHAUS MB45, USA) at 104ºC. The bulk and tapped density were measured and described elsewhere (Abdullah, 2007).

The Carr's compression Index (Carr, 1965) and Hausner ratio (Hausner, 1967) obtained indicated that *Ficus deltoidea* powder has poor flowa compared to Avicel powder which has good flow characteristics, which may be used to infer their compressibility characteristic later.

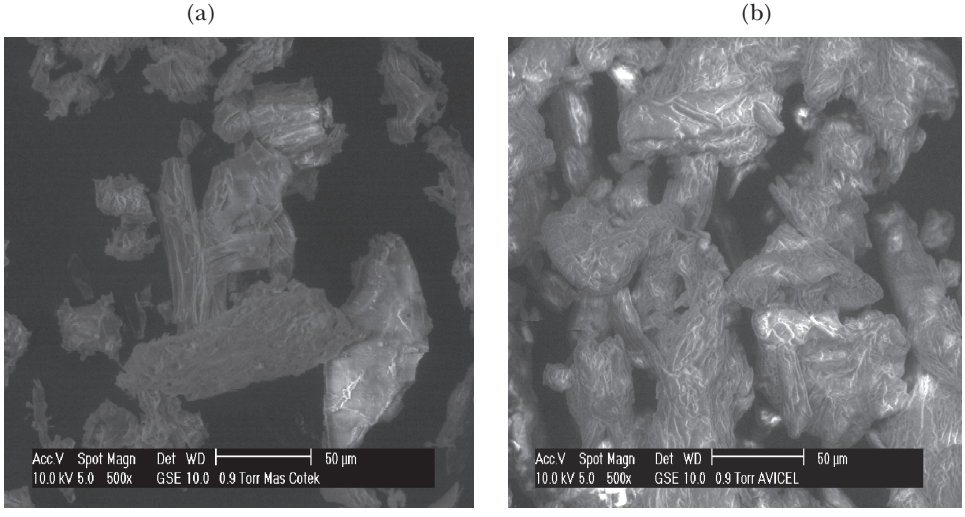

Fig. 1: SEM images for (a) Ficus deltoidea *and (b) Avicel powders at 500x magnifications*

TABLE 1
Material properties of *Ficus deltoidea* and Avicel powders

Material Properties	*Ficus deltoidea*	Avicel
Estimated Particle Size (µm)	100-150	80
Moisture Content (%)	11.34	4.45
Bulk Density (kg/m^3)	250	340
Tapped Density (kg/m^3)	333	423
Carr Index (%) (Carr, 1965)	25	19.6
Hausner Ratio (Hausner, 1967)	1.30	1.24
Flowability	Poor flowability	Good flowability

Uniaxial Die Compaction

The *Ficus deltoidea* tablets were prepared using a 13-mm-diameter cylindrical uniaxial die (Runnig Sdn. Bhd, Selangor). *Ficus deltoidea* powder (0.5 ± 0.01g) was poured into the stainless steel die using a plastic funnel to facilitate the flow of the powder. Then, the die was tapped for about 20 times to form a homogenous density distribution within the powder. Upon loading, a universal testing machine (Instron 5566, USA) was used for tabletting, with pressures ranging from 7.5 to 75 MPa and at a constant crosshead speed of 5 mm/min.

The data were recorded by a computer connected to the machine in the form of force-displacement curves. Upon unloading and ejection, the thicknesses of the tablets were measured using a digital vernier caliper and the volumes of the tabletted powder were obtained.

Tensile Strength Test

Tensile strength was determined by a diametrical compression test also known in the pharmaceutical industry as ''hardness'' test. In this test, the tablets were placed between two flat plates as shown in *Fig. 2.* The tests were conducted at a crosshead speed of 5 mm/min until an ideal fracture occurred (Newton *et al.*, 1971).

Fig. 2: A tensile strength test for a tablet

Effect of Binder

Mixtures of *Ficus deltoidea* and Avicel powders were prepared at 0.5 and 1.0 g of feed powders with the percentages of Avicel binder being 10, 20, 30, 40, and 60 %. Pure *Ficus deltoidea* and pure Avicel powders were also tabletted separately. These samples were compacted at various loads using the Instron machine.

RESULTS AND DISCUSSION

Pressure – Volume Relationship

Fig. 3 shows the pressure – volume relationship of 0.5 g of feed powder containing pure *Ficus deltoidea* and Avicel powders. Generally, as the pressure increases, the volume decreases, or in other words the density increases as the pressure increases. This could be explained based on the fact that the tabletting process may be divided into two main processes; rearrangement and deformation processes of the powders. Upon loading (at low pressure) the particles rearrange and slid to fill in the void spaces in the powder bed, creating higher inter-particle friction. As the pressure increases, further powder rearrangement and deformation occurs, thus forming a closer packing structure such that the compactibility of the powder increases. Intermolecular forces, such as van der

Waals forces were postulated to exist at this stage (Nyström *et al.*, 1993). During the final stage of tabletting process, the powder starts to deform permanently. The compressibility of the powder decreases in which tablet volume reduces slightly as the pressure increases. This may be due to the formation of large bonding points (junctions of contact), hence increasing the inter-particle contact area. Consequently, stronger bonds form between the particles that may have prevented further volume reductions. The trend of the findings in *Fig. 3* is similar to those of Yusof (2005) for compaction of maize with Avicel powders, and Abdullah (2007) for tabletting of 1.0 g of *Ficus deltoidea*. *Fig. 3* shows that the compressibility of Avicel powder is better compared to *Ficus deltoidea* powder as indicated by a large amount of volume reduction. Thus, the density of the Avicel tablet is higher than the *Ficus deltoidea* tablet. This agrees well with Avicel characteristics, commonly known as a universal binder.

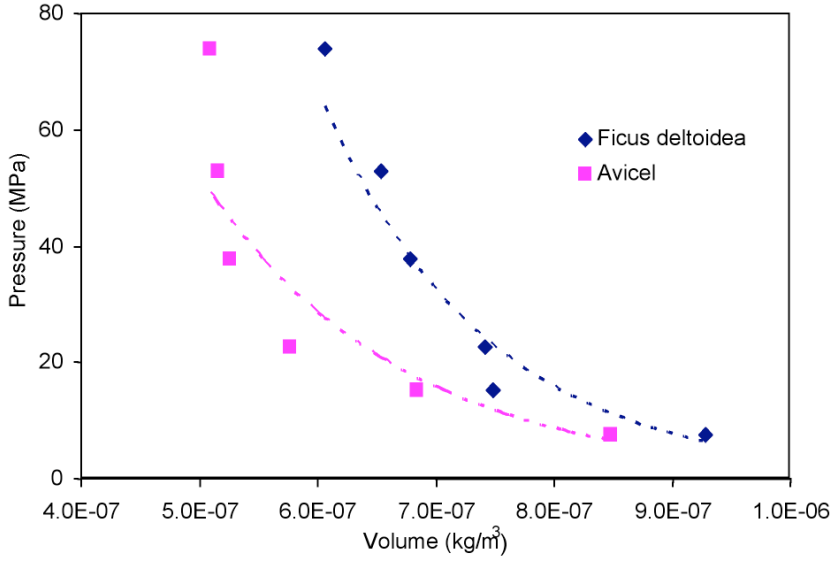

Fig. 3: Pressure vs volume for 0.5g of feed powder. The lines are the trend lines

Validation of the Experimental Data

The experimental data obtained were verified using a classical model of Kawakita (Kawakita and Lüdde, 1970/71). Constant *a* in the Kawakita relationship is considered to represent the initial porosity and constant *b* is related to the resisting force, or the cohesiveness of the powders (Kawakita and Lüdde, 1970/71). Table 2 shows *a* and *b* values for 0.5 and 1.0 g mixtures of *Ficus deltoidea* and Avicel powders with the compositions of Avicel powders ranging from 0 to 100%. There are some inconsistencies in the values of the constants as the compositions of Avicel increases and this is due to the segregation problem, which occurred in the feed powder mixture, which is unavoidable in a solid powder mixture (Yusof, 2005). Nevertheless, these values are comparable to the values for paracetamol powder with *a* and *b* values are 0.48 and 1.11 respectively (Mohammed, 2004). The *a* and *b* values for other herbal powders such as *Eurycoma longifolia jack* are 0.81 and 0.55 (Ahmad, 2007) and for *Morinda citrifolia* are 0.60 and 0.19 (Md Nor, 2007).

TABLE 2
The constant *a* and *b* from Kawakita's plot

Weight	0.5 g			1.0 g		
Composition of Avicel (%)	*a*	*b*	R^2	*a*	*b*	R^2
0	0.64	0.22	0.9989	0.79	0.08	0.9681
10	0.75	0.20	0.9971	0.74	0.14	0.9937
20	0.73	0.17	0.9968	0.75	0.13	0.9956
30	0.71	0.24	0.9993	0.72	0.17	0.9981
40	0.72	0.24	0.9993	0.70	0.19	0.9990
60	0.81	0.48	0.9996	0.69	0.20	0.9995
100	0.77	0.43	0.9996	0.75	0.12	0.9995

Tensile Strength

Fig. 4 shows the tensile strength as a function of load applied to 0.5 g of the mixture of *Ficus deltoidea* and Avicel powders. Avicel was used as a binder at various compositions, ranging from 0 to 100 % Avicel. Obviously, the tensile strength of pure Avicel is the strongest among the other samples. This finding agrees well with those of Ahmad (2007) and Md Nor (2007) for tabletting of *Eurycoma longifolia jack* and *Morinda citrofolia* herbs, respectively. Similar finding was found for tabletting of 1.0 g of the mixtures of *Ficus deltoidea* and Avicel powders (Abdullah, 2007).

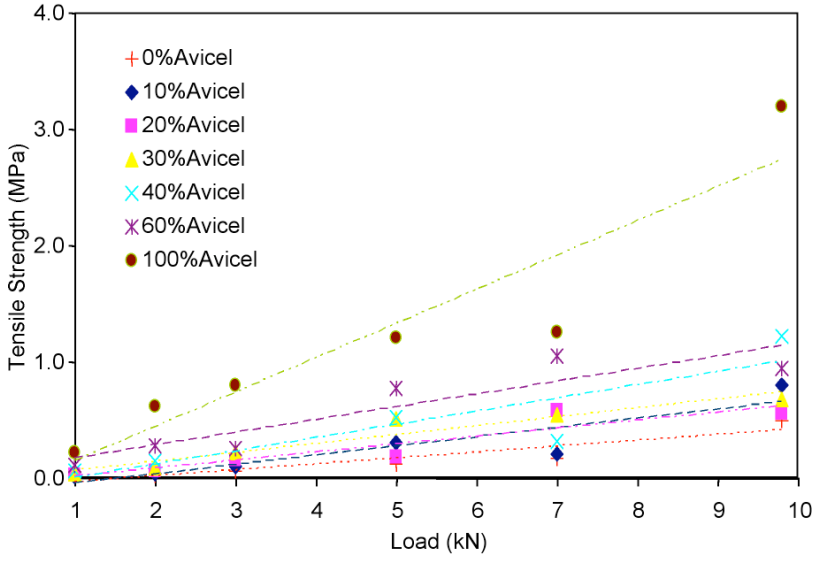

Fig. 4: Tensile strength vs load for 0.5 g of feed powder. The lines are the trend lines

CONCLUSIONS

The *Ficus deltoidea* powder was investigated upon tabletting. It was found that as the pressure to produce the tablet increases, the volume decreases, and the density increases. Therefore, higher pressure can produce a more tough and coherent tablet. The effect of binder was studied by the tensile strength versus load relationship. It was found that the tensile strength of pure Avicel (100% Avicel) was the strongest when compared with that of the mixed *Ficus deitoldea*- Avicel powders. The experimental results obtained for the tabletting study were also verified with an established model and they were found comparable to those in the literature. In conclusion, this study may be used to understand the tabletting characteristic of *Ficus deltoidea* herb.

ACKNOWLEDGEMENTS

The authors wish to thank the Universiti Putra Malaysia for the financial support through the young lecturers scheme (PLB), funding no. 5315831.

REFERENCES

Abdullah, R. (2007). Uniaxial die compaction of *Ficus deltoidea* (Thesis, Universiti Putra Malaysia, 2007).

Ahmad, S. (2007). Mechanical granulation by tabletting of *Eurycoma longifolia jack* (Thesis, Universiti Putra Malaysia, 2007).

Carr, R.L. (1965). Evaluating flow properties of powders. *Chemical Engineering, 72,* 163-167.

Cooper, Jr. A.R. and Eaton, L.E. (1962). Compaction behaviour of several ceramic powders. *Journal of the American Ceramic Society, 45,* 97-101.

Hausner, H.H. (1967). Friction conditions in a mass of metal powder. *International Journal of Powder Metallurgy, 3, 4,* 7-13.

Heckel, R.W. (1961). An analysis of powder compaction phenomena. *Transaction of Metallurgy. Society. AIME, 221,* 671-675.

Kawakita, K. and Lüdde, K.H. (1970/71). Some consideration on powder compaction equations. *Powder Technology, 4,* 61-68.

Ismail, M.K. (2006, April 7). Mas Cotek herba berkhasiat pencabar Tongkat Ali. *Utusan Malaysia*, http://www.frim.gov.my/fin/file/ACFA93.jpg.(date cited:7 Jun 2007)

Md Nor, C.R. (2007). Uniaxial die compaction of *Morinda citrifolia*. (Thesis, Universiti Putra Malaysia, 2007).

Mohammed, H. (2004). Contact mechanical aspects of pharmaceutical compaction (PhD Thesis, Imperial College London, London, 2004).

Newton, J.M., Rowley, G., Fell, J.T., Peacock, D.G. and Ridgeway, K. (1971). Computer analysis of the relation between tablet strength and compaction pressure. *Journal of Pharmacy and Pharmacology, 23,* 195-S201.

Nyström, C., Alderborn, G., Duberg, M. and Karehill, P.G. (1993). Bonding surface area and bonding mechanisms-two important factors for the understanding of powder compactability. *Drug Development and Industrial Pharmacy, 17 & 18,* 2143-2196.

YUSOF, Y. A., SMITH, A. C. and BRISCOE, B. J. (2005). Roll compaction of maize powder. *Chemical Engineering Science, 60(14),* 3919-3931.

YUSOF, Y. A. (2005). Rolling-mill granulation of powders (PhD thesis, United Kingdom Imperial College London, London, 2005).

ISSN: 0128-7680
Pertanika J. Sci. & Technol. **16 (1)**: 23 - 30 (2008)

Anti Windup Implementation on Different PID Structures

Farah Saleena Taip*[1] and Ming T. Tham[2]
[1]Department of Process and Food Engineering, Faculty of Engineering, Universiti Putra Malaysia, 43400 UPM, Serdang, Selangor, Malaysia
[2]School of Chemical Engineering and Advanced Materials, Newcastle University, Newcastle upon Tyne, NE1 7RU, United Kingdom
**E-mail: saleena@eng.upm.edu.my*

ABSTRACT

Although there have been tremendous advances in control theory over the last 25 years, the PID controller remains very popular and is still widely used in industry. A vital aspect of its implementation is the selection of a suitable set of parameters, as an improperly tuned controller might lead to adverse effects on process operation and worse, cause system instability. In industry, there are various types of PID controllers in addition to the 'textbook' PID but most tuning methods were developed based on this ideal algorithm. Another issue that is always associated with PID controllers is integral windup and the most popular method to overcome this problem is to add an anti windup compensator. This article includes the assessment of three anti windup strategies in combination with different tuning methods. The characteristics of PID controllers tuned using these approaches are evaluated by application to simulated FOPTD processes with different time-delay to time-constant ratios. Different measures were used to assess their performance and robustness properties, and the applicability of the tuning relationships to more typical (non-ideal) PID controllers is also considered. In general, the anti windup compensators successfully reduced the degradation effect caused by integral windup. It was found that the effectiveness of the different anti windup schemes varied depending on controller tuning methods and controller structures.

Keywords: Anti windup, PID, saturation

INTRODUCTION

The Proportional-Integral-Derivative (PID) controller remains the most popular control algorithm used in industry despite the continuous advances in control theory. It has a simple and easily understood structure but at the same time, can provide excellent control performance over a wide range of dynamic characteristics. Controllers are tuned to minimize or eliminate offset; to minimize the effect of disturbances; to ensure and maintain stability; and to provide smooth and rapid response. Practically, constraints always exist in any control system and may have negative effects on the closed loop response. Actuator saturation is among the most common nonlinearity in any control system. It is a form of input constraint and should not be neglected in a control design system. When the actuator saturates, the plant input will be different from the controller output, the integrator will continue to integrate the error causing the windup. Windup was initially associated with integral action, which may also occur during switching between controllers. This is because a control scheme has to satisfy multiple objectives, thus needs to operate in a different control mode (Bak, 2000; Astrom and Hagglund, 1995; Seborg *et al.*, 1998; Chau, 2002; Coughanowr, 1981).

* Corresponding Author

A well known methodology that has been used to counter windup is anti windup compensation. This methodology gave rise to a compensator which during saturation, suppresses the degradation caused by saturation (i.e. large overshoot, long settling time). Anti windup is a popular approach in handling saturation. The main objective of all anti windup schemes is to stabilise the system and to recover as much performance as possible in the presence of actuator saturation (Bohn, Atherton, 1995; Goodwin *et al.*, 2001; Astrom and Hagglund, 2001).

The objective of this research was to investigate how different controller tuning methods fare under the presence of saturation will also be investigated. Focus will be on the classical anti windup strategy and some extension of the classical anti windup structures. The different anti windup structures will be tested on different PID controllers tuned by different methods, to see the effectiveness of anti windup schemes with different tuning methods and different PID structures. The robustness properties of these anti windup compensators will also be studied.

Different PID Structures

There is only one form of PI controller. PID controllers, however, can have different structures.

Ideal PID (PIDI)

The PID algorithm reported in most publications is the "ideal PID" which has the following transfer function:

$$\frac{U(s)}{E(s)} = G_C(s) = K_C\left(1 + \frac{1}{T_I s} + sT_D\right) \tag{1}$$

The proportional gain (K_c), integral time (T_I) and derivative time (T_D) are the tuning constants. $U(s)$ is the output of the controller, while $E(s) = X(s) - Y(s)$ is the error between setpoint, $X(s)$, and controlled output, $Y(s)$ and $G_C(s)$ is the controller transfer function. PID controllers used in industry may not have the same structure though (Astrom and Hagglund, 1995; Goodwin *et al.*, 2001; Astrom, 1996; Clair, 2000).

Series PID (PIDS)

There is a slightly different version of the PID controller, known as the "series" or "interacting" controller.

$$G_C'(s) = K_C'\left(1 + \frac{1}{sT_I'}\right)(1 + sT_D') \tag{2}$$

The controller transfer function is denoted as $G_C'(s)$. The proportional gain (K_c'), integral time (T_I') and derivative time (T_D') are the tuning constants for the series controller. It is called interacting because the derivative and integral terms interact with each other (Astrom and Hagglund, 1995; Goodwin *et al.*, 2001; Astrom, 1996; Clair, 2000).

"Commercial" PID (PIDC)

The derivative term in Eq. 1 causes realization problems, and a more practical form is:

$$G_C(s) = K_C\left(1 + \frac{1}{T_I s} + \frac{T_D s}{1 + sT_D / N}\right) \tag{3}$$

The derivative term in Eq. 1 is cascaded with a low-pass filter with a time-constant, T_D/N is usually chosen to be between 5 and 20. The sensitivity of the algorithm to noise is increased with higher values of N (Astrom and Hagglund, 1995; Goodwin *et al.*, 2001; Astrom, 1996; Clair, 2000).

Setpoint Weighted or Output Filtered PID (PIDF)

Normally, a PID controller is driven by the error between the setpoint and the controlled output. However there is a more flexible structure given by:

$$U(s) = K_C\left[\left(bX(s)\right) + \frac{1}{sT_I}\left(X(s) - Y(s) + \frac{T_D s}{1 + sT_D / N}\left(cX(s) - Y(s)\right)\right)\right] \tag{4}$$

Here, the responses to setpoint changes depend very much on the values of b and c, which are either "0" or "1". By setting them equal to zero, "kicks" in the controller output are avoided when there is a large step-change in setpoint (Astrom and Hagglund, 1995; Goodwin *et al.*, 2001; Astrom, 1996).

Different Anti Windup Schemes

Three anti windup schemes based on 'back calculation' technique are discussed. They are the classical anti windup, alternative anti windup and modified anti windup. The Classical Anti Windup (CAW) is previously known as 'back-calculation' or 'tracking', this anti windup scheme is easily incorporated in PI/D controllers. The principle behind it is to recalculate the integral action when the output saturates and come into effect only when there is saturation and maintain the original 'normal' behaviour when there is no saturation. An extra feedback loop is added by feeding the difference between the control output, u, and the plant input or the saturated plant input, $sat(u)$ to the integrator with a gain of $1/T_I$. T_I is the parameter that needs to be specified, and determines the rate at which the controller output is reset (Astrom and Hagglund, 1995).

By limiting the controller output, the speed of actuator response will also be limited, if the actuator is described by linear dynamics, followed by saturation. To account for this, an alternative structure is introduced where an unrestricted control signal is applied to the process and a dead zone is used to generate the feedback signal. The structure is called Alternative Anti Windup (AAW). The dead zone range is the same as the linear range of the actuator. The dead zone gain, b, represents the ratio between integral time and the tracking time, $b = \frac{T_I}{T_I}$ and usually is set equal to 1, as it corresponds with $T_I = T_I$, (the suggested value for classical anti windup). A high value of b may reduce overshoot but at the expense of slower response (Bohn and Atherton, 1995).

Both classical and alternative anti windup are very sensitive to changes to the parameters, T_I and b. In the alternative anti windup scheme, if the dead zone gain is large, a very high initial controller output (due to P and D terms) will give a very large feedback signal to the integrator. Therefore, an additional limit on the proportional and derivative part is introduced. By incorporating the additional limit, another design parameter is introduced, and it is known as 'r', which represents the ratio range of the proportional-derivative limiter and the dead zone range. This structure which is known as Modified Anti Windup (MAW) allows a large value of dead zone gain to be selected, without causing slower response. The responses are relatively insensitive to changes in r (Bohn and Atherton, 1995).

Simulation Studies

To assess the effectiveness of different types of anti windup structures, they have been applied to different controller structures. The design parameter, for classical anti windup has been chosen to be $T_t = T_I$ for PI and $T_t = \sqrt{T_I T_D}$ for PID, while for both parameters for alternative anti windup and modified anti windup; b and r are chosen to be 1, as suggested. The anti windup strategies were applied to all PID structures except the Series PID. The structure of Series PID does not require anti windup, as this PID form can be implemented to counter actuator saturation. The three different anti windup structures were applied to PID controllers that were tuned using different tuning methods. The methods vary from the classical methods, like Ziegler-Nichols (ZN), Cohen-Coon (CC), to more recent methods like Direct Synthesis (DS), Simplified IMC (SIMC), Abbas tuning method (AA) and gain phase mergin method (GPM) (Abbas, 1997; Ho *et al.*, 1999; Coughanowr, 1981; Seborg *et al.*, 1989; Skogestad, 2002). The process considered was first order with process and time delay (FOPTD) with process gain, $K_p = 2$, process time constant, $\tau_p = 4$ and the delay, $\theta = 2$ where R = 0.5. The simulations were done using MATLAB, where the simulation time was 200s.

RESULTS AND DISCUSSION

Integral Absolute Error, (IAE), and the percentage overshoot (PO) were used as performance measurements. The three anti windup schemes were compared based on different PID controllers. Extensive simulations were done to observe the effect of saturation. In general, saturation will degrade the closed loop performance, leading to larger IAE, larger overshoots and longer settling times. Systems with faster responses (i.e. tuned using ZN and CC) tend to result in larger differences compared to the process tuned using the GPM method.

Performance

In general, insignificant differences were observed in PI controlled system. For the Ideal PID controller, all anti windup strategies performed well in reducing the overshoot for all tuning methods. The MAW scheme was designed to provide faster response compared to the classical anti windup (Bohn and Atherton, 1995), explaining the smallest amount of overshoot reduction in comparison to the other two schemes. With the GPM method, responses of the different anti windup are quite identical with about 10% reduction in overshoot.

An analysis of the overshoots in the responses under the different anti windup schemes are shown in *Fig. 1.* Each bar represents a different anti windup method; CAW,

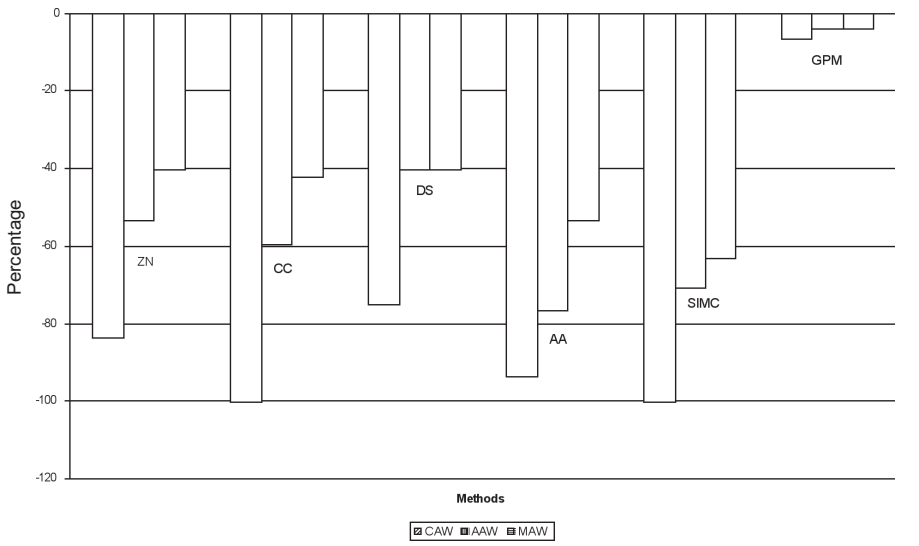

Fig. 1: Differences in overshoots for different anti windup (PIDI)

AAW and MAW. Six different tuning methods were considered and they are indicated as ZN, CC, DS, AA, SIMC and GPM. The y-axis represents the percentage change in overshoot when different anti windup compensators were applied. A negative value means that the percentage of overshoot is reduced by the anti windup scheme, while a positive value means that the percentage overshoot is increased by applying anti windup.

As one of the main objectives of having anti windup is to reduce the overshoot that will occur when there is saturation, the main focus will be in the negative region, as this shows the degree of reduction in the overshoot for a system without anti windup and when different anti windup schemes are applied. The anti windup schemes undoubtedly showed excellent performances in reducing the overshoot, with the CAW consistently yielding the 'best' performance across different tuning methods, for all PID structures.

For the Ideal PID controller, the differences in IAE between the three anti windup structures are more significant (*Fig. 2*). The CAW showed tremendous improvement in reducing or eliminating overshoot, compared to the other two schemes, which consequently reduced largest IAE as well. All the anti windup schemes effectively reduced the IAE. The MAW scheme in general, contributed to the least reduction in IAE, ranging between 0.4 to 26% reductions.

The differences between the three anti windup schemes became more prominent when applied to the Commercial PID. The CAW scheme was clearly the most effective anti windup scheme in terms of reducing overshoot; it reduces overshoots by between 50 – 100% for all tuning methods considered. On the other hand, the MAW only managed to reduce overshoot by 4 to 60%. The AAW showed acceptable performance, where the overshoot was reduced by between 40 to 100% for different tuning methods.

Overall, the CAW scheme was the most effective in terms of reducing overshoot as it eliminated the overshoot for controllers tuned using CC, DS, AA and SIMC methods, but at the expense of longer settling times and larger IAE compared to other anti windup schemes. Insight into the behaviour of different anti windup schemes can be gained by examining the closed loop response in *Fig. 3*. Systems with MAW scheme displayed

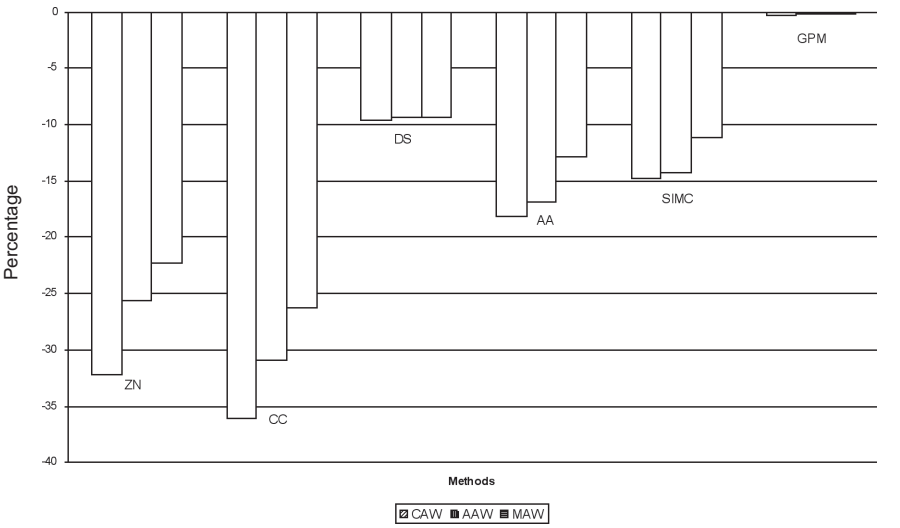

Fig. 2: Differences in IAE for different anti windup (PIDI)

highest overshoot among all other anti windup structures. The CAW scheme portrayed the best performance. Similar trends were observed for different tuning methods ±25% of the nominal case and performances were indicated by IAE values and percentage overshoot.

An increase in gain will definitely make the closed loop response more oscillatory, thus making an anti windup compensator less effective but the CAW scheme still exhibited the best performance on all PID controllers. Table 1 shows the percentage change in overshoot for a PI controller, when the gain is increased by 25%. The table can be divided into three main columns, according to the different anti windup schemes.

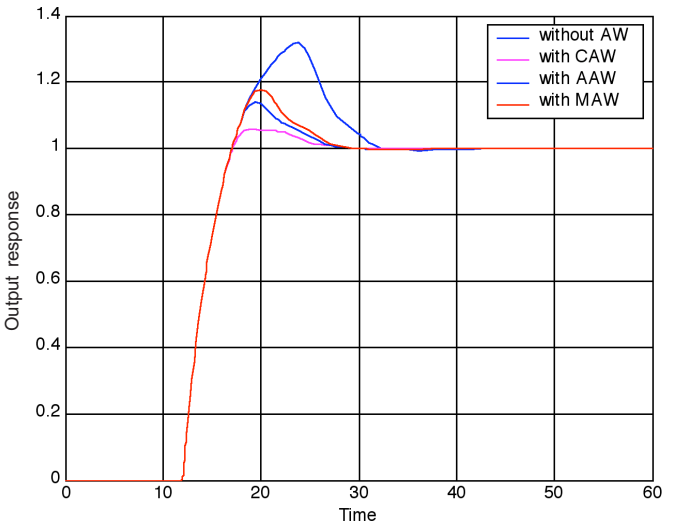

Fig. 3: Responses of different anti windup schemes for ZN tuned PIDF controller

TABLE 1
Percentage overshoot change by different anti windup schemes for PI with mismatch in gain (+25%)

Method	Classical anti windup		Alternative anti windup		Modified anti windup	
	Nominal	PMM	Nominal	PMM	Nominal	PMM
ZN	-99	-20	-99	-20	-65	-20
CC	-55	-40	-55	-40	-48	-40
DS	-20	-8	-20	-8	-20	-8
AA	-75	-25	-75	-25	-75	-25
SIMC	-20	-8	-20	-8	-20	-8
GPM	-44	-14	-44	-14	-44	-14

Each main category can be divided into two, representing the nominal case and when there is process model mismatch, (PMM). They refer to the overshoot reduced by the application of anti windup. Large differences between the nominal case and when mismatch is considered can be seen in the least robust tuning procedures, like ZN and CC, for all anti windup schemes.

As expected, by lowering the process gain, the closed loop response will become slower. Therefore, the anti windup schemes were more effective in reducing the overshoot. It can be seen that the CAW scheme still gave the best performance, even with mismatch in the gain.

As the process time constant is set 25% higher than the nominal value, the closed loop response was faster for controllers tuned using certain methods. The PI controller with CAW scheme gave quite a consistent performance with small differences between nominal and when mismatch was considered. The AAW and MAW schemes were severely affected. The detrimental effects in all PID controllers are more significant, with the classical anti windup scheme being the most affected in the Ideal PID controller. As the process time constant is reduced by 25%, the closed loop responses are slightly affected. The effectiveness of the anti windup schemes were slightly reduced for the PI controller. However, the change is more significant in other PID controllers; with certain tuning methods showing some reduction in the effectiveness while some portrayed slight improvements. For a slower system (tuned using DS, SIMC, and GPM methods), reducing the process time constant may not deteriorate the performance as much as for controllers tuned by other methods.

Mismatch in time delay does not have a significant overall impact on the effectiveness of the three anti windup compensators. The effect of lowering the dead time was not very significant in the PI controller. A similar observation was made for other PID controllers. Generally, in all PID controllers, the change is between 10%-20% for the three anti windup schemes.

CONCLUSIONS

Actuator saturation undeniably will cause deterioration to a closed loop performance but the degree of degradation differs according to tuning method. Overall, the GPM method was the least affected when there is saturation. Generally, the classical anti windup

scheme showed the most preferable performance in reducing the adverse effect caused by saturation while the modified anti windup exhibited the least preferable performance. The CAW scheme also portrayed consistent performance through out the different PID structures. However, the responses of different anti windup also differ according to different controller settings, although the CAW scheme was generally suitable for all tuning methods. The tuning methods that yield more aggressive response like ZN and CC methods may not be suitable with the MAW scheme that resulted in faster responses. However, for a conservative method like the GPM method, applying MAW scheme may still provide a good and acceptable response. The alternative anti windup scheme resulted in similar response with CAW scheme for the PI controller, because the tuning parameters chosen for both CAW and AAW schemes resulted in the same value for the PI controller.

When process model mismatch is considered, the CAW scheme was the least robust, as it was the most affected especially for the Ideal PID controller. Even though the CAW scheme was the most affected when there is model mismatch, it still exhibited the best performance, especially in reducing the overshoot.

REFERENCES

Abbas, A. (1997). A new set of controller tuning relations. *ISA Transactions, 36*(3), 183-187.

Astrom, K. and Hagglund, T. (1995). *PID Controllers: Theory, Design and Tuning* (2nd ed.). New York: Research Triangle Park.

Astrom, K. (1996). *PID Control. The Control Handbook.* Florida: CRC Press.

Astrom, K. and Hagglund, T. (2001). The future of PID control. *Control Engineering Practice, 9,* 1163-1175.

Bak, M. (2000). *Control of Systems with Constraints.* Denmark: Department of Automation, Technical University of Denmark.

Bohn, C. and Atherton, D.P. (1995). An analysis package comparing PID anti-windup strategies. *IEEE Control System Magazine, 2,* 34-40.

Chau, P. (2002). *Process Control.* UK: Cambridge University Press.

Coughanowr, D. (1981). *Process Systems Analysis and Control.* New York: McGraw Hill.

Clair, D.W. (2000). The PID algorithm. Retrieved from http://members.aol.com/pidcontrol/pid_algorithm.htm

Goodwin, G., Graebe, S.F. and Salgado, M.E. (2001). *Control System Design.* New Jersey: Prentice Hall.

Ho, W.K., Lim, K.W., Hang, C.C. and Ni, L.Y. (1999). Getting more phase margin and performance out of PID controllers. *Automatica, 35,* 1579-1585.

Seborg, D., Edgar, T. and Mellichamp, D. (1989). *Process Dynamics and Control.* New York: John Wiley.

Skogestad, S. (2002). Simple analytic rules for model reduction and PID controller tuning. *Journal of Process Control, 13,* 291-309.

ISSN: 0128-7680
Pertanika J. Sci. & Technol. **16 (1)**: 31 - 39 (2008)

Water-oil Flows Transition from Stratified to Inter-dispersed in Horizontal Pipeline System

Siti Aslina Hussain[*1], Wan Hassan Mohd Jamil[2], Xiao Yu Xu[3] and Geoffrey F. Hewitt[4]
[1]Department of Chemical and Environmental Engineering, Faculty of Engineering, Universiti Putra Malaysia, 43400 UPM, Serdang, Selangor Darul Ehsan, Malaysia
[2]Geowell. Sdn. Bhd., 151 Jalan Aminuddin Baki, Taman Tun Dr Ismail, 56000 Kuala Lumpur, Malaysia
[3,4]Department of Chemical Engineering, Imperial College London, South Kensington Campus, London SW7 2AZ, UK
**E-mail: aslina@eng.upm.edu.my*

ABSTRACT

The spatial distribution of water and oil in horizontal pipe flows was studied experimentally at differing inlet water fractions and mixture velocities. Under most conditions the pattern was oil-continuous in water-dispersed or water-continuous in oil-dispersed and there is entrainment in the form of drops of phase into the other. The investigations were carried out through the cross-sectional phase distribution in the flow of mixtures of water and oil in a horizontal 0.0254 m bore stainless steel section. The phase fraction distribution was determined using a traversing beam gamma densitometer, with the beam being traversed at 0º, 45º and 90º of the vertical line passing through the axis of the tube. Measurements were made at 1.0 m and 7.72 m along the 9.7 m test section length tube. The measurements were made using the **T**wo-phase **O**il **W**ater **E**xperimental **R**ig (**TOWER)** facility, which allows the two fluids to be fed to the test section before separation and return again to the test line. The flow developed naturally from an initial stratified flow in which the oil and water were introduced separately at the top and the bottom of the test section respectively. It was found that the liquids were fully inter-dispersed by the time it reached the end of the test section. The phase fraction distribution was shown to be homogeneously mixed near the outlet of the test section.

Keywords: Water-oil flows, phase distribution, stratified-dispersed flow, inlet water fraction, mixture velocities

INTRODUCTION

Multiphase flow is the simultaneous flow of two or more phases in direct contact in a given system. It is important in many areas of chemical and process engineering and in the petroleum industry, e.g. in production wells and in subsea pipelines. The behavior of the flow will depend on the properties of the constituents, the flow rates and the geometry of the system. There are four combinations of two-phase flows namely, gas-liquid, gas-solid, liquid-liquid and solid-liquid. Liquid-liquid flows, the subject of this study are extremely important particularly in two-phase flow applications in horizontal pipes, for instance in the oil industry. In liquid-liquid flow system, it is important to understand the nature of the interactions between the phases and to observe the ways in which the phases are distributed over the cross section of the pipe or know as flow pattern.

The mean in-situ volume fraction will not normally be the same as the input volume fraction. The flow behavior is also influenced by the density and viscosity of the phases and the diameter of the pipe. Studies of such parametric effects include those of Charles *et al.* (1961), Arirachakaran *et al.* (1989) and Shi *et al.* (1999). Most previous studies have

* Corresponding Author

focused on general flow patterns and their delineation through flow pattern maps. There have been only a few studies focused specifically on dispersed flows in horizontal pipelines. Moreover, the present detailed understanding of the phenomena involved is very limited. In the dispersed flow region, there exist two types of flow configurations, namely oil-in-water dispersions and water-in-oil dispersions.

A number of recent studies on oil-water dispersions have focused on horizontal pipelines and, in particular, on the evaluation of the behavior of the droplets in the system. Extensive studies have been done on the flow patterns and the transition between them resulting in a better understanding of the two-phase flow structure. It is important to understand the nature of the interactions between the phases and how these influence the flow patterns and the resulting flow pattern maps, the droplet behavior and the phase distributions. Arirachakaran *et al.* (1989) and Angeli (1996, 2000) found that dispersed flow for oil-water systems in horizontal pipes occurs when the liquid-liquid mixture is moving at high velocity. In horizontal flow, the flow pattern will inevitably be more complex because the gravitational force acts perpendicular to the direction of flow. Thus, there is a tendency for the dispersed phase to move vertically (i.e. normal to the tube axis) under the influence of gravity (upwards, due to buoyancy, if the dispersed phase is the lighter phase and downwards if the dispersed phase is the heavier). This tendency is affected by the action of turbulent eddies in the continuous phase which act towards making uniform the distribution of the dispersed phase due to turbulent diffusion. The actual distribution is a manifestation of the balance between gravity-induced separation and turbulence-induced mixing.

Earlier work on liquid-liquid flows in horizontal channels (Angeli, 1996; Soleimani, 1999; Siti Aslina, 2006a, 2006b) included studies of the phase distribution. These studies demonstrated the tendency for the dispersed phase to separate to the top or the bottom of the channel depending on its density relative to the continuous phase. The higher the velocity, the more the fluids were well mixed indicating the increasing dominance of turbulence over gravity. In these earlier experiments, the measurements were made in what was expected to be a relatively fully developed flow at the end of the test section (typically 300-400 tube diameters from the inlet). However, it is likely that further insight could be gained regarding the turbulent mixing and gravity separation processes by studying the development of the flow along the channel and this was the underlying theme of this study. The inlet conditions were such that the heavier phase (water) was introduced at the bottom of the tube and the lighter phase (oil) was introduced at the top of the tube. The initial conditions were therefore of well-separated phases though it would be expected that dispersion of the relevant phase would occur quite quickly downstream of the entrance.

The objectives of this study were to investigate the tendency of flow structure to be affected by the action of turbulent eddies in the continuous phase which results in uniform distribution of the dispersed phase due to turbulent diffusion. The current experimental work is natural free flow from mixing equipment at the inlet of the pipe and therefore the actual distribution is a manifestation of the balance between gravity-induced separation and turbulence-induced mixing along the pipe, from partially stratified to fully homogeneous flow.

MATERIALS AND METHODS

Experimental Setup and Measurement Techniques

The **T**wo-phase **O**il and **W**ater **E**xperimental **R**ig is a liquid-liquid flow facility designed for studying flows in 0.0254 m horizontal pipes channel. The TOWER facility allows the

phenomena occurring during the simultaneous horizontal flow of two liquids, such as oil and water, in a pipe channel to be observed. The TOWER facility flow loop is illustrated in detail by Siti Aslina (2004).

Water and oil were supplied separately from two 0.681m^3 storage tanks to the stainless steel test sections. The test section had an inside diameter of 0.0243m and was made up of six successive pipe section of lengths of 1m, 1m, 1.87m, 1.87m, 3.85m and 0.1m respectively, giving a total length of 9.7m. The pipe sections are linked together with flanged connections designed to give a continuous and smooth inner bore. The final 0.11m section was made from acrylic resin to allow the flow to be observed.

The mixture of the two fluids after the test section was separated in a liquid-liquid separator which has 4m^3 horizontal vessel made from PVC reinforced with steel. It consists of a 1.94 m long, 0.54 m ID tank, containing a 0.54 m diameter, 0.3 m long Knitmesh™ coalescer. The Knitmesh™ coalescer was fitted to promote efficient separation of the fluids and is made from filaments of two different materials, metal and plastic, knitted together. These two materials are wetted by water and oil respectively and can therefore collect droplets of either fluid in a continuum of the other. The combination of different materials can also significantly improve the rate of coalescence of captured droplets which pass up or down (depending on which phase is continuous) the Knitmesh™ pad, meeting at the junction points of the two materials.

The two liquid phases used in the experiments were: tap water fed directly into the water tank through a plastic hose and oil (density, 801kg/m^3, viscosity, 1.6 cp and interfacial tension air-oil-water, 0.027 N/m^2, 0.017 N/m^2). The oil was pumped from the supply drums into the oil tank through a special branch in the suction line of the oil pump.

Measurements were taken using an advanced technique known as Gamma Densitometer System. A gamma densitometer system has been developed for use on the TOWER facility. The platform was designed such that the beam could be traversed with the beam in the horizontal (0º), vertical (90º) and inclined (45º) orientations. At each orientation it was thus possible to obtain the water hold-up profile. Collection of these three sets of data for a given flow condition also allowed the derivation of tomographic images of phase distribution across the channel (Soleimani, 1999; Siti Aslina, 2004). The basic equations for gamma densitometry and the factors influencing measurement accuracy are discussed in detail in Soleimani (1999), Siti Aslina (2004) and Siti Aslina *et al* (2006, 2007).

The hold-up of the oil and water phases in terms of the measured intensity I and the full tube values I_{oil} and I_{wat} are given by the following equations (Siti Aslina, 2004; Siti Aslina *et al.,* 2006, 2007):

$$\varepsilon_{oil} = \frac{\mathrm{In}\left(I / I_{wat}\right)}{\mathrm{In}\left(I_{oil} / I_{wat}\right)} \tag{1}$$

$$\varepsilon_{wat} = \frac{\mathrm{In}\left(I / I_{oil}\right)}{\mathrm{In}\left(I_{wat} / I_{oil}\right)} = 1 - \varepsilon_{oil} \tag{2}$$

In the experiments, I_{oil} , I_{wat} and I were determined, and the errors lead to an error approximately ±0.26 mm corresponding to an error approximately ±1% in phase hold-up (i.e. at the central chord position. This measurement error is much higher in the oil-water system than an oil-air system due to the small density difference between oil and water. For each flow condition, 75 chordal mean phase fraction measurements were

made with 25 at each orientation. The average phase fraction could be determined from the results at each orientation by taking the average of the chordal mean values weighted according to chord length. Thus, for any given flow conditions and axial location, the average phase fraction determined at the three respective beam orientations were in reasonable agreement.

Measurements of local chordal mean phase fraction were made using the Gamma Densitometry System (GDS) at 1.0 m and 7.72 m from the inlet. The measurements were taken at 1.8 m/s and 2.76 m/s mixture velocities and three input water fractions (i.e. 60%, 46% and 40%). The data obtained for chordal mean phase fractions could also be interpreted using a tomographic algorithm (Hu and Stewart, 2002).

RESULTS AND DISCUSSION

Effect of Inlet Water Fraction

Input water fraction is a very important variable. At the lowest water fraction studied (40%), the water would be expected to be dispersed in the oil and at the highest (60%) the oil would be expected to be dispersed in the water. However, tomography reveals that the phase mixing patterns are extremely complex as will be seen by examining the full set of tomographic data in the following figures. The effect of input water fraction can be illustrated by considering four examples as follows:

(i) Mixture Velocity 1.8 m/s, Axial Location 1.0 m (*Fig. 1*)

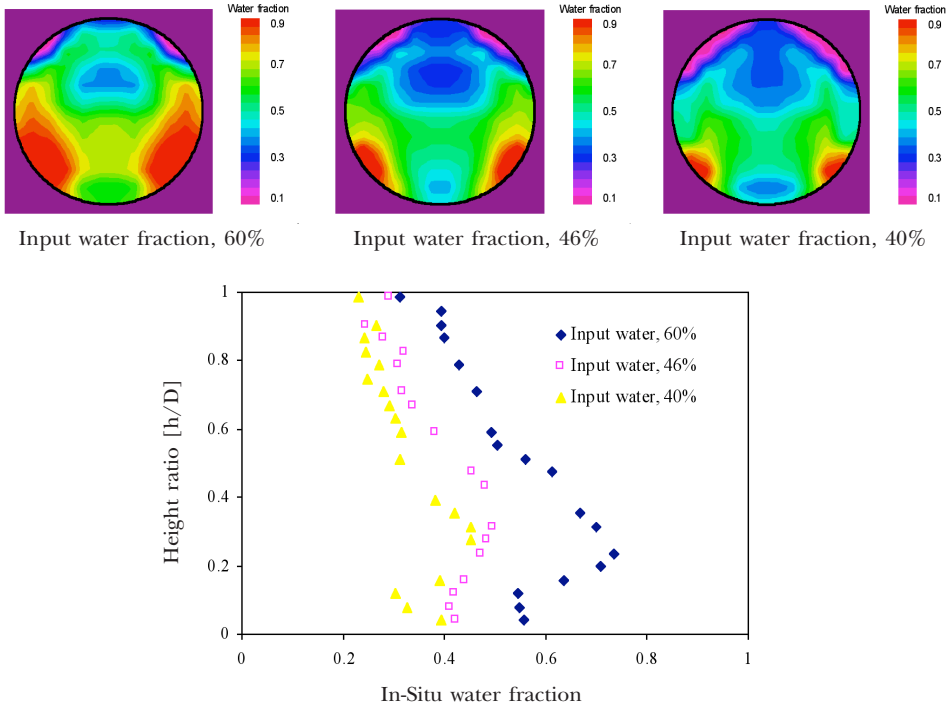

Fig. 1: Cross-sectional phase distributions (obtained by the gamma tomographic method) and vertical water fraction distributions (obtained from the vertical gamma scan) for a velocity of 1.8 m/s and at a position 1m from inlet

At the inlet, the oil is introduced at the top of the channel and the water at the bottom. The phase distribution observed at 1.0 m for a mixture velocity of 1.8 m/s (the lowest velocity studied) may strongly reflect this initial distribution with oil-rich and water-rich zones being seen at the top and bottom of the pipe on either side of a line passing vertically through the axis. Mixing in and around this line may be most intense, leading to the rather unexpected phase distribution observed.

(ii) Mixture Velocity 2.76 m/s, Axial Location 1.0 m (*Fig. 2*)

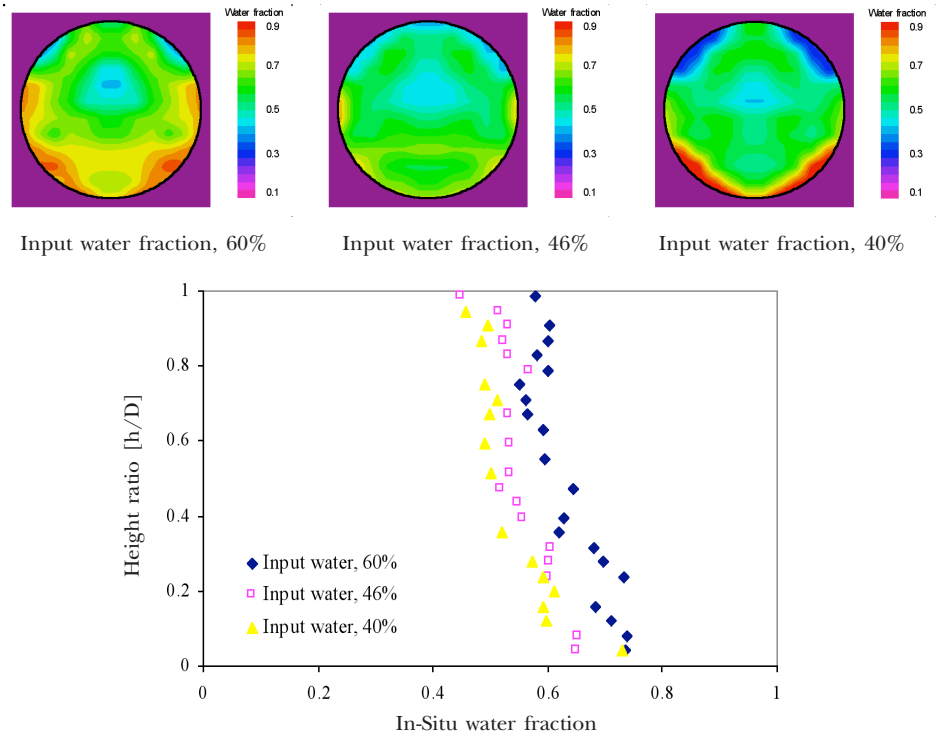

Fig. 2: Cross-sectional phase distributions (obtained by the gamma tomographic method) and vertical water fraction distributions (obtained from the vertical gamma scan) for a velocity of 2.76 m/s and at a position 1m from inlet

In this case, at the highest mixture velocity, the phase distributions are more uniform, though a high concentration of water is still observed at the bottom of the pipe, and a high concentration of oil near the top of the pipe, for an input water fraction of 40% where the dispersion is water-in-oil. For 46% input water fraction, (near the expected phase inversion point) the water fraction is reasonably constant across the pipe. For 60% input water fraction, an oil-in-water dispersion would be expected and the oil phase concentration would be expected to be higher (as is observed) at the top of the pipe due the tendency of the (lighter) oil drops to rise upwards.

(iii) Mixture Velocity 1.8m/s, Axial Location 7.72 m (*Fig. 3*)

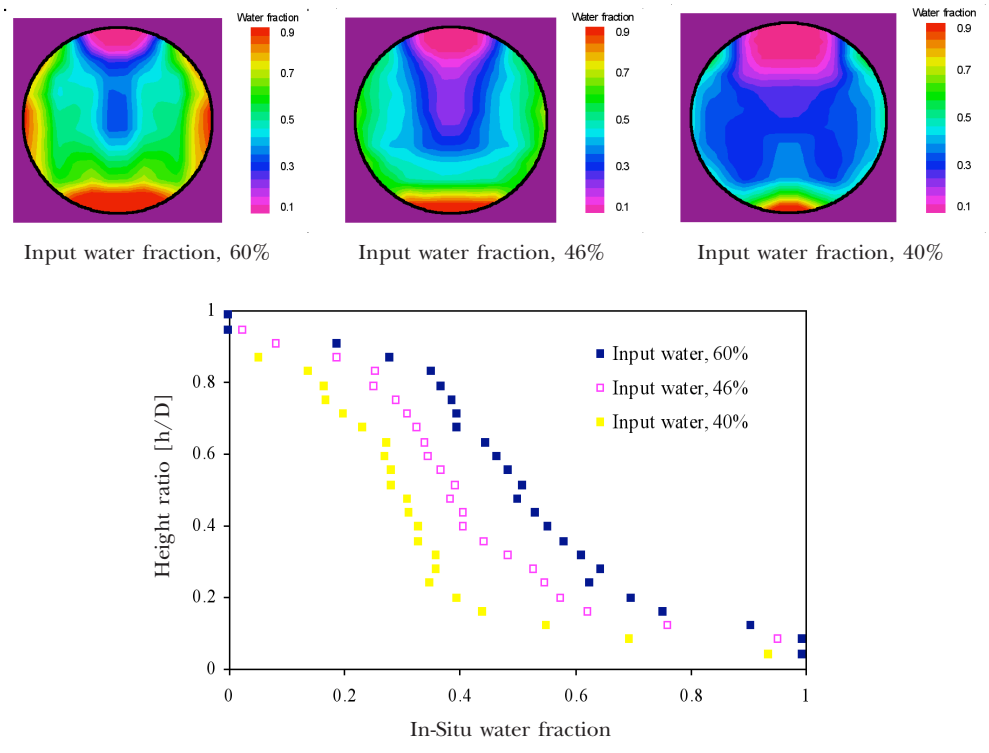

Fig. 3: Cross-sectional phase distributions (obtained by the gamma tomographic method) and vertical water fraction distributions (obtained from the vertical gamma scan) for a velocity of 1.8 m/s and at a position 7.72 m from inlet

For this axial distance, there was time for the two phases to partially separate with an oil "rivulet" at the top of the pipe and a water "rivulet" at the bottom of the pipe. The region between is mixed with some separation of the heavier and lighter phases observed.

(iv) Mixture Velocity 2.76m/s, Axial Location 7.72 m (*Fig. 4*)

At this higher velocity, partial separation is also observed. However, the shape of the regions with near-pure fluid is much more complex. At 46% and 60% input water fractions, the water layer is seen to be spreading around the tube. For 40% input water fraction (water-in-oil dispersion) a region of high oil concentration also appears half way along the circumference from the bottom as shown in *Fig. 4* (water fraction 60%) and (water fraction 46%). This is consistent with the behavior seen in stratifying annular gas-liquid flows (Badie, 2000). Water is constantly separating from the core mixture and forms a downstream-draining layer near the wall which thickens near the bottom of the tube. Re-entrainment of the draining layer may occur near the wall which thickens near the bottom of the tube. Re-entrainment of the draining layer may then occur preferentially from this layer, as well as in the region near the bottom of the tube. The distributions seen in *Fig. 4* (water fraction

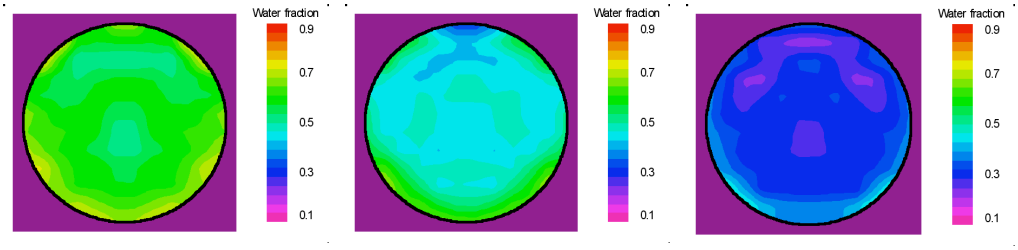

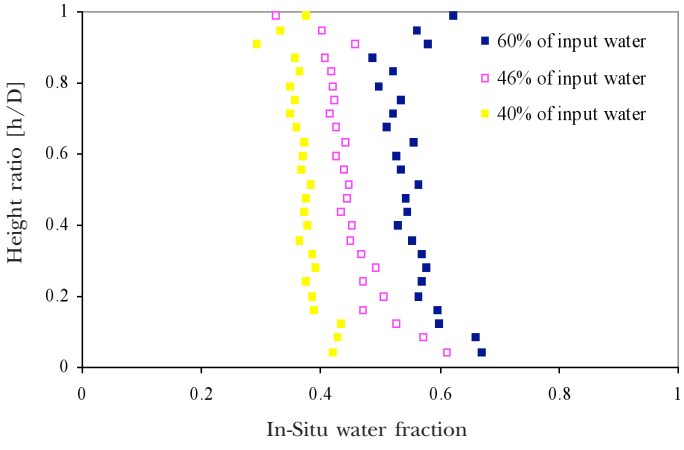

Fig. 4: Cross-sectional phase distributions (obtained by the gamma tomographic method) and vertical water fraction distributions (obtained from the vertical gamma scan) for a velocity of 2.76 m/s and at a position 7.72 m from inlet

40%) indicate that there is a tendency for the phases to mix as they pass along the channel.

Local Volume Fractions Results with Previous Studies

Measurements of the vertical distributions of chordal mean void fraction were made by Soleimani (1999, 2000) for conditions similar to those used in current experiments. Comparisons between the results of this study and that reported by Soleimani are shown in *Figs. 5* and *6*. For the highest velocity (2.76 m/s here and 3.0 m/s for the data of Soleimani), there is reasonable qualitative agreement between the two data sets. Soleimani (1999, 2000) found that there is a transition of phases and therefore at 46% of input water as in *Fig. 5*, there is a higher oil concentration at 0.58, height ratio. The current data shows greater phase separation with lower water concentration at the top of the pipe and higher at the bottom. This is probably accounted for by the fact that a static mixer immediately downstream of the inlet was used in Soleimani's study resulting in good agreement where the phases distributed well across tube area. This may explain the mixing instability and internal forces with higher input velocity that appear in the fluid system.

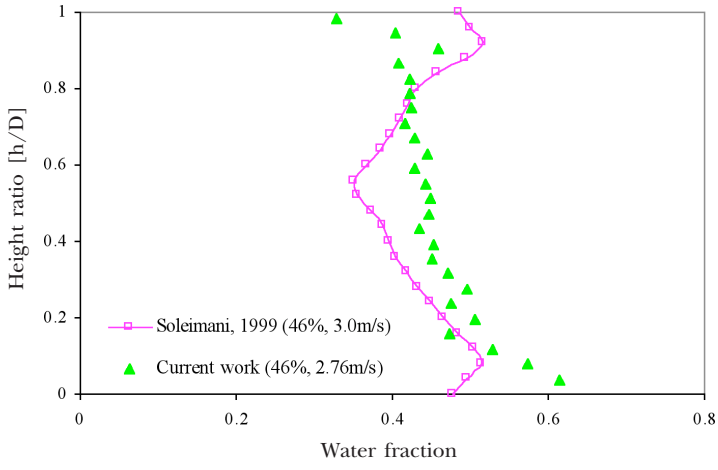

Fig. 5: Comparison of present data for vertical distribution of water phase fraction across the cross section for an input water fraction of 46% and at 7.72 m from the inlet with that of Soleimani (1999)

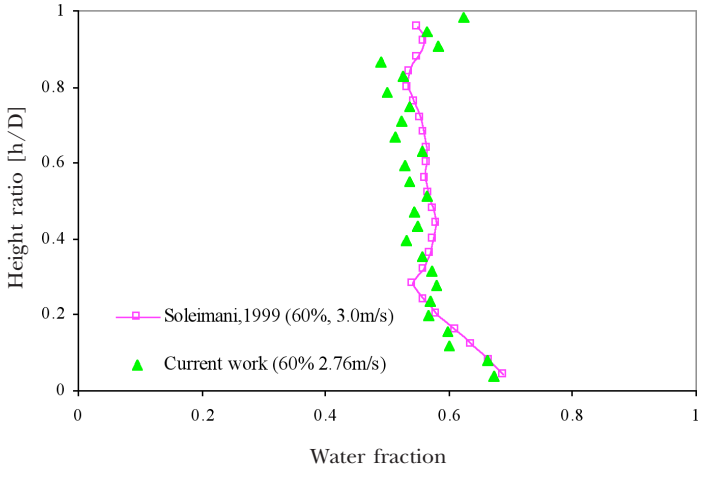

Fig. 6: Comparison of present data for vertical distribution of water phase fraction across the cross section for an input water fraction of 60% and at 7.72 m from the inlet with that of Soleimani (1999)

CONCLUSIONS

The experimental results reported here serve mainly to illustrate the complexity of the processes in liquid-liquid flows. If flow pattern is regarded as a characteristic type of phase distribution then it has been demonstrated that this depends not only on phase flow rates but also on the axial position. Pressure gradient (not reported here) passes through a maximum pressure point with distance before becoming relatively independent of distance towards the end of the pipe. This may reflect energy losses associated with intense mixing near the inlet. At high enough mixture velocities, the phases ultimately became mixed (dispersion of water-in-oil or oil-in-water).

The results for the vertical distributions of chordal mean volume fraction are in reasonable qualitative agreement with those obtained by Soleimani (1999, 2000). The key results are shown in *Fig. 4* and show the tendency of the phase to mix and approach uniform distribution as the flow proceeds along the channel. In general, the tomography results illustrate the great complexity of liquid-liquid dispersed flows, reflecting the many competing processes (turbulence, gravitational separation, droplet break-up and coalescence) which are occurring in the channel.

REFERENCES

Angeli, P. (1996). Liquid-liquid in horizontal pipes (Ph.D thesis, Imperial College, Imperial College of Science, Technology & Medicine, London, England, 1996).

Angeli, P. and Hewitt, G.F. (2000). Flow structure in horizontal oil-water flow. *International Journal Multiphase Flow, 26,* 1117-1140.

Arirachakaran, S., Oglesby, K.D., Malinowsky, M.S., Shoham, O. and Brill, J.P. (1989). An analysis of oil/water flow phenomena in horizontal pipes. SPE paper 18836. In *SPE Prod. Operating Symposium*, March 13-14 (p. 155-167). Oklahoma.

Badie, S. (2000). Horizontal stratifying/annular gas-liquid flow (Ph.D thesis, Imperial College of Science, Technology & Medicine, London, England, 2000).

Charles, M.E, Govier, G.W. and Hodgson, G.W. (1961). The horizontal pipeline flow of equal density oil-water mixture. *Can. J. Chem. Eng., 39,* 27-36.

Hu, B. and Stewart, C. (2002). XrayCT 1.1 calculation principle and user's manual. Three Plex Project, MPS/188. Department of Chemical Engineering and Chemical Technology, Imperial College of Science, Technology & Medicine, London, England.

Rashmi, W., Siti Aslina, H. and Thomas, C.Y.S. (2006). Analysing liquid holdup for dispersed flow using CFD. In *11th Asian Pacific Confederation of Chemical Engineering (APCChE Congress 2006)*, 28-30 August. Kuala Lumpur.

Shi, H., Cai, J.Y. and Jepson, W.P. (1999). Oil-water distributions in large diameter horizontal pipelines. Multiphase flow and heat transfer. *Proc. of the Fourth International Symposium* (p. 73-80). Xi'an China.

Siti Aslina, H. (2004). Experimental and computational studies of liquid-liquid dispersed flows (PhD Thesis, Imperial College of Science, Technology & Medicine, London, England, 2004).

Siti Aslina, H., Siti Mazlina, M.K. and Wan Hassan, M.J. (2006). *In-situ* phase fractions for oil and water occupied in pipe channel. *International Journal of Engineering and Technology, 3(2)*, 248-256.

Siti Aslina, H. and Siti Mazlina, M.K. (2006). *In-situ* phase fractions for oil and water occupied in pipe channel. *Seminar on Engineering and Technology (SET 2006)*, 4-5 September. Kuala Lumpur.

Siti Aslina, H. (2006a). Local volume fraction on liquid-liquid dispersion. *The Eleventh Asian Congress of Fluid Mechanics*, 22-25 May. Kuala Lumpur.

Siti Aslina, H. (2006b). Experimental investigation of two-phase local volume fraction using gamma densitometer system technique on liquid-liquid dispersion. *11th Asian Pacific Confederation of Chemical Engineering (APCChE Congress 2006)*, 28-30 August. Kuala Lumpur.

Siti Aslina, H., Siti Mazlina, M.K. and Wan Hassan, M.J. (2007). Influence of oil and water holdup on mixture velocity in horizontal flows. *Journal of Chemical Engineering of Japan* (In Press).

SOLEIMANI, A. (1999). Phase distribution and associated phenomena in oil-water flows in horizontal tubes. (Ph.D Thesis, Imperial College of Science, Technology & Medicine, London, England, 1999).

SOLEIMANI, A. (2000). Spatial distribution of oil and water in horizontal pipe flow. *SPE Journal, 4*(5), 394-401).

ISSN: 0128-7680
Pertanika J. Sci. & Technol. **16 (1)**: 41 - 48 (2008)

Growth of Gold Particles on Glassy Carbon from a Thiosulphate-Sulphite Aged Electrolyte

S. Sobri*[1], S. Roy[2], E. Kalman[3], P. Nagyp[3] and M. Lakatos[4]

[1]Department of Chemical and Environmental Engineering, Faculty of Engineering, Universiti Putra Malaysia, 43400 UPM, Serdang, Selangor, Malaysia

[2]School of Chemical Engineering and Advanced Materials, Merz Court, University of Newcastle upon Tyne, NE1 7RU, UK

[3]Chemical Research Centre of the Hungarian Academy of Sciences (CHEMRES), H-1025 Budapest, Pusztaszeri ut 59-67, Hungary

[4]Institute for Materials Science and Technology of the Bay Zolt·n Foundation (BAYATI), H-1116 Budapest, Fehervari ut. 130, Hungary

**E-mail: eeza@eng.upm.edu.my*

ABSTRACT

Interest has grown in developing non-toxic electrolytes for gold electrodeposition to replace the conventional cyanide-based bath for long term sustainability of gold electroplating. A solution containing thiosulphate and sulphite has been developed specially for microelectronics applications. However, at the end of the electrodeposition process, the spent electrolyte can contain a significant amount of gold in solution. This study has been initiated to investigate the feasibility of gold recovery from a spent thiosulphate-sulphite electrolyte. This paper presents the microscopy observations of crystal growth of gold on glassy carbon as a function of deposition potentials and time. It was found that the initial deposition of gold at less cathodic potential corresponds to an electrochemical diffusion control of gold discharge from which spherical nuclei are obtained. When a certain induction time for spherical growth has passed, the initial growing nuclei become unstable and the thin gold deposit begins to develop tips which eventually grow larger and produce dendrites. The dendritic growth is controlled by surface diffusion limitations of gold nuclei.

Keywords: Gold electrodeposition, thiosulphate-sulphite, glassy carbon

INTRODUCTION

The emerging use of gold-based connectors in microtechnology has initiated the need to search for stable and non-toxic electrolytes for gold electrodeposition because the classical cyanide-based bath has been found to be incompatible with positive photoresists used during the process (Osaka *et al.,* 2001; Liew *et al.*, 2003, Green *et al.*, 2003; Liew, 2002; Watanabe *et al.*, 1999). One electrolyte being examined is a solution containing thiosulphate and sulphite, which was initially proposed by Osaka *et al.* (2001). This electrolyte was reported to be highly stable, requires no stabilizing additives and contained phosphoric acid as buffering agent.

Recently, a mixed thiosulphate-sulphite ligand bath has been formulated by Newcastle University with aurochloric acid, Au (III) Cl^{-4}, as the starting material (Liew *et al.*, 2003). Subsequent reduction and complexation by thiosulphate led to the formation of

* Corresponding Author

$Au(S_2O_3)_2^{3-}$. This electrolyte was found to be stable at near neutral pH and showed good compatibility with positive photoresists (Green *et al.*, 2003). The mixed ligand bath proved to be satisfactory for an industrial process and is used as electrolyte to electrodeposit gold for microelectronics applications.

Since the discharge of gold with effluent is a major economic and environmental concern, this study was carried out to investigate whether gold can be recovered from aged thiosulphate-sulphite electrolyte and to determine the microstructure of the deposits/particles obtained. Currently, there is no reliable information concerning gold recovery from thiosulphate-sulphite plating baths. The recovery process is expected to be of value if the recovered gold can be tailored for suitable applications, for example in catalysis, sensors, electronics and others (Hutchings, 1996; Corti *et al.*, 2002; Goodman, 2002).

In a previous work to investigate the nucleation mechanism of gold (Sobri and Roy, 2005), glassy carbon and graphite had been used as electrodes. The two forms of carbon were chosen due to the differences in their structures. It was found that at the early stages of the reduction process, the deposition of gold on glassy carbon exhibits an instantaneous nucleation of non-overlapping particles. At longer times, the particles begin to overlap and the deposition follows a classic progressive nucleation phenomenon. Deposition of gold on graphite, however, does not follow the classical nucleation phenomenon.

MATERIALS AND METHODS

Glassy carbon (Goodfellow Cambridge Ltd, UK) was used as the electrode. The substrate was 99.5% pure with 1 mm thickness. The electrode was cut into 1 cm^2 and attached to a copper wire using silver loaded epoxy adhesive and hardener (RS Components, UK). In order to avoid metal deposition on copper wire and silver paste used for contact, the metallic area was covered with multi-purpose silicone sealant (Dow Corning Ltd, UK).

Gold was deposited from the thiosulphate-sulphite aged electrolyte. Details on electrolyte preparation are reported in Liew *et al.* (2003). The bath mainly consist of $Au(S_2O_3)_2^{3-}$ as well as trace amounts of Na^+ ions. The concentration of the predominant species, Au+, was 8.981 g/L. The electrochemical experiments were performed in a three-electrode H-cell. The cell was separated into anode and cathode compartments by a glass frit. 45 ± 1 ml volume of aged gold thiosulphate-sulphite plating solution was equally divided in each compartment.

A potentiostat (Sycopel Scientific) controlled by a computer was used to carry out the experiments. The working electrode was mounted in the cell and held in place by the use of a metal clip. 2.0 × 2.5 cm^2 platinised-titanium sheet was used as the auxiliary electrode. All potential measurements were made with respect to a saturated mercurous sulphate electrode (SMSE).

Current-time transients were accomplished by applying the potentials from the rest potential to the deposition potentials of lower than –0.7 V for 60 seconds. Prior to each chronoamperometry measurements, the carbon surface was gently polished using wet silicon carbide paper grit 4000 (Struers Ltd., UK) and then washed thoroughly with distilled water before being transferred to the experimental cell.

In order to study the growth of gold with time, a set of current-time transients were accomplished by applying the potentials from the rest potential to the deposition potentials of –0.925 V and –1.20 V, for durations of 1, 10, 100, 500 and 1000 seconds. The two deposition potentials were chosen as it shows transition from growth of single particulates to aggregates. Atomic Force Microscopy (AFM) analysis for gold deposits was

recorded using a Nanoscope Dimension™ 3100 with operational frequency of 2 Hz. The AFM was operated in contact mode, scanning at 25 mm imaging resolutions. Scanning Electron Microscopy (SEM) analysis was also performed using a Hitachi model SE570 SEM at an acceleration voltage of 20 kV.

RESULTS AND DISCUSSION

Fig.1 contains representative scanning electron micrographs of gold nanoparticles on glassy carbon after 60 seconds of potential application. These images illustrate the influence of overpotentials on crystal distribution and size. As shown in the images, deposition at –0.775 V yields a smaller number of nuclei. Notably, the nuclei are of nearly the same size, the average size being 680 ±10 nm. At intermediate overpotential, two distinct nuclei sizes are visible, with average particle sizes of 650 nm and 160 nm. As the applied potential is lowered, homogeneous nanocrystals ranging in diameter from 80 to 100 nm are obtained. A manual image analysis showed that the range of crystal diameter had a relative deviation of less than 1% for potentials below –1.0 V.

Fig. 2 contains representative atomic force micrographs of gold nanoparticles on glassy carbon at 25 mm resolution. These images illustrate the distribution of gold nuclei at an overpotential of –0.925 V after 1s, 10s, 100s, 500s and 1000s deposition

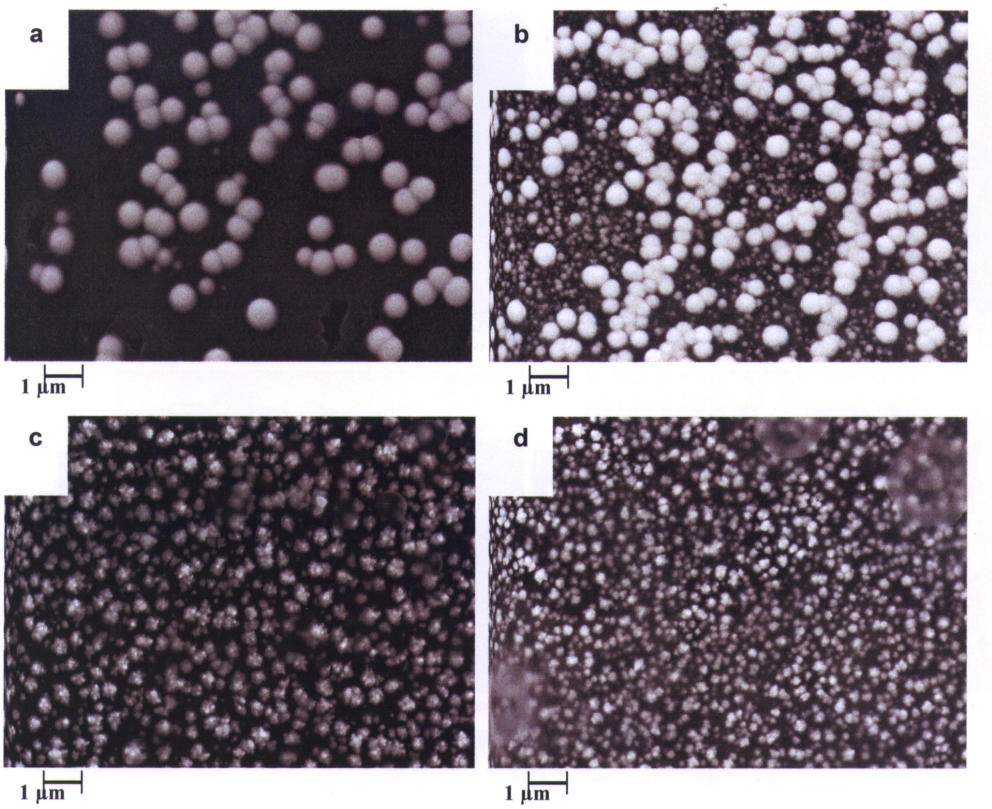

Fig. 1: SEM images of gold on glassy carbon as a function of deposition overpotentials: (a) –0.775 (b) –0.925 (c) –1.075 (d) –1.20V

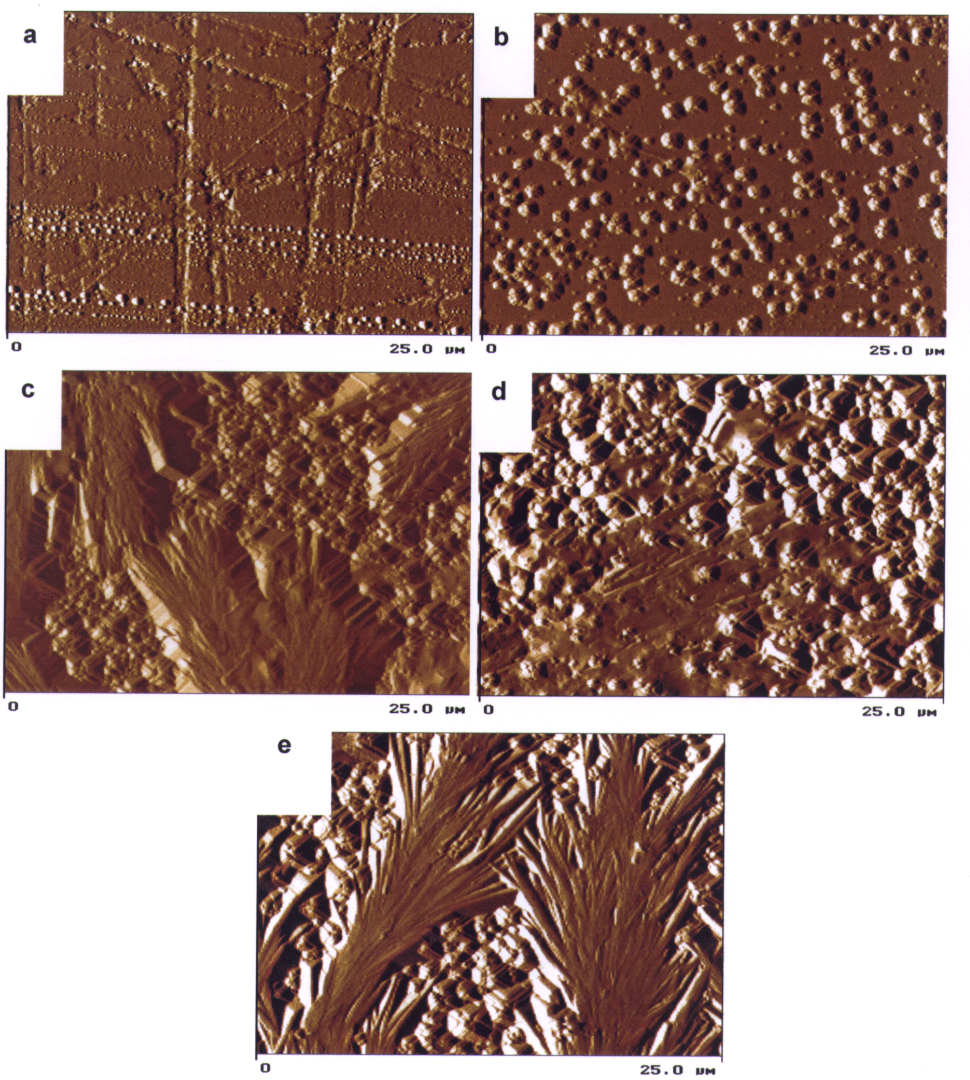

Fig. 2: AFM images of gold on glassy carbon at –0.925V at (a) 1s (b) 10s (c) 100s (d) 500s (e) 1000s

time. As shown in the images, deposition at 1s yields a number of large nuclei. During this stage, each nuclei grows independently of each other. These gold nuclei deviate little in size, with average size of 120 nm. Between 1s and 10s, a fraction of the gold nuclei begin to coalesce while some remain as single particle. The average size of gold aggregates is 550 nm.

Deposition at longer periods results in complete coverage of gold aggregates on the substrate surface. The particles are clustered into larger aggregates and measurement of the diameter of the particles or aggregates was not possible. The 3-D images in *Fig. 3* demonstrate the changes in surface feature from single particulates at 1s to smooth gold deposits at 1000s.

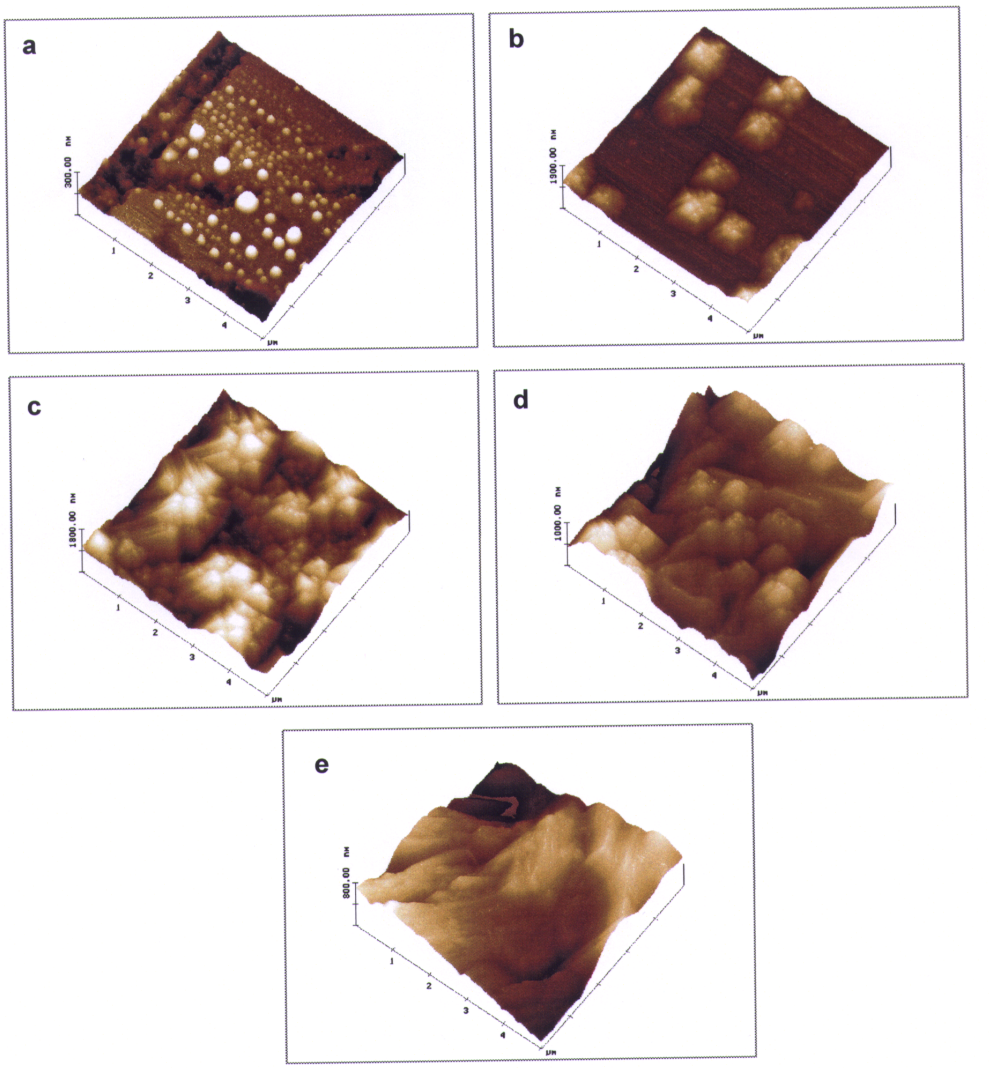

Fig. 3: 3–dimensional images of gold on glossy carbon at –0.925V at (a) 1s (b) 10s (c) 100s (d) 500s (e) 1000s

Fig. 4 represents the micrographs of gold nanoparticles on glassy carbon deposited at an overpotential of –1.20 V and 25 mm imaging resolution. The images presented indicate that the growth of gold nuclei exhibits a needle-like structure which occurs even before the first second had elapsed.

In order to determine the density of gold nuclei as a function of overpotential, 15 μm^2 areas were randomly chosen from the micrographs of the substrate surface with each of the area being $1\mu m^2$. The values are listed in Table 1. The density of nuclei increased with increasing overpotential for gold reduction. These nuclei density values are an order of magnitude 10^1–10^2 smaller compared to those reported for gold deposition from chlorides (Schmidt *et al.*, 1997), which could be due to the difficulty of reduction from sulphite based electrolytes.

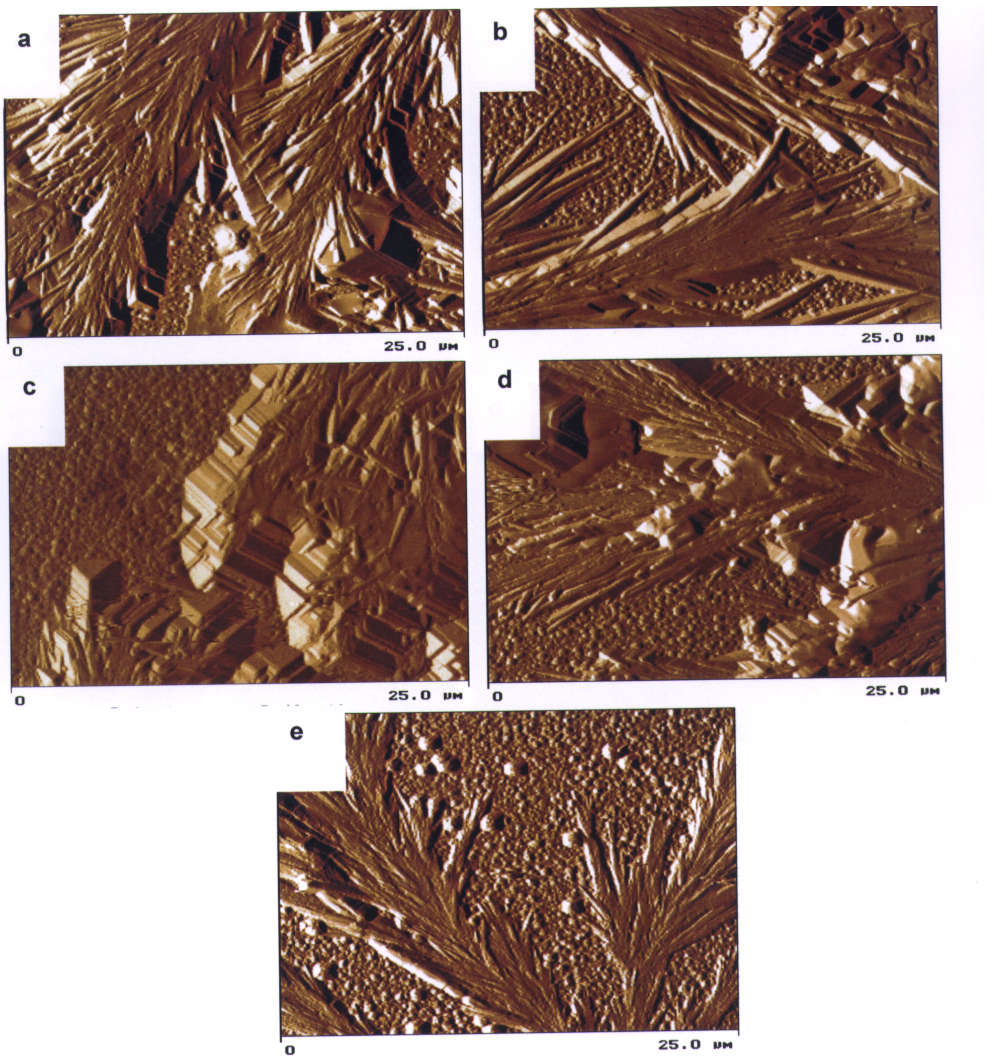

Fig. 4: AFM images of gold on glassy carbon at –1.20V at (a) 1s (b) 10s (c) 100s (d) 500s (e) 1000s

TABLE 1
Nuclei density of gold glassy carbon as a function overpotential

η(V)	Average particle density calculated from SEM (10^{-8}/cm^{-2})
–0.775	4
–0.925	8
–1.075	13
–1.200	19

The microscopy images at more negative overpotentials indicate that the growth of gold nuclei exhibits a needle-like structure. This characteristic was affirmed by the observed microscopy images at 200 magnifications, as shown in *Fig. 5*. Each 'branch' is formed from a nucleus or centre of crystallisation, which proceeds to send out radial arms. From these primary arms, secondary and tertiary arms begin to sprout and this is repeated until a surface pattern, known as dendrites, is formed on the surface. These gold dendrites develop by the addition of nuclei onto its branches.

It can also be seen that the dendrites arms grow outward and thickened as the deposition time increased. They continue to grow until its outer arms are in contact with neighbouring dendrites, in which this contact acts as a boundary of the grain. Further growth results in thickening of the existing dendrites arms, as can be seen from *Fig. 5*. Images recorded both by AFM and SEM, revealed that the spaces between the dendrites arms are also ultimately filled with particles.

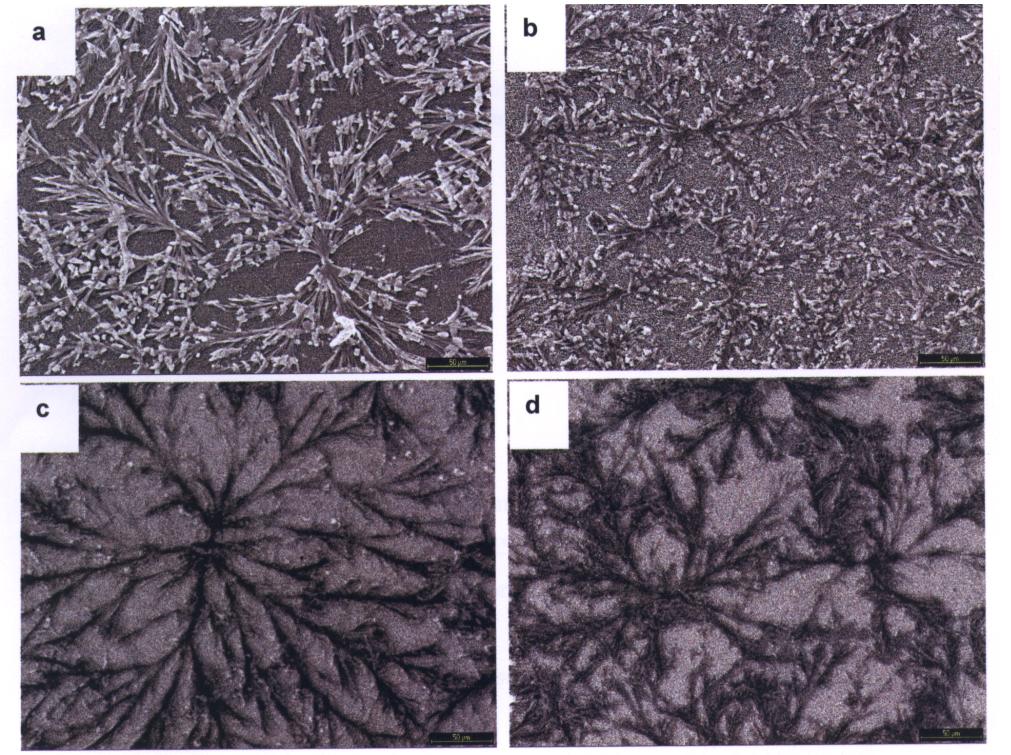

Fig. 5: SEM images of gold on glassy carbon at –1.20V at (a) 10s (b) 100s (c) 500s (d) 1000s

CONCLUSIONS

The electrodeposition of gold was studied from gold thiosulphate-sulphite aged electrolyte. Electrochemistry and microscopy analysis were applied to characterize Au^{+} crystals deposited on the carbon substrates. Microscopy observations demonstrated that the particle size and density can be controlled by varying the deposition potentials and time.

Deposition at less cathodic overpotentials yields a smaller number of large particles. As the applied potential is lowered, homogenenous Au crystals ranging in diameter from 80-100 nm are obtained. The particle density increases with overpotential, signifying the increase in number of nucleation sites. It is also evident that single crystals can be obtained shortly after applying a potential whereas at longer times the particle tend to coalesce and form larger aggregates with diameters ranging from 100 to 300 nm. AFM images also show that the growth of gold nuclei at more cathodic overpotential exhibits a needle-like structure and the substrate is ultimately filled with gold aggregates.

ACKNOWLEDGEMENTS

S. Sobri acknowledges a Short Term Scientific Mission (STSM) grant from COST D19-00935. The work was carried out in a facility funded by JIF-4NESCEQ grant. Grant Staines, D. Arranyi and K. Papp helped with SEM and AFM measurements.

REFERENCES

Corti, C.W., Holliday, R.J. and Thompson, D.T. (2002). Developing new industrial applications for gold: Gold nanotechnology. *Gold Bull. (Geneva), 35*(4), 111.

Goodman, P. (2002). Current and future uses of gold in electronics. *Gold Bull. (Geneva), 35*(1), 21.

Green, T.A., Liew, M.J. and Roy, S. (2003). Electrodeposition of gold from a thiosulfate-sulfite bath for microelectronic applications. *J. Electrochem. Soc., 150,* C104.

Hutchings, G.J. (1996). Catalysis: A golden future. *Gold Bull. (Geneva), 29*(4), 123.

Liew, M.J. (2002, July). Title of thesis. (PhD Thesis, University of Newcastle upon Tyne, UK, 2002).

Liew, M.J., Roy, S. and Scott, K. (2003). Development of a non-toxic electrolyte for soft gold electrodeposition: An overview of work at University of Newcastle upon Tyne. *Green Chem., 5,* 376.

Osaka, T., Kato, M., Sato, J., Yoshizawa, K., Homma, T., Okinaka, Y. and Yushioka, O. (2001). Mechanism of sulfur inclusion in soft gold electrodeposited from the thiosulfate-sulfite bath. *J. Electrochem. Soc., 148,* C659.

Schmidt, U., Donten, M. and Osteryoung, J.G. (1997). Gold electrocrystallization on carbon and highly oriented pyrolytic graphite from concentrated solutions of LiCl. *J. Electrochem. Soc., 144,* 2013.

Sobri, S. and Roy, S. (2005). Gold electrocrystallization from a spent thiosulfate-sulfite electrolyte. *J. Electrochem. Soc., 152,* C593.

Watanabe, H., Hayashi, S. and Honma, H. (1999). Microbump formation by noncyanide gold electroplating. *J. Electrochem. Soc., 146,* 574.

ISSN: 0128-7680
Pertanika J. Sci. & Technol. **16 (1)**: 49 - 59 (2008)

Development of Gluten Extensibility Measurement Using Tensile Test

D. N. Abang Zaidel[1], N. L. Chin[1*], R. Abd. Rahman[2] and R. Karim[2]
[1]Department of Process and Food Engineering, Faculty of Engineering, Universiti Putra Malaysia, 43400 UPM, Serdang, Selangor, Malaysia
[2]Department of Food Technology, Faculty of Food Science and Technology, Universiti Putra Malaysia, 43400 UPM, Serdang, Selangor, Malaysia
**E-mail: chinnl@eng.upm.edu.my*

ABSTRACT

Gluten is a viscoelastic mass obtained from washing wheat flour dough. A simple set-up of tensile test was built to determine gluten extensibility, which is one of the most common measurements used in determining the quality of gluten. The main problem encountered in performing gluten and dough extensibility test is holding of the sample so that it breaks within the sample and not at the jaws that hold the sample. In this research, gluten strips of about 5.0 ± 0.5 g were clamped to the set-up which was attached to Instron 5566 series and then extended at the centre by a hook at crosshead speed of 300 mm min^{-1}. Extensibility parameters such as original gluten length, gluten length at fracture, measured force, actual force acting on the gluten strips, strain, strain rate and stress were obtained using the formulas derived from the results of measurements. The performance of gluten extensibility between strong and weak flour dough were compared. The results of the study showed that gluten obtained from strong flour has greater extensibility compared to weak flour.

Keywords: Extensibility, gluten, tensile test

NOMENCLATURE

A_o	original cross-sectional area of gluten	(mm^2)
A_t	fiknal cross-sectional area of gluten	(mm^2)
d	distance (gap) between the two clips	(mm)
F_m	measured force	(N)
F_a	actual force	(N)
l_o	gluten original length	(mm)
l_t	gluten final length at fracture	(mm)
V_o	original volume of gluten	(mm^3)
V_t	final volume of gluten	(mm^3)
y_o	gluten original position	(mm)
y_t	final hook displacement at gluten fracture	(mm)
α	angle of deformation	(^{o})
ε_H	Hencky strain	(dimensionless)
$\dot{\varepsilon}$	strain rate	(S^{-1})
α	stress	(N mm^{-2})

* Corresponding Author

INTRODUCTION

A cohesive, viscoelastic dough is obtained when water is mixed with wheat flour. Gluten is a cross-link of protein network developed during mixing of flour-water dough. Water is responsible for hydrating the protein fibrils in wheat flour and start the interactions between the proteins cross links with the disulphide bonds (Faubion and Hoseney, 1989). At the early stage of mixing, gluten fibrils are formed as the water is in contact with flour particles. As the mixing proceeds, more protein becomes hydrated and the glutenins tend to align because of the shear and stretching forces imposed. At this stage, gluten networks are more developed by the cross-linking of protein with disulphide bonds. At optimum dough development, the interactions between the polymers cross-links are becoming stronger which leads to an increase in dough strength, maximum resistance to extension and restoring force after deformation (Letang *et al.*, 1999). When the dough is mixed longer past its optimum development, the cross-links begin to break due to the breaking of disulphide bonds. The glutenins become depolymerised and the dough is overmixed. The presence of smaller chains in the dough makes the dough stickier (Letang *et al.*, 1999).

By washing the dough under running water, the starch is removed and the remaining viscoelastic mass obtained is gluten. Nowadays, the uses of gluten in industry have been intensely applied in various food and non-food industries. Day *et al.* (2006) reported that due to the unique cohesive properties of gluten it has become a commercial material in food industry such as in bakery, breakfast cereals, noodles, sausages and also meat substitutes. Its application has been expanding to other sectors such as pet food, aquaculture feed, natural adhesives and also as biodegradable films.

Rheological properties of gluten are always being connected to the quality of its end product: textural attributes, shape and expansion (Amemiya and Menjivar, 1992; Tronsmo *et al.*, 2003; Anderssen *et al.*, 2004). The rheological properties of gluten and dough were studied in terms of small and large deformation measurements (Amemiya and Menjivar, 1992; Janssen *et al.*, 1996; Uthayakumaran *et al.*, 2002; Tronsmo *et al.*, 2003). Small deformation is a fundamental rheological measurement that involves dynamic oscillation shear measurement. However, Tronsmo *et al.* (2003) found that at small strains, the result of small deformation could not be used as a correlation to the gluten quality as compared to large deformation measurements. Large deformation is more suitable to test the gluten quality used as food product since it can be related to its eating quality. A material experiences a large deformation when the stress exceeds the yield value. The commonly adapted method for large deformation test of dough and gluten is extension. Various instruments are available to perform the extension of dough and gluten such as the extensograph, texture analyser and also Instron. In this test, the sample is clamped at two ends and pulled or extended by a hook at the centre of the sample at a constant speed. Large deformation is applied to the sample until it is fractured and the material is unable to regain the original shape. In the past, many works were done regarding extensibility of gluten and dough using attachment on the Universal Testing Machine such as texture analyser and Instron (Kieffer *et al.*, 1998; Tronsmo *et al.*, 2003; Dunnewind *et al.*, 2004; Sliwinski *et al.*, 2004a; Sliwinski *et al.*, 2004b). Tronsmo *et al.* (2003) performed a uniaxial extension on dough and gluten using the Kieffer dough and gluten extensibility rig for the TA.TX2i texture analyser to test the rheological properties. They used six different wheat flours to study the difference in the breadmaking performance and determined the maximum resistance to extension and total extensibility.

The main problem encountered in performing gluten and dough extensibility test is to hold the sample so that it breaks within the sample and not at the jaws that hold the sample. Thus this research focused on a new tensile test set-up which was built to measure the extensibility of gluten. This new set-up was attached to Instron (5566 series, Instron Corporation, USA). Gluten extensibility was determined by studying the rheological properties of gluten of two types of flour; Diamond N and SP-3.

MATERIALS AND METHODS

Sample Preparation

Two types of flour, Diamond N (12.33% protein) and SP-3 (8.81% protein), were used in this study and referred to as strong and weak flour, respectively. Dough was prepared by mixing 200 g of flour with water (63.4% for strong flour; 59.5% for weak flour) in a mixer (5K5SS, KitchenAid, Belgium) for 8 minutes. Treated drinking water was used to avoid any effect or reaction from other types of minerals on protein in the flour during flour-water mixing. The dough was left to stand in water for 1 hour at room temperature to rest (AACC. 1976). The rested dough was washed under running tap water at a flow rate of 2.5 to 2.8 ml s^{-1} to remove starch until gluten was obtained. At the end of the washing, 1 to 2 drops of water from the gluten was squeezed into a container containing clear water (AACC. 1976). Starch was absent in gluten if cloudiness does not appear. The gluten, dried between dry cloths, was shaped into a ball shape and pressed to a thickness of 10 mm (*Fig. 1*) with the palm. Then, a paper clip with 10 mm gap (*Fig. 2(a)*) was used to press onto the gluten to print 10 mm width strips (*Fig. 1*) as a guide for cutting using a paper cutter (*Fig. 2(b)*). Finally, the strips were cut to 70 mm length. The 10 mm × 10 mm × 70 mm gluten strips of approximately 5.5 ± 0.5 g were immersed in tap water at room temperature and left for 30 minutes to rest (Chen *et al.*, 1998; Chiang *et al.*, 2006).

Extensibility Set-up

The rested gluten strips were then clamped at two ends using plastic clips arranged at 40 mm distance nailed to a 15.2 cm × 21.6 cm wooden platform cut according to the size of the Instron base platform. The wood was held tightly to the Instron platform using a

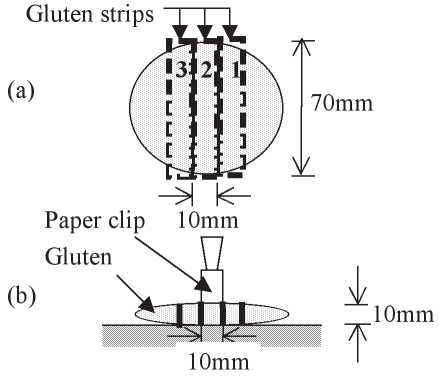

Fig. 1: Gluten imprint using paper clip (a) top (b) cross-sectional view

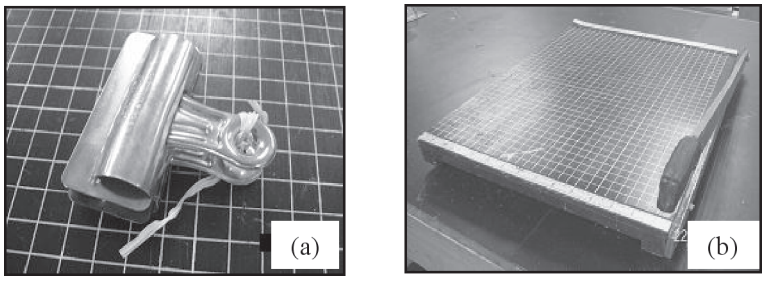

Fig 2: (a) Paper clip used to print 10 mm width of the gluten strips and (b) paper cutter used for gluten cutting

G-clamp. The tensile test started as the gluten was pulled up by the hook at a speed of 300 mm min^{-1} and stopped when the gluten fractured. The tensile test set-up (*Fig. 3*) consists of a hook bent into a V-shaped using a metal rod of 3.2 mm diameter and fitted to the Instron (5566 series, Instron Corporation, USA). The clip was set 10 mm above the wood plane for easy opening of the clamps when placing the gluten strips. *Fig. 4* shows the schematic diagram of a tensile test set-up at top and side views. To ensure that the gluten does not bend during placement on the set-up, the hook was levelled with the lower part of the plastic clips as shown in *Fig. 4(b)*.

The measured force (F_m) was exerted on the gluten at a vertical axis as shown in *Fig. 5*. Extensibility parameters: the original length of gluten (l_o), the final length of gluten at fracture (l_t) and actual force (F_a), and rheological parameters: strain (o_H), strain rate and stress (ε_H), were determined.

(i) Derivation of Extensibility Parameters

Equation [1] was used to determine the original length of gluten (l_o) before extension. *d* was 40 mm in this study. The final length of gluten at fracture (l_t) was calculated using equation [2]:

$$l_o = 2\sqrt{(d/2)^2 + (y_o)^2} \tag{1}$$

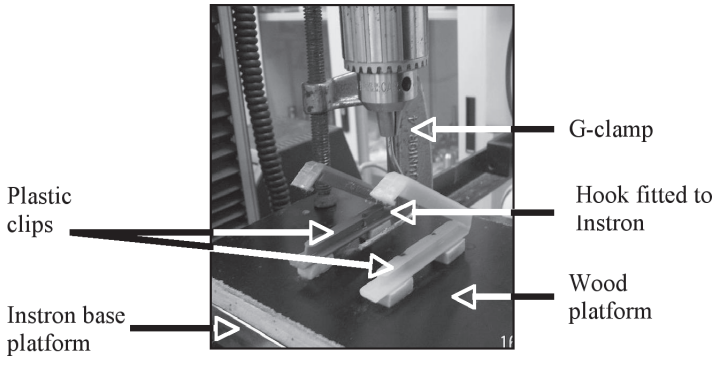

Fig. 3: Tensile test set-up for gluten extensibility on Instron (5566 series, Instron Corporation, USA)

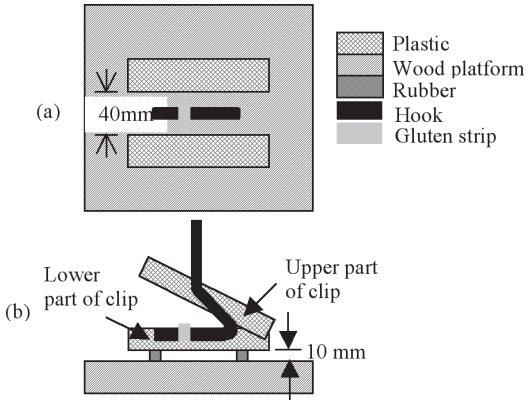

Fig. 4: Tensile test set-up diagram from(a) top and (b) side view

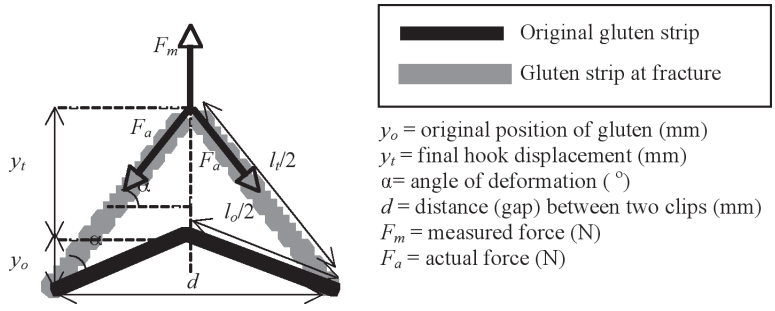

Fig. 5: Schematic diagram of forces acting on gluten and the length of gluten during tensile test [10]

$$l_t = 2\sqrt{(d/2)^2 + (y_o + y_t)^2} \tag{2}$$

Assuming that the hook passes exactly through the centre of the gap, the measured force (F_m) was divided equally over both stretched gluten at each side of the hook (Kieffer *et al.* 1998). Thus, the actual force (F_a) that acted upon the stretched gluten was determined using equation [4] while equation [3] shows the expression of the angle of deformation (α) in terms of the measured and actual force acting upon the gluten.

$$\sin\alpha = \frac{F_m/2}{F_a} = \frac{y_t + y_o}{l_t/2} \tag{3}$$

$$F_a = \frac{F_m l_t}{4(y_t + y_o)} \tag{4}$$

(ii) Derivation of Rheological Parameters

The extension parameters obtained earlier were used to determine the rheology parameters such as strain, strain rate and stress. The Hencky strain (ε_H) acting on gluten was calculated using equation [5] and the strain rate was calculated by a derivative of Hencky strain ($\dot{\varepsilon}$) with time as shown in equation [6]:

$$\varepsilon_H = \ln\left(\frac{\sqrt{(d/2)^2 + (y_o + y_t)^2}}{\sqrt{(d/2)^2 + (y_o)^2}}\right) \tag{5}$$

$$\dot{\varepsilon} = \frac{d\varepsilon_H}{dt} = \frac{dl}{l_t dt} = \frac{1}{l_t} \cdot \frac{2(y_t + y_o)}{\sqrt{9^2 + (y_t + y_o)^2}} \cdot \frac{dy_t}{dt} = \frac{4v(y_t + y_o)}{{l_t}^2} \tag{6}$$

where v is the speed of hook (mm min^{-1}). The final cross-sectional area of gluten strip can be calculated by assuming the volume of gluten was constant throughout the test (Muller *et al.*, 1961; Sliwinski *et al.*, 2004a) as shown in equation (7).

$$\begin{aligned} V_o &= V_t \\ A_o l_o &= A_t l_t \\ A_t &= \frac{A_o l_o}{l_t} \end{aligned} \tag{7}$$

where V_o is the original volume of gluten (mm^3), V_t is the final volume of gluten (mm^3), A_o is the original cross-sectional area of gluten (mm^2) and A_t is the final cross-sectional area of gluten (mm^2). From equation (8), the stress (σ) acting on the gluten was calculated by dividing the actual force (F_a) with the final cross-sectional area of gluten strip (A_t).

$$\sigma = \frac{F_a}{A_t} \tag{8}$$

Data Analysis

The experiments were conducted using three replications. The mean value and standard deviation of three replications were calculated using Microsoft Excel. Data from the force-extension graph obtained from Instron was used to calculate the extensibility parameters. Curves of strain-hook extension, strain rate-hook extension and stress-strain were obtained to study the performance of the tensile test set-up.

RESULTS AND DISCUSSION

Figs. 6(a) to *6(d)* illustrate the tensile test for gluten extensibility from the beginning until the fracture of gluten. The gluten strip bent slightly upward at the hook as it was clamped (*Fig. 6 (a)*). This explains the original hook position (y_o) in equation (1) which is to prevent bending of the gluten sample. Previous studies by Uthayakumaran *et al.* (2002) and Dunnewind *et al.* (2004) reported that precaution has to be taken to prevent sagging during clamping of the test sample. *Fig. 6(b)* shows the gluten being pulled upward as the hook was moving at a crosshead speed 300 mm min^{-1}. Studies on the effect of various speeds on the extension of dough and gluten piece have been done (Dunnewind *et al.*, 2004; Sliwinski *et al.*, 2004a; Sliwinski *et al.*, 2004b) and the results showed that the deformation at fracture increased with increasing speed. *Fig. 6(c)* shows that as the hook was displaced further upward the gluten strip became thinner at point 2 and 4 before it fractured (*Fig. 6(d)*) at its maximum extensibility. In this set-up, the gluten test piece did not fracture at the clamping area.

Fig. 7(a) shows the typical force-extension curve for gluten from strong and weak flour mixed for 8 minutes. For both flours, an increase of force was observed with increasing hook displacement and decreased after reaching a peak. A similar trend was reported for gluten and dough in uniaxial extension tests (Dunnewind *et al.*, 2004; Sliwinski *et al.*, 2004a; Sliwinski et al., 2004b). Generally these curves resemble the curves from extensograph measurements. From these curves, the force needed to extend the gluten increased during tensile deformation and reached a maximum before gluten ruptured and then decreased after rupture. It was observed that gluten from strong flour was more extensible than weak flour as indicated by the higher measured and actual force, hook displacement, final length at fracture, stress, strain and strain rate (Table 1).

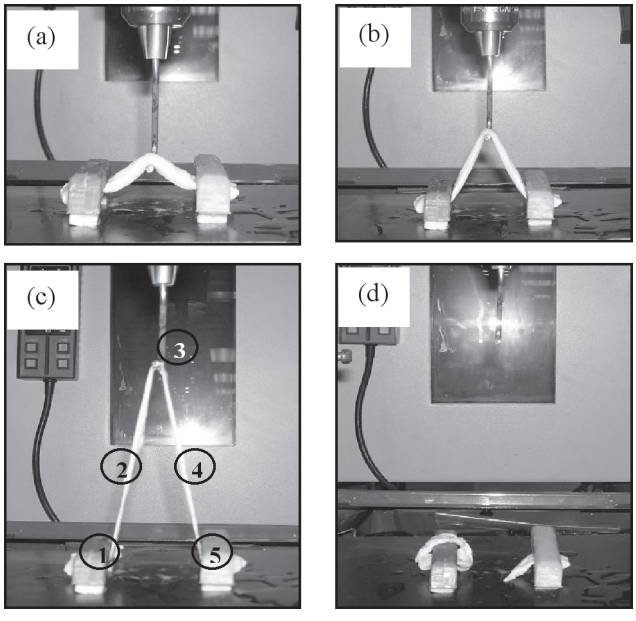

Fig. 6: Tensile test showing gluten extensibility at various stages: (a) gluten clamped at clips (b) gluten pulled upward by hook (c) gluten became thinner (d) gluten fractured

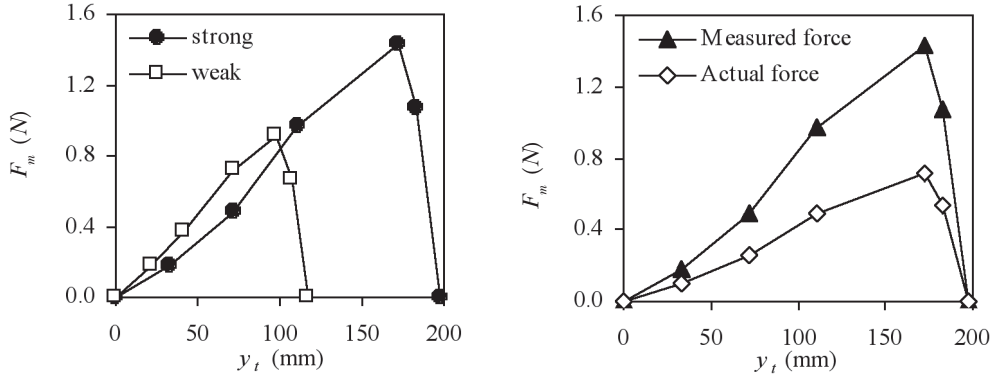

Fig. 7: (a) Measured force-hook displacement curve for gluten from strong and weak flour (b) Measured and actual force versus hook displacement for gluten from strong flour

Higher force and extensibility of strong flour gluten suggests that strong flour has stronger gluten network and the extensibility was influenced by the protein content of the flour (C'uric' *et al.*, 2001). *Fig. 7(b)* shows the curves of measured and actual force against hook extension for gluten from strong flour. It was found that the measured force was double the actual force acting on the gluten (Dunnewind *et al.*, 2004).

Figs. 8(a) and *(b)* show the strain and strain rate versus hook displacement curves for strong and weak flour mixed for 8 minutes. From these curves, strain increased and strain rate increased and reached a maximum then decreased as the hook displaced upward. These curves gave similar patterns as the extensograph and the Kieffer rig (Dunnewind *et al.*, 2004). Strain increased as the gluten extended upward and reached a maximum at gluten fracture. It was observed that strain rate for weak flour gluten was higher than for strong flour at the beginning of the extension. As the hook expanded more, the strain rate of both flours was slightly the same.

In *Fig. 9*, the stress-strain curves determined in the extension are shown for gluten from strong and weak flour mixed for 8 minutes. Both flours show an increase in stress with increasing strain and reached a peak at fracture of a sample. In the stress-strain

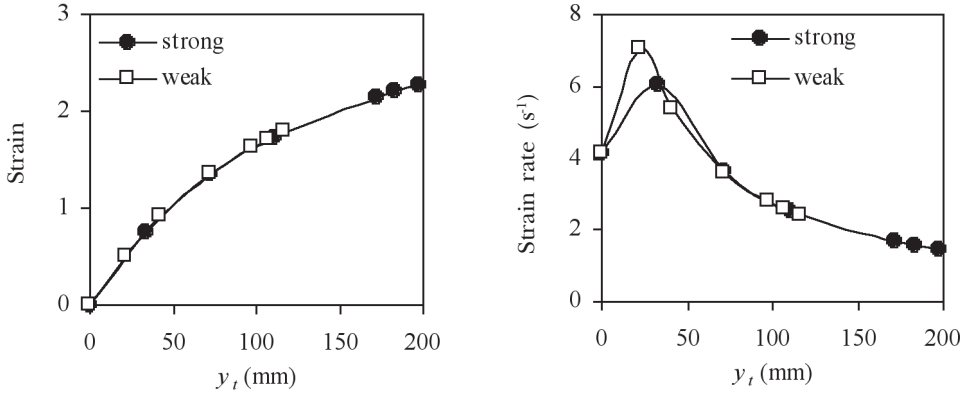

Fig. 8: Curves of (a) Hencky strain (b) Strain rate versus hook extension for gluten from strong and weak flour

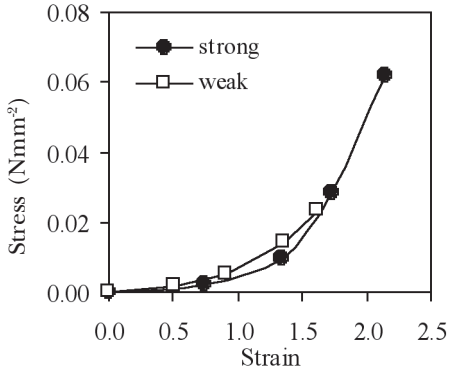

Fig. 9: Stress-strain curve for gluten from strong and weak flour. The point of fracture is indicated with an arrow

TABLE 1
Extensibility parameters for gluten of strong and weak flour mixed for 8 minutes

Flour	y_t(mm)	F_m(N)	l_t(mm)	F_a(N)	ε_H	$\dot{\varepsilon}$ (s^{-1})	σ(N mm^{-2})
Strong	0 ± 0.0	0 ± 0.00	41.8 ± 0.0	0 ± 0.00	0 ± 0.00	4.13 ± 0.00	0 ± 0.0000
	33.3 ± 0.0	0.18 ± 0.01	88.3 ± 0.0	0.10 ± 0.01	0.75 ± 0.00	6.06 ± 0.00	0.0021 ± 0.0001
	72.2 ± 5.6	0.49 ± 0.02	161.5 ± 10.8	0.25 ± 0.01	1.35 ± 0.06	3.62 ± 0.21	0.0098 ± 0.0009
	111.1 ± 11.1	0.97 ± 0.04	237.7 ± 21.9	0.49 ± 0.02	1.73 ± 0.09	2.53 ± 0.21	0.0282 ± 0.0033
*	**172.2 ± 5.6**	**1.43 ± 0.15**	**325.6 ± 11.0**	**0.72 ± 0.08**	**2.14 ± 0.03**	**1.66 ± 0.05**	**0.0618 ± 0.0060**
	183.3 ± 4.8	1.07 ± 0.24	369.7 ± 9.6	0.54 ± 0.12	2.21 ± 0.03	1.57 ± 0.04	0.0489 ± 0.0101
	197.2 ± 2.8	0 ± 0.00	397.4 ± 5.5	0 ± 0.00	2.28 ± 0.01	1.46 ± 0.02	0 ± 0.0000
Weak	0 ± 0.0	0 ± 0.00	41.8 ± 0.0	0 ± 0.00	0 ± 0.00	4.13 ± 0.00	0 ± 0.0000
	22.2 ± 2.8	0.18 ± 0.06	69.3 ± 4.4	0.11 ± 0.04	0.50 ± 0.07	7.04 ± 0.20	0.0018 ± 0.0007
	41.7 ± 0.0	0.37 ± 0.03	103.4 ± 0.0	0.20 ± 0.02	0.91 ± 0.00	5.35 ± 0.00	0.0049 ± 0.0004
	72.2 ± 2.8	0.72 ± 0.06	161.5 ± 5.4	0.37 ± 0.03	1.35 ± 0.03	3.61 ± 0.12	0.0143 ± 0.0010
*	**97.2 ± 2.8**	**0.91 ± 0.07**	**210.3 ± 5.5**	**0.46 ± 0.04**	**1.62 ± 0.03**	**2.80 ± 0.07**	**0.0234 ± 0.0023**
	106.9 ± 1.4	0.66 ± 0.06	229.4 ± 2.7	0.34 ± 0.03	1.70 ± 0.01	2.58 ± 0.03	0.0185 ± 0.0018
	116.7 ± 4.8	0 ± 0.00	248.6 ± 9.5	0 ± 0.00	1.78 ± 0.04	2.39 ± 0.09	0 ± 0.0000

Bold and * – values for gluten at fracture
± standard deviation of mean of three replications

curves, the point of fracture of the gluten sample is indicated. The fracture stress and strain determined for gluten mixed for 8 minutes is shown in Table 1. The gluten from weak flour showed lower value for fracture stress compared to the strong flour due to the low stress-level, low strain hardening and the small fracture strain. These results are in agreement with previous observations (Sliwinski *et al.*, 2004a; Sliwinski *et al.*, 2004b).

CONCLUSIONS

Determining the extensibility of gluten using the tensile test set-up was successful in terms of providing the extensibility measurements. The extensibility parameters of gluten from strong flour gave higher values than for weak flour in terms of the length at fracture, measured and actual force, strain and also stress.

ACKNOWLEDGEMENTS

The authors wish to thank the Malayan Flour Mill Sdn Bhd, Pasir Gudang, Johor Bahru for supplying the flour for this study.

REFERENCES

AACC. (1976). Method 38-10. Gluten – Hand washing method. In *Approved Methods of the American Association of Cereal Chemists* (Vol. 1, 7th ed.). Minnesota, USA: AACC, Inc.

Amemiya, J.I. and Menjivar, J.A. (1992). Comparison of small and large deformation measurements to characterize the rheology of wheat flour doughs. *Journal of Food Engineering, 16*, 91-108.

Anderssen, R.S., Bekes, F., Gras, P.W., Nikolov, A. and Wood, J.T. (2004). Wheat-flour dough extensibility as a discriminator for wheat varieties. *Journal of Cereal Science, 39*(2), 195-203.

Chen, C.S., Chen, J.J., Wu, T.P. and Chang, C.Y. (1998). Optimising the frying temperature of gluten balls using response surface methodology. *Journal of the Science of Food and Agriculture, 77*, 64-70.

Chiang, S.H., Chen, C.S. and Chang, C.Y. (2006). Effect of wheat flour protein compositions on the quality of deep-fried gluten balls. *Journal of Food Chemistry, 97*(4), 666-673.

Ćurić, D., Karlović, D., Tušak, D., Petrović, B. and Dugum, J. (2001). Gluten as a standard of wheat flour quality. *Journal of Food Technology Biotechnology, 39*(4), 353-361.

Day, L., Augustin, M.A., Batey, I.L. and Wrigley, C.W. (2006). Wheat-gluten uses and industry needs. *Trends in Food Science & Technology Journal, 17*(2), 82-90.

Dunnewind, B., Sliwinski, E.L., Grolle, K. and Van Vliet, T. (2004). The Kieffer dough and gluten extensibility rig – an experimental evaluation. *Journal of Texture Studies, 34*, 537-560.

Faubion, J.M. and Hoseney, R.C. (1989). The viscoelastic properties of wheat flour doughs. In H.A. Faridi and J.M. Faubion (Eds.), *Dough Rheology and Baked Product Texture* (p. 29-66). New York: Van Nostrand Reinhold.

Janssen, A.M., van Vliet, T. and Vereijken, J.M. (1996). Rheological behaviour of wheat glutens at small and large deformations. Comparison of two glutens differing in bread making potential. *Journal of Cereal Science, 23*, 19-31.

Kieffer, R., Wieser, H., Henderson, M.H. and Graveland, A. (1998). Correlations of the breadmaking performance of wheat flour with rheological measurements on a micro-scale. *Journal of Cereal Science, 27*, 53-60.

LETANG, C., PIAU, M. and VERDIE, C. (1999). Characterization of wheat flour-water doughs. Part I: Rheometry and microstructure. *Journal of Food Engineering, 41*, 121-132.

MULLER, H.G., WILLIAMS, M.V., RUSSELL EGGITT, P.W. and COPPOCK, J.B.M. (1961). Fundamental studies on dough with the Brabender Extensograph. I – Determination of stress-strain curves. *Journal of Science & Food Agriculture, 12*, 513-523.

SLIWINSKI, E.L., KOLSTER, P., PRINS, A. and VAN VLIET, T. (2004a). On the relationship between gluten protein composition of wheat flours and large-deformation properties of their doughs. *Journal of Cereal Science, 39*, 247-264.

SLIWINSKI, E.L., KOLSTER, P. and VAN VLIET, T. (2004b). Large-deformation properties of wheat flour dough in uni- and biaxial extension. Part I. Flour dough. *Rheologica Acta, 43*, 306-320.

TRONSMO, K.M., MAGNUS, E.M., BAARDSETH, P. and SCHOFIELD, J.D. (2003). Comparison of small and large deformation rheological properties of wheat dough and gluten. *Cereal Chemistry, 80*(5), 587-595.

UTHAYAKUMARAN, S., NEWBERRY, M., PHAN-THIEN, N. and TANNER, R. (2002). Small and large strain rheology of wheat gluten. *Rheologica Acta, 41*, 162-172.

ISSN: 0128-7680
Pertanika J. Sci. & Technol. **16 (1)**: 61 - 71 (2008)

Studies of N,N-Dibutyltrimethylenediamine and N, N, N'Triethylenediamine for CO_2 Absorption and Desorption

Ammar Mohd Akhir*[1], Yudy Halim Tan[2] and David W. Agar[2]
[1]Department of Process and Food Engineering, Faculty of Engineering, Universiti Putra Malaysia, 43400 UPM, Serdang, Selangor, Malaysia
[2]Chair of Technical Chemistry B, Faculty of Bio - and Chemical Engineering, University Dortmund, 44221 Dortmund, Germany
**E-mail: ammar@eng.upm.edu.my*

ABSTRACT

CO_2 gas emissions and their increasing role in global warming have become an issue of much concern. Chemical absorption is preferred for lowering the partial pressure of CO_2. The potential of completely new amines N,N-Dibutyltrimethylenediamine and N,N,N'-Triethylenediamine which are both categorized and widely known as diamine (amine that may contains two active nitrogen atoms without going through any conventional mixing process) were investigated for CO_2 absorption and desorption processes. In order to investigate the potential of these diamines for CO_2 absorption and desorption, experiments and analysis were conducted to determine the absorption rate, absorption capacity, desorption rate and desorption effectivity of CO_2.

Keywords: CO_2, absorption, desorption, diamine, N,N Dibutyltrimethylenediamine, N,N,N'-Triethylenediamine

INTRODUCTION

In recent times, the emission of greenhouse gases and their increasing role in global warming has become a big concern. Amongst the known greenhouse gases, carbon dioxide (CO_2) resulting from combustion of fossil fuels activities such as electricity generation and fuel usage in the transportation sector accounts for around 46% of total CO_2 emissions in Europe alone. CO_2 emissions in European Union (EU) countries are projected to reach 3.8 $GtCO_2$ in 2010 and 4.1 $GtCO_2$ in 2020. These projected growth shows an increment of 1.07% per year between 1995 and 2010 and 0.64% per year between 2010 and 2020 (Viguier, n.d.).

Consequently, this on-going issue with CO_2 emissions has spurred researchers around the world to develop new and effective CO_2 capture technologies that can be implemented strategically in sectors which contribute greatly towards CO_2 emissions.

Removal of CO_2 from fuel gas and hydrogen (H_2) stream has been practiced in many industrial processes such as ammonia manufacture, H_2 production, coal gasification and in oil and gas purification. Aqueous amine solutions are the usual solvents for CO_2 removal. One of the most popular types of aqueous amine solutions is mixed amines systems or 'activated amine solution' which contains small amounts of a primary or secondary amine that acts as an activator (high absorption rate) and a tertiary amine (high absorption capacity). Typical mixed amines systems that are investigated include among others MEA-MDEA, DEA-MDEA and MEA-Piperazine.

MATERIALS AND METHODS

Diamine is an amine which already contains a primary or secondary amine and a tertiary amine in one solution and the supplied diamine solution can be used directly without undergoing conventional or the usual mixing process such as in MEA-MDEA or DEA-MDEA systems. Details about diamines used in this study are shown in Table 1.

TABLE 1
Diamines used

Diamine	Description
1) N,N-Dibutyltrimethylenediamine (Diamine 1) • CAS No.: 102-83-0 • Supplier: Merck, Hohenbrunn, Germany • Purity: ≥ 99%	Possess primary and a tertiary amine properties
2) N,N,N'-Triethylenediamine (Diamine 2) • CAS No.: 105-04-4 • Supplier: Sigma-Aldrich, Steinheim, Germany • Purity: 98%	Possess secondary and a tertiary amine properties

These diamines were selected with due consideration of economic feasibility (price), location of nitrogen atoms in the molecule (primary-secondary-tertiary combination) and the structure of the hydrocarbon group linked to them.

The method for CO_2 absorption and desorption was adapted from Tan (2005) and Zhu (2006). The absorption and desorption experiments were carried out with 1 to 4 M of both N,N-Dibutyltrimethylenediamine and N,N,N'-Triethylenediamine solutions. The volume of all the solutions was 5 ml.

Absorption Experiment

The absorption was carried out in rubber sealed Schott GL 18 test tubes. The required amine solutions were prepared directly inside the test tubes and weighed using a Mettler PT 1200. Reaction gas, CO_2 was supplied to the amine solutions in the test tube by using a PTFE tube (inner diameter = 1/16 inch, outer diameter = 0.04 inch) that penetrates through the test tube cap and rubber seal.

The flow of CO_2 from the gas tank was regulated using a pressure gauge which maintains the CO_2 flow at 1 bar and then by magnetic valve connected to a Bronckhorst flow controller box. This flow controller box can regulate gas flowrate. For absorption experiments, 20 mlN/min of CO_2 flowrate was used. The water bath temperature for absorption was maintained at 25°C.

Each test tube containing amine solution was weighed every 5 minutes. The absorption was considered to be in complete equilibrium after three consecutive constant weights of the test tubes. The whole process of absorption was about 1 hour to 2 hours at the most. The process flow diagram of absorption experiment is shown in *Fig. 1.*

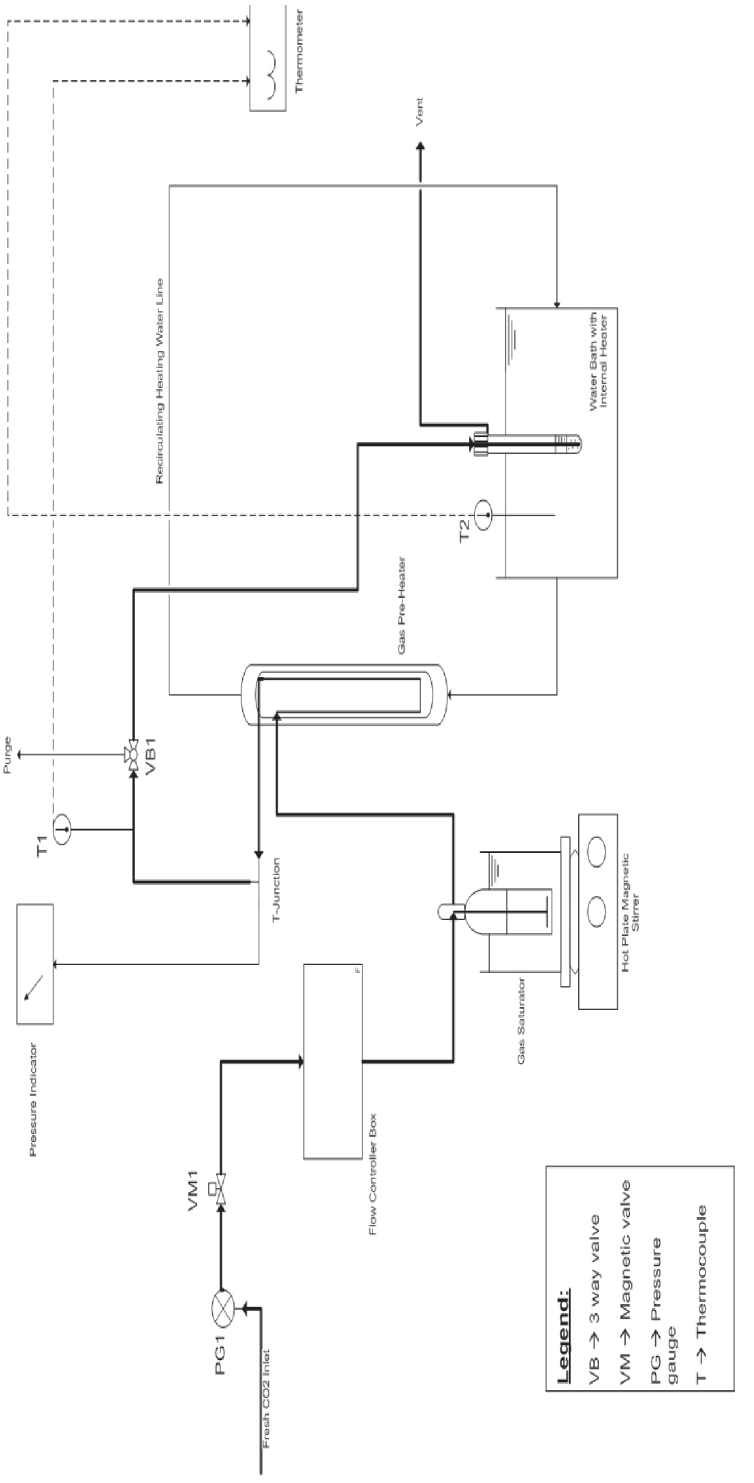

Fig. 1: Process flow diagram of absorption experimental set-up

The operating parameters for absorption experiment were:

- Volume of amine solution = 5 ml
- Concentration of amine solution = 1 M, 2 M, 3 M and 4 M
- Flowrate of CO_2 = 20 mlN/min
- Pressure = 1.05 bar
- Temperature = 40°C
- Sampling time interval for gravimetric analysis = 5 minutes

Desorption Experiment

The desorption process was carried out subsequently after the absorption process. The desorption process also lasted for about 1 to 2 hours by heating the CO_2 loaded amine solution stepwise from 40°C up to 80°C at 10°C intervals.

The PTFE tube was closed at the tip by using a rubber loop. The test tubes containing CO_2 loaded amine solution were hung by a support up to a depth whereby the amine solution inside the test tube was fully immersed in the heating oil. Additionally, a magnetic stirrer was inserted into each test tube.

As desorption by heating is a non-steady state process and can not reach steady condition, a strictly fixed condition was chosen. First, the temperature of the heating oil was brought to the desired temperatures (40°C to 80°C). Then the test tubes containing CO_2 loaded amine solution were immersed into the heating oil. Every 5 minutes, gas was released from the test tube by detaching the rubber loop at the tip of the PTFE tube and then the rubber loop was attached back to the tip of the PTFE tube. These steps were done for 15 minutes (3 times detaching and attaching the rubber loop). After that, the weight of each tube was recorded. The sketch of desorption experimental set-up is shown in *Fig. 2*.

To achieve the study objectives, the results of the absorption and desorption characteristics of optimized N,N-Dibutyltrimethylenediamine-H_2O system and N,N,N'-Triethylenediamine-H_2O system were analyzed.

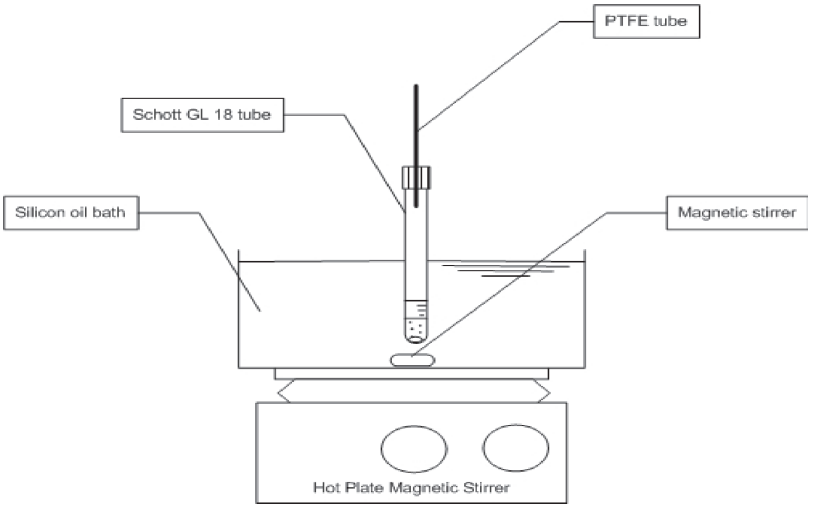

Fig. 2: Desorption experimental set-up

Furthermore, since it was assumed that diamines might have 2 active nitrogen atoms that can react with CO_2 (as this is the main reason why the potential of diamines for CO_2 absorption and desorption was investigated), the results of CO_2 absorption and desorption characteristics were compared between 2 active nitrogen atoms and 1 active nitrogen atom diamine systems.

Optimization of N,N-Dibutyltrimethylenediamine-H_2O System

TABLE 2
Selected results for N,N-Dibutyltrimethylenediamine-H_2O system

Molarity	Max. CO_2 Absorbed (g)	Max. CO_2 Desorbed (g)	n CO_2 Absorbed*n Amine^{-1}	% CO_2 Desorbed	Solid Formation
1	0.32	0.1	1.4545	0.3125	No
2	0.57	0.28	1.2955	0.4912	No
3	0.72	0.35	1.0909	0.4861	No
4	0.69	0.26	0.7841	0.3768	No

Fig. 3 shows the absorption curves of the experiments for different concentrations of the N,N-Dibutyltrimethylenediamine-H_2O system. The results show that the rate of CO_2 absorption is of the order 1 M > 2 M > 3 M > 4 M solution. It is also clear that solutions of lower concentration absorbed more CO_2 per mol of amine.

Fig. 4 shows the desorption curves of the experiments for different concentrations of the N,N-Dibutyltrimethylenediamine-H_2O system. The highest CO_2 desorption occurs at 80°C for all concentrations. The desorption efficiency was as follows; 1 M < 3 M < 4 M

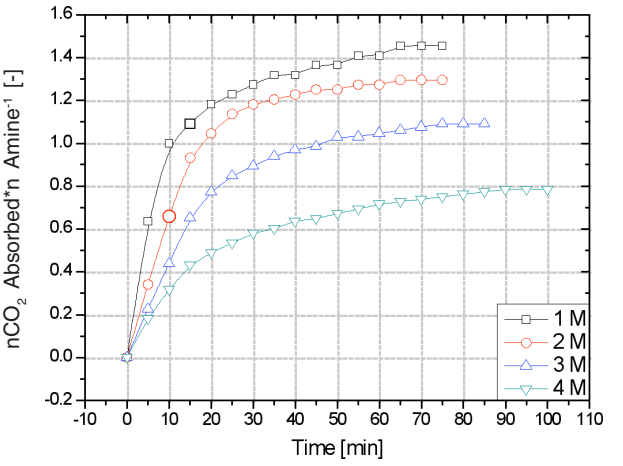

Fig. 3: Mol CO_2 absorbed / mol amine [-] vs. time [min] for N,N-Dibutyltrimethylenediamine-H_2O system

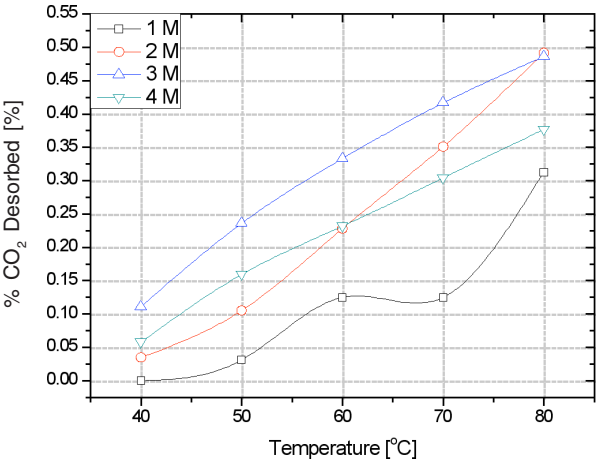

Fig. 4: % CO_2 desorbed [%] vs. temperature [°C] for N,N-Dibutyltrimethylenediamine-H_2O system

< 2 M. The 2 M solution desorbed CO_2 better than 3 M and 4 M solutions because increase in viscosity was not significant in the 2 M solution as compared to 3 M and 4 M solutions.

The optimum concentration for N,N-Dibutyltrimethylenediamine-H_2O system was 2 M. The 1 M solution was ruled out due to low CO_2 desorption capability. The 3 M and 4 M solutions were ruled out because the significant increase in viscosity had an effect on CO_2 absorption and desorption capabilities.

Optimization of N,N,N'-Triethylenediamine-H_2O System

TABLE 5
Selected results for N,N,N'-Triethylenediamine-H_2O system

Molarity	Max. CO_2 Absorbed (g)	Max. CO_2 Desorbed (g)	n CO_2 Absorbed*n Amine^{-1}	% CO_2 Desorbed	Solid Formation
1	0.28	0.07	1.2727	0.25	No
2	0.51	0.09	1.1591	0.1765	No
3	0.74	0.2	1.1212	0.2703	No
4	0.93	0.45	1.0568	0.4839	No

Fig. 5 shows the absorption curves of the experiments for different concentrations of the N,N,N'-Triethylenediamine-H_2O system. The rate of CO_2 absorption was 1 M > 2 M > 3 M > 4 M solutions. The results showed that solutions with lower concentration absorbed more CO_2 per mol of amine.

Fig. 6 shows the desorption curves of the experiments for different concentration of the N,N,N'-Triethylenediamine-H_2O system. The highest CO_2 desorption occurred at

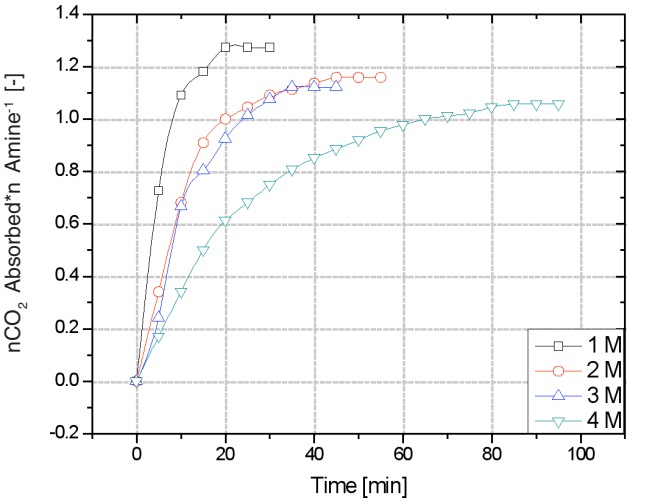

Fig. 5: Mol CO_2 absorbed / mol amine [-] vs. time [min] for N,N,N'-Triethylenediamine-H_2O system

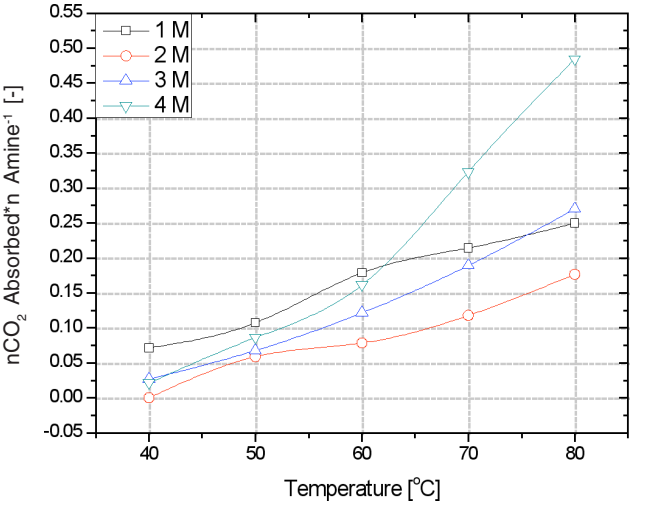

Fig. 6: % CO_2 desorbed [%] vs. temperature [°C] for N,N,N'-Triethylenediamine-H_2O system

80°C for all concentrations. The desorption efficiency was 2 M < 1 M < 3 M < 4 M. The 4 M solution desorbed CO_2 better than 1 M, 2 M and 3 M solutions because of higher amine content available in the 4 M solution in comparison to the other solutions.

The optimum concentration for N,N-Dibutyltrimethylenediamine-H_2O system was 4 M solution. The 1 M, 2 M and 3 M solutions were ruled out due to low CO_2 desorption capabilities.

Comparison of Both Optimized Systems (Two Active Nitrogen Atoms in Diamines)

TABLE 6
Selected results for two active nitrogen atoms in diamines comparison

Amine Solutions	Max. CO_2 Absorbed (g)	Max. CO_2 Desorbed (g)	n CO_2 Absorbed*n $Amine^{-1}$	% CO_2 Desorbed
2 M N,N-Dibutyltrimethylenediamine-H_2O system	0.57	0.28	1.2955	0.4912
4 M N,N,N'-Triethylenediamine-H_2O system	0.93	0.45	1.0568	0.4839

Fig. 7 shows the comparison of absorption curves for the different optimized systems involved. The rate of CO_2 absorption for all optimized systems is as follows; 2 M N,N-Dibutyltrimethylenediamine-H_2O>4 M N,N,N'-Triethylenediamine-H_2O. The CO_2 absorption capacity per mole of amine for 2 M N,N-Dibutyltrimethylenediamine-H_2O was greater than 4 M N,N,N'-Triethylenediamine-H_2O.

Fig. 8 shows the comparison of desorption curves for the different optimized systems involved. The highest CO_2 desorption occurred at 80°C for all the systems involved. The desorption efficiency of 4 M N,N,N'-Triethylenediamine-H_2O was smaller than that for 2 M N,N-Dibutyltrimethylenediamine-H_2O. Both diamines systems desorbed almost 50% CO_2 due to the presence of the two active nitrogen atoms.

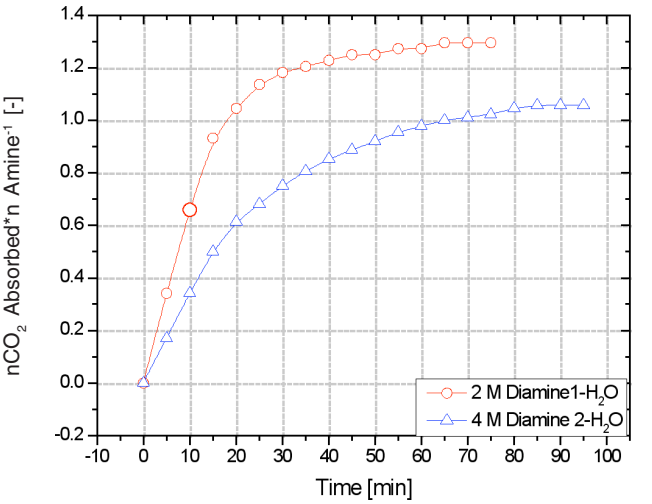

Fig. 7: Mol CO_2 absorbed / mol amine [-] vs. Time [min] for two active nitrogen atoms comparison

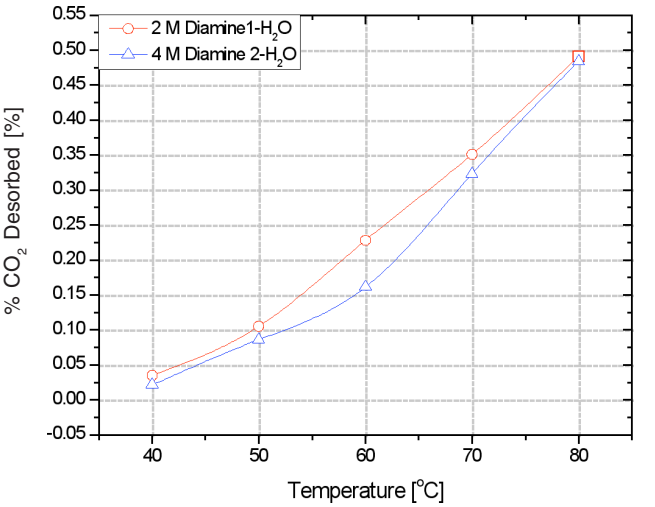

Fig. 8: % CO_2 desorbed [%] vs. temperature [°C] for two active nitrogen atoms comparison

Comparison of All Optimized Systems (One Active Nitrogen Atom in Diamines)

TABLE 7
Selected results for one active nitrogen atom in diamines comparison

Max. CO_2 Amine Solutions	Max. CO_2 Absorbed (g)	Max. CO_2 Desorbed (g)	n CO_2 Absorbed*n Amine^{-1}	% CO_2 Desorbed
2 M N,N-Dibutyltrimethylenediamine-H_2O system	0.1425	0.07	0.6478	0.1228
4 M N,N,N'-Triethylenediamine-H_2O system	0.2325	0.1125	0.5284	0.121

Results from the screening of N,N-Dibutyltrimethylenediamine-H_2O and N,N,N'-Triethylenediamine-H_2O systems presented earlier reveal the optimum concentration of each system. Here, the results for N,N-Dibutyltrimethylenediamine-H_2O and N,N,N'-Triethylenediamine-H_2O systems are assumed to have only one active nitrogen atom that can react with CO_2. These results are shown in Table 7.

Fig. 9 shows the comparison of absorption curves for the optimized systems involved. The rate of CO_2 absorption for 2 M N,N-Dibutyltrimethylenediamine-H_2O was greater than that for 4 M N,N,N'-Triethylenediamine-H_2O. The CO_2 absorption capacity per mole of amine for 2 M N,N-Dibutyltrimethylenediamine-H_2O was greater than for 4 M N,N,N'-Triethylenediamine-H_2O.

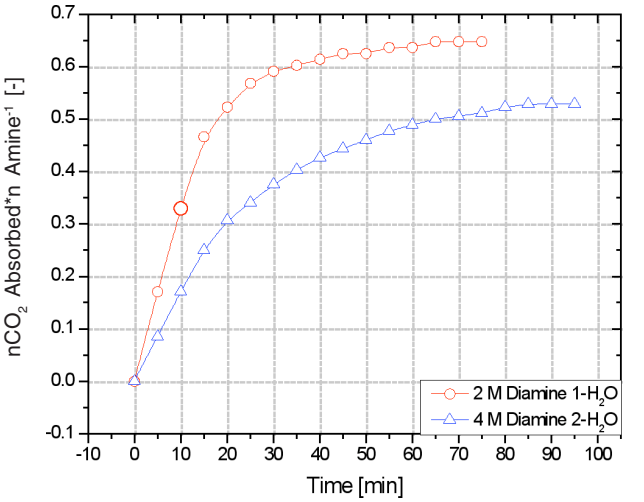

Fig. 9: Mol CO_2 absorbed / mol amine [-] vs. temperature [°C] for one active nitrogen atom comparison

Fig. 10 shows the comparison of desorption curves for the optimized systems involved. The highest CO_2 desorption occurs at 80°C for all the systems involved. The desorption efficiency for 2 M N,N-Dibutyltrimethylenediamine-H_2O was less than that for 4 M N,N,N'-Triethylenediamine-H_2O. Both diamine systems desorbed less CO_2 than systems with 2 active nitrogen atoms due to the lack of 1 active nitrogen atom.

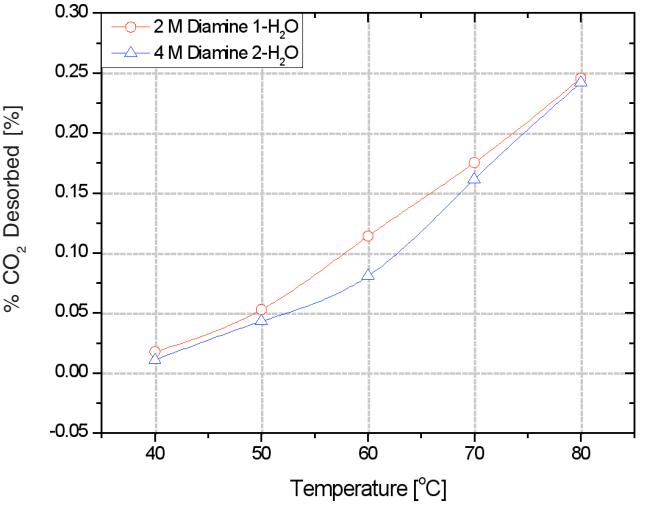

Fig. 10: % CO_2 Desorbed [%] vs. temperature [°C] for one active nitrogen atom comparison

CONCLUSIONS

After thorough investigation and analysis, it was found that both aqueous diamines (N,N-Dibutyltrimethylenediamine-H_2O and N,N,N'-Triethylenediamine-H_2O) systems have the potential to be used as a chemical solvent for CO_2 absorption and desorption. This statement is valid provided that there are 2 active nitrogen atoms within the diamines molecules that can react with CO_2.

Other conclusions that can be drawn are as follows:

1. The optimized concentration for N,N-Dibutyltrimethylenediamine-H_2O system at 40°C and 80°C CO_2 absorption and desorption temperatures respectively is 2 M.
2. The optimized concentration for N,N,N'-Triethylenediamine-H_2O system at 40°C and 80°C CO_2 absorption and desorption temperatures respectively is 4 M.

The assumption regarding 2 active nitrogen atoms reacting with CO_2 needs validation with further investigations.

ACKNOWLEDGEMENTS

The research was accomplished with support from the Chair of Technical Chemistry B, Universitäe Dortmund, Germany.

REFERENCES

VIGUIER, L. L., BABIKER, M. H. and REILLY, J.M. (n.d.). Carbon emissions and The Kyoto Commitment in The EU, MIT Joint Program on the Science and Policy of Global Change Report 70. Massachusetts Institute of Technology.

TAN, Y.H. (2005). Experimental study of CO_2 absorption into aqueous lipophilic amine solution. (MSc. Thesis, Universitaet Dortmund, 2005).

ZHU, F. (2006). Reaktiontechnische untersuchungen zur CO_2 absorption in thermomorphischen systemen (TMS) in Einer Blasensauele, Studienarbeit Universitaet Dortmund.

ISSN: 0128-7680
Pertanika J. Sci. & Technol. **16 (1)**: 73 - 81 (2008)

CVD Whiskerization Treatment Process for the Enhancement of Carbon Fiber Composite Flexural Strength

Suraya Abdul Rashid*[1], Christina Vargis[1], Robiah Yunus[1] and Suryani Shamsudin[2]
[1]Chemical and Environmental Engineering Department, Faculty of Engineering, Universiti Putra Malaysia, 43400 UPM, Serdang, Selangor, Malaysia
[2]Advanced Material Research Centre (AMREC) SIRIM Berhad, Lot 34, Jalan Hi-Tech 2/3, Kulim Hi-Tech Park, 09000 Kulim, Kedah, Malaysia
**E-mail: suraya@eng.upm.edu.my*

ABSTRACT

Carbon fiber composite performance can be enhanced by applying an optimum level of fiber surface treatment such as whiskerization. The main objectives of this study were to conduct whiskerization through carbon nanotube (CNT)-coating of carbon fiber via chemical vapour deposition (CVD) at various conditions (temperature and hydrogen flow rate) and to investigate the enhancement in flexural strength of composites fabricated from these CNT-coated carbon fibers. The results indicated that CNTs were able to grow onto the carbon fibres with the highest amount of whiskerization occurring for samples nearest the reactant gas inlet of the CVD Rig. Various whiskerization behaviours were observed at different reaction temperatures and flow rates. From flexural tests, it was found that whiskerization treatment on carbon fibers increases the flexural strength of its composites between 44-122%.

Keywords: Carbon fibers, carbon nanotubes, composites, flexural strength

INTRODUCTION

Carbon fibers are the main reinforcing fibers used in high performance polymer matrix composites. Carbon fiber which has a very smooth surface causes the bond between fiber and matrix to be the weakest feature of the combination when laminated. Therefore, though carbon fiber possesses superior modulus as compared to glass fiber, it bonds poorly with matrix materials (Milewski *et al.,* 1971). Consequently carbon fibers were considerably inferior to boron and glass fibers that were being used in structural materials. These observations led investigators to develop various surface treatments that could improve the fiber-matrix interfacial bonding (Donnet *et al.,* 1998).

These surface treatments may be classified into oxidative treatments and non-oxidative treatments. Non-oxidative treatments that improve the fiber-resin bonding involves the deposition of more active forms of carbon on the carbon fiber surface, such as the growth of carbon whiskers (on the fiber surface) in a process called whiskerization (Donnet *et al.,* 1998). It is believed that these carbon whiskers are either carbon nanotubes (Thostenson *et al.,* 2001) or carbon nanofibers which are known for their superior strength (Downs and Baker, 1995).

Fiber bundles or fibrous textures (fabrics) can be coated using vapor-phase processes. A process of this kind which is well suited for coating fiber bundles is the method known as chemical vapor deposition, or CVD (Huber and Schmaderer, 1992). CVD of films and

* Corresponding Author

coatings involve the chemical reaction of gaseous reactants on or near the vicinity of a heated substrate surface (Choy, 2003). In this study, carbon nanotubes (CNTs) were grown on carbon fibers through a CVD process known as whiskerization treatment.

Milewski *et al.* (1971), Downs and Baker (1995) and Kowbel *et al.* (1997) found that whiskerization provided immense improvement in the surface bond by 500%, 475% and 250% respectively. Donnet *et al.* (1998) reported that whiskerization contributes immense improvement in inter-laminar shear strength (ILSS). A good measure of increment in surface bonding is by measuring the flexural strength of composites which correlates well with ILSS (Jang and Yang, 2000).

The objectives of this study were (i) to carry out whiskerization treatment by coating untreated PAN-based carbon fiber with CNTs at various reaction temperatures (800-1000^{o}C) and hydrogen flow rates (100-500ml/min) conditions and to characterize the CNT-coated fibers at these conditions and (ii) to investigate the effect of these varying whiskerization treatment conditions on the flexural strength of carbon fiber-epoxy composite.

MATERIALS AND METHODS

Whiskerization Treatment

In this study, the whiskerization treatment was carried out using a custom-built CVD Rig. A description of the apparatus has been reported by Suraya *et al.* (2006). Whiskerization treatment was conducted on carbon fibers by bubbling hydrogen gas into benzene and then flowing this reaction gas into the quartz tube where ferrocene and carbon fiber tows were positioned. Ferrocene decomposes under high temperature and expels organic compounds whilst the Fe ions are left to diffuse into exposed pores on the carbon fibers. Benzene vapour which enters the furnace decomposes into carbon atoms. These carbon atoms are attracted to the heated Fe ions which act as catalysts, thus stimulating whisker nucleation and growth. This treatment was conducted at reaction temperatures of 800^{o}C, 900^{o}C and 1000^{o}C at a heating rate of 5^{o}C/min. At each of the reaction temperature, the hydrogen flow rate was varied at 100ml/min, 300ml/min and 500ml/min. The reactor was cooled under argon gas before collecting the treated fiber.

Fiber Characterization

The treated fiber samples from each treatment condition were then analyzed using scanning electron microscopy (SEM) (JEOL JSM-6400 model). The CNTs grown on the carbon fiber surfaces were characterized using HRTEM model Philip Tecnai 20.

Composite Processing

Composites were then fabricated from carbon fiber and epoxy resin using the hand layup method before being subjected to flexural test according to ASTM D790 using Instron Universal Testing Machine. A SEM, model JEOL JSM-6400, was then used to characterize the fracture surface of these composites.

RESULTS AND DISCUSSION

Characterization of CNT-coated Fiber

A total of nine sets of treatment conditions were experimented, and the details of the designations used for these treatment conditions are given in Table 1.

TABLE 1
Description of the treatment condition designations used

Designation	Hydrogen Flow Rate (ml/min)	Reaction Temperature (°C)
A	100	800
B	300	800
C	500	800
D	100	900
E	300	900
F	500	900
G	100	1000
H	300	1000
I	500	1000

For each treatment, CNT-coated fiber samples were taken from three main regions along the reaction tube to examine the pattern of CNT growth on the carbon fibers along the reaction tube. *Fig. 1* illustrates these three regions in the quartz tube denoted as regions 1, 2 and 3.

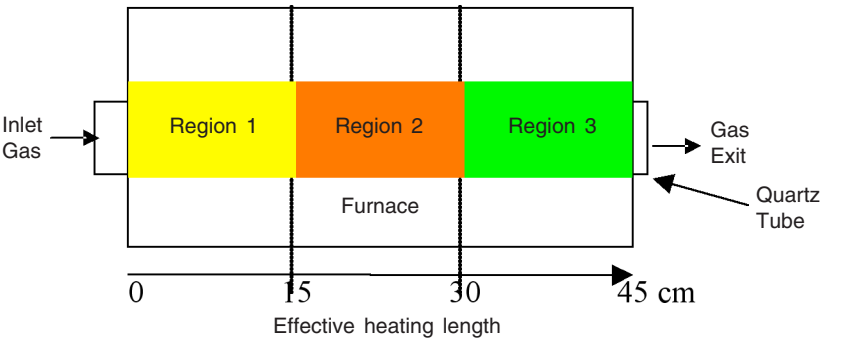

Fig. 1: Positions of the three regions in the reaction tube where CNT-coated fiber samples were taken to examine the whiskerization pattern

Fig. 2 depicts the SEM micrographs of CNT-coated carbon fibers for condition A. CNTs tend to grow from carbon fibers only at region 1. This pattern was evident for all treatment conditions. CNTs are likely to form at the inlet region of a CVD reactor where the ferrocene vapour is fed because the Fe particles (resulting from ferrocene decomposition) will increase in diameter with an increase in the axial distance and only the catalyst particles at the inlet with relatively smaller diameters are capable of performing as the growth seed for CNT growth. As the larger Fe particles form towards the reactor exit, they become too large and inactive for CNT growth (Moisala *et al.* 2006; Kuwana and Saito, 2005).

Figs. 3 to *5* depict the SEM micrographs of CNT-coated carbon fibers for conditions A to I at region 1. CNT-coated fibers consist mainly of relatively short CNT length at a

reaction temperature of 800°C whereas at higher reaction temperatures (900°C and 1000°C), longer strand-like CNT is noticeable on CNT-coated fibers. Zhao *et* al. (2005) reported similar findings where low temperature CVD processes produced short MWCNTs while high temperature CVD produces long MWCNTs. HRTEM analysis was carried out in order to examine the alignment of parallel graphitic sheets of individual CNTs (grown on carbon fibers) at 800, 900 and 1000°C, and the images are shown in *Fig. 6 (a, b, c)*. The alignment of graphitic sheets parallel to the tube axis is evident in all the figures, with the parallel graphitic sheet of CNTs being more aligned and distinct as the temperature increases. This is because as the temperature increases, the carbon diffusion rate (from benzene decomposition) increases. Consequently, the growth rate of CNTs increases and the graphitic sheets build up with a less defect (Lee *et al.*, 2003).

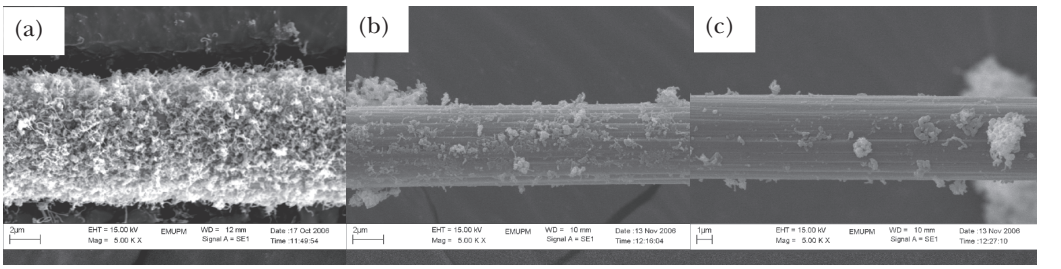

Fig. 2: SEM micrograph of CNT-coated carbon fiber at a reaction temperature of 800°C and 100ml/min of hydrogen gas flow rate, A, at (a) region 1, (b) region 2 and (c) region 3 along the reaction tube

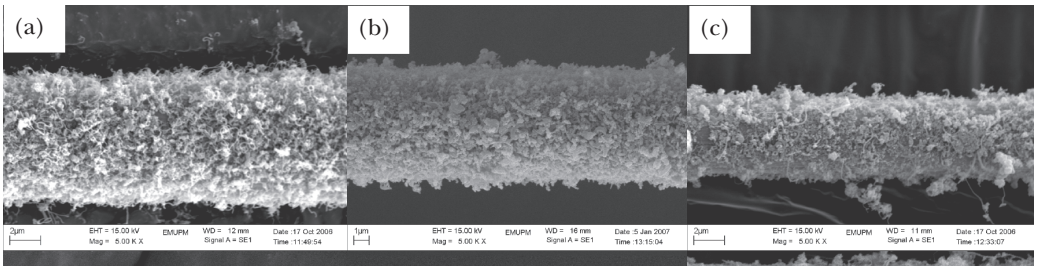

Fig. 3: SEM micrograph of CNT-coated carbon fibers at (a) 100ml/min, (b) 300ml/min and (c) 500ml/min of hydrogen gas flow rate and a reaction temperature of 800°C at region 1

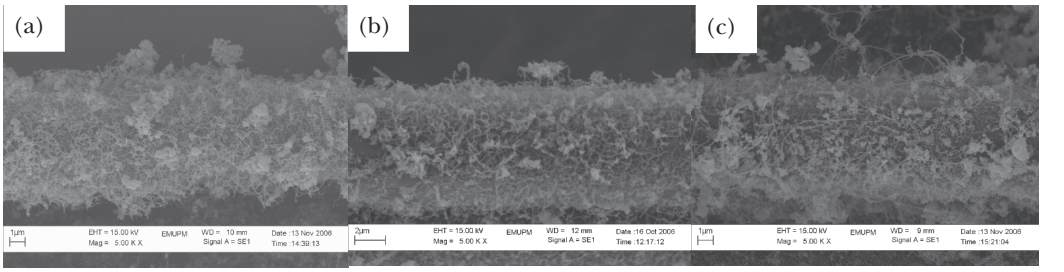

Fig. 4: SEM micrograph of CNT-coated carbon fibers at (a) 100ml/min, (b) 300ml/min and (c) 500ml/min of hydrogen gas flow rate and a reaction temperature of 900°C at region 1

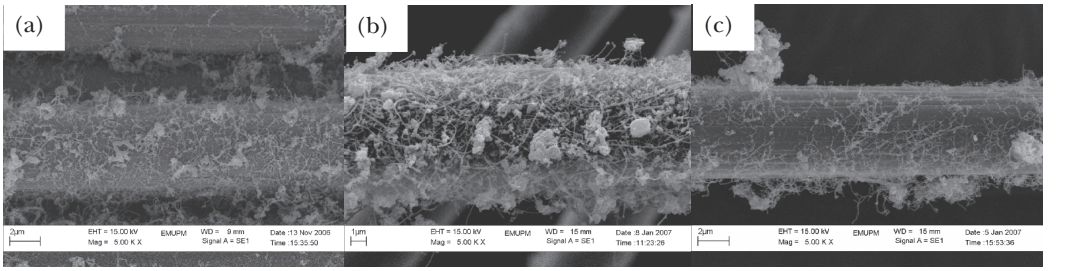

Fig. 5: SEM micrograph of CNT-coated carbon fibers at (a) 100ml/min. (b) 300ml/min and (c) 500ml/min of hydrogen gas flow rate and a reaction temperature of 1000ºC at region 1

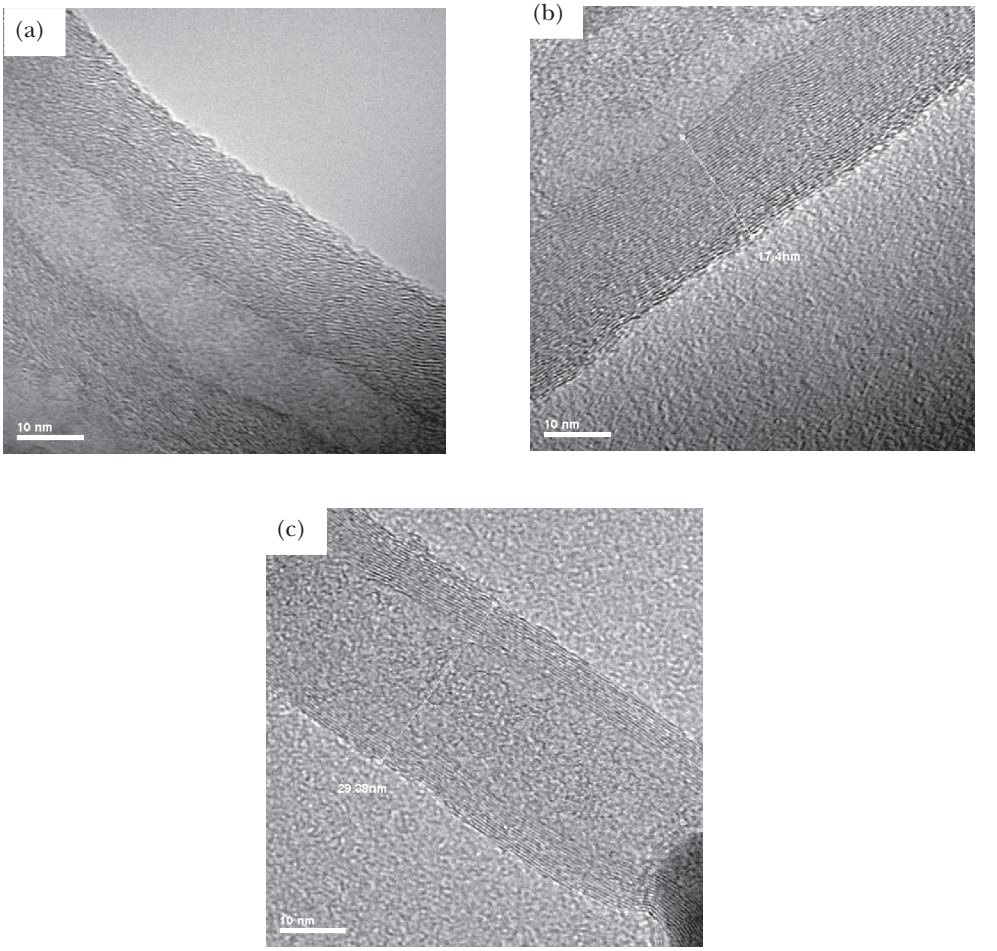

Fig. 6: HRTEM micrographs on CNT grown at (a) 800ºC, (b) 900ºC

Figs. 7 to *9* show the SEM micrographs of CNT-coated carbon fibers for conditions A to I at region 1 at a lower magnification. The micrographs show that most of the CNT-coated fibers at the lower hydrogen flow rate of 100ml/min comprises of fibers with amorphous carbon impurities (indicated by clumps) and relatively uneven CNT coating. At higher hydrogen flow rates of 300 and 500ml/min, the clumps on the CNT-coated fibers disappeared and the CNT coatings on the fiber were relatively more even. These observations were much more evident at lower temperatures especially at 800°C. This trend could be due to the role of hydrogen in hindering or preventing the formation of surface carbide (Fe_3C) which is the cause for low carbon deposition rates. Yang and Yang (1986) reported that surface carbide is essentially inactive for benzene decomposition.

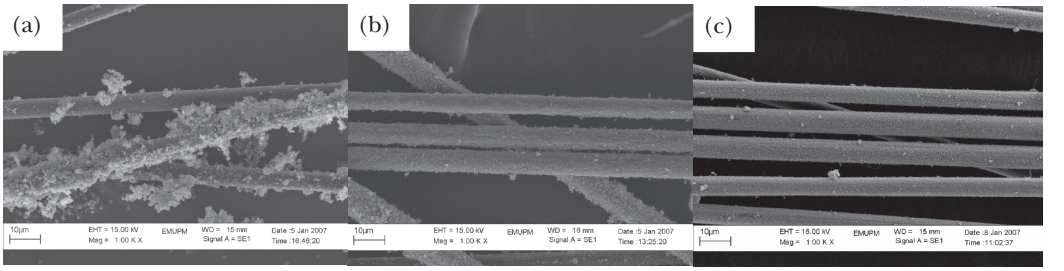

Fig. 7: SEM micrograph of CNT-coated carbon fibers at (a) 100ml/min, (c) 300ml/min and (c) 500ml/min of hydrogen gas flow rate and a reaction temperature of 800°C at region 1

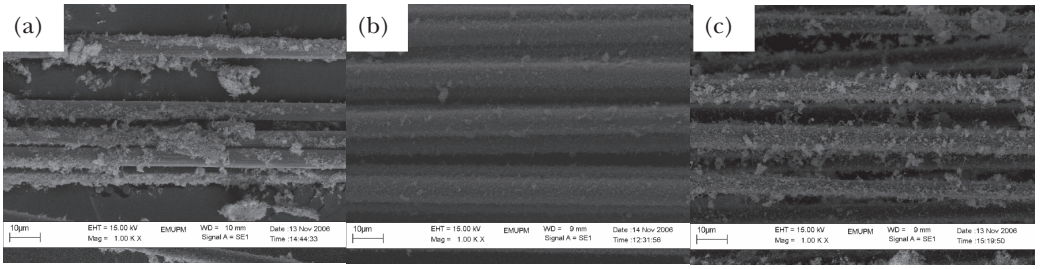

Fig. 8: SEM micrograph of CNT-coated carbon fibers at (a) 100ml/min, (c) 300ml/min and (c) 500ml/min of hydrogen gas flow rate and a reaction temperature of 900°C at region 1

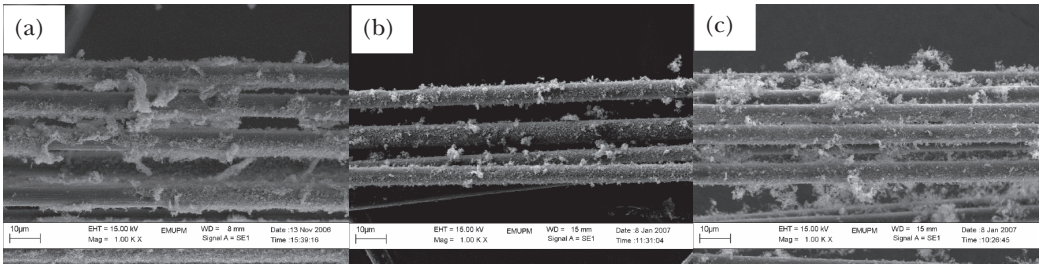

Fig. 9: SEM micrograph of CNT-coated carbon fibers at (a) 100ml/min, (c) 300ml/min and (c) 500ml/min of hydrogen gas flow rate and a reaction temperature of 1000°C at region 1

Carbide is formed, along with amorphous carbon and graphite, which deactivates the Fe activity for carbon deposition. In the presence of H_2, a high activity is obtained probably because a metallic surface is maintained, thus sustaining the activity. This explains the reduced impurities and even coating of CNT at higher hydrogen flow rate.

Whiskerization treatment on carbon fibers increases the flexural strength of composites by 44-122%. The extent of increment in flexural strength varies according to the whiskerization treatment conditions. The flexural strength of composites made from untreated and CNT-coated carbon fibers are listed in Table 2. The carbon nanotubes grown on carbon fibers improves the surface geometry of fibers by providing greater mechanical grip for matrix material which when combined with the fibers forms composites. The CNT-coated fibers have a considerable degree of cohesion even before they are impregnated with matrix filler material because the CNTs from adjacent fibrils overlap, intertwine and occupy all of the interstitial voids located between adjacent bundles of fibers (Milewski *et al.,* 1971). This type of fiber-matrix adhesion mechanism is called mechanical interlocking and results in enormous increase in flexural strength when these fibers are combined with matrix material. The resulting composite behaves in a manner resembling more nearly an isotropic material.

TABLE 2
Flexural strength of composites made from untreated and CNT-coated carbon fibers

Whiskerization Treatment Condition	Flexural Strength (MPa)	Increment (%)
Untreated	1.45	-
800°C, 100ml/min	3.22	122
800°C, 300ml/min	3.03	109
800°C, 500ml/min	2.84	96
900°C, 100ml/min	2.62	81
900°C, 300ml/min	2.30	59
900°C, 500ml/min	2.27	57
1000°C, 100ml/min	2.25	55
1000°C, 300ml/min	2.23	54
1000°C, 500ml/min	2.09	44

Effect of Varying Reaction Temperature and Hydrogen Flow Rate

Fig. 10 compares the flexural strength of composites fabricated from CNT-coated carbon fibers at various temperatures for various hydrogen flow rates. As the whiskerization treatment reaction temperature increases from 800°C to 1000°C, at 100ml/min of hydrogen, the flexural strength of composites fabricated at these conditions decreases but is still more than composites fabricated from untreated carbon fibers. This same pattern is observed for 300 and 500 ml/min of hydrogen as the reaction temperature increases from 800°C to 1000°C. This can be attributed to the increased reaction temperature causing the surface activity of the fiber surface to decrease (Wang *et al.* 2006), resulting in lesser fiber and epoxy interaction and this in turn lowers the flexural strength of the composite. Therefore though whiskerization treatment at higher temperatures (900°C and 1000°C) enhances the flexural properties of composites by 44-

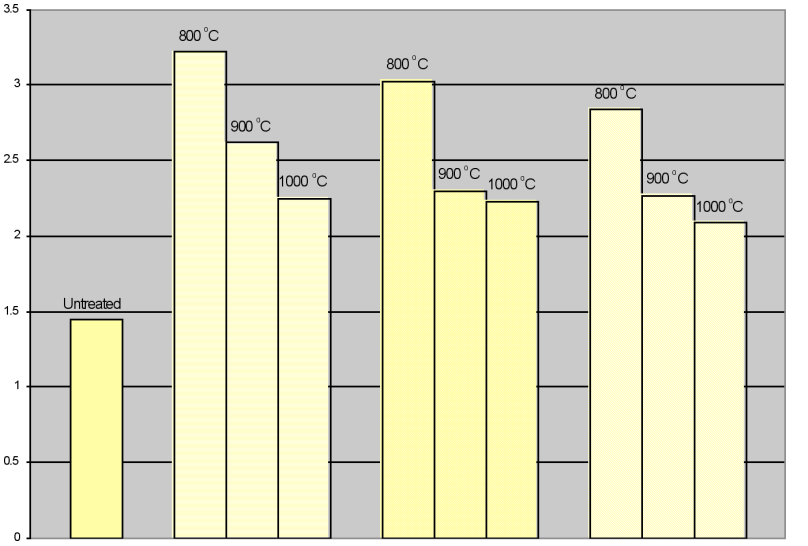

Fig. 10: Flexural strength of composites fabricated from untreated and CNT-coated carbon fibers

81%, this enhancement is less compared to flexural strength of composites fabricated from carbon fibers treated at 800°C with corresponding increment of 96-122%.

Alternatively, comparing the flexural strength of composites fabricated from CNT-coated carbon fibers at various hydrogen flow rates at the same reaction temperature indicates an overall decrease in the flexural strength of composites fabricated for all three reaction temperatures. Nevertheless the difference in flexural strength for the various hydrogen flow rates at the same temperature is not very significant with a mere 7-13% decrement. Therefore, it can be concluded that the hydrogen gas flow rate (used during whiskerization) does not play a major role in flexural strength of these CNT-coated carbon fiber composites.

CONCLUSIONS

Observation of SEM micrographs of treated carbon fiber samples taken at various points in each region showed that CNTs tend to grow from carbon fibers only at region 1 for all treatments. Observation of SEM micrographs of CNT-coated carbon fibers at reaction temperatures of 800°C, 900°C and 1000°C showed that the CNTs grown on the carbon fibers increased in length and distinctness of parallel graphitic sheets alignment as the reaction temperature increased from 800 to 1000°C. On the other hand, as the hydrogen flow rate increased from 100 to 500 ml/min, SEM micrographs depicted that the CNT coatings on the fibers were relatively more even. The amorphous carbon impurities (indicated by clumps) on the CNT-coated fibers also disappeared as the hydrogen flow rate increased from 100 to 500 ml/min but this was only observed at a reaction temperature of 800°C.

Whiskerization of carbon fibers increases the flexural strength of composites by 44-122%. Higher reaction temperature and hydrogen flow rate during carbon fiber whiskerization lowers the flexural strength of its composites with the latter condition having less impact on the strength.

ACKNOWLEDGEMENTS

The authors would like to acknowledge the financial support provided by the Ministry of Science, Technology and the Environment, Malaysia (MOSTE) under programme No. 03-01-01-0065-PR0072/08-05 and also acknowledge the SEM analysis service of Universiti Putra Malaysia, Bioscience Institute, Microscopy and Nanoscience Imaging Institute as well the HRTEM analysis service of Advanced Materials Research Centre (AMREC) SIRIM Berhad.

REFERENCES

Choy, K.L. (2003). Chemical vapour deposition of coatings. *Progress in Material Science, 48,* 57-100.

Donnet, J.B., Wang, T.K., Peng, J.C.M. and Rebouillat, S. (1998). *Carbon Fibers* [(p. 162). Marcel Dekker Inc.: New York.

Downs, W.B. and Baker, R.T.K. (1995). Modification of the surface properties of carbon fibers via the catalytic growth of carbon nanofibers. *Journal of Materials Research, 10*(3), 625-633.

Huber, R. and Schmaderer, F. (1992). Application of CVD-coated multifilament fibers. *Materials & Design, 13,* 2.

Jang, J. and Yang, H. (2000). The effect of surface treatment on the performance improvement of carbon fiber/polybenzoxine composites. *Journal of Materials Science, 35,* 2297-2303.

Kowbel, W., Bruce, C., Withers, J.C. and Ransone, P.O. (1997). Effect of carbon fabric whiskerization on mechanical properties of C-C composites. *Composites Part A, 28A,* 993-1000.

Kuwana, K. and Saito, K. (2005). Modeling CVD synthesis of carbon nanotubes: Nanoparticle formation from ferrocene. *Carbon, 43,* 2088-2095.

Milewski, J.V., Brook, S. and Shyne, J.J. (1971). Method of treating the surface of a filament. *United State Patent Office, 3,* 580, 731.

Lee, Y.T., Kim, N.S., Park, J., Han, J.B., Choi, Y.S., Ryu, H. and Lee, H.J. (2003). Temperature-dependent growth of carbon nanotubes by pyrolysis of ferrocene and acetylene in the range between 700 and 1000°C. *Chemical Physics Letters, 372,* 853-859.

Moisala, A., Nasibulin, A.G., Brown, D.P., Jiang, H., Khriachtchev, L. and Kauppinen, E.I. (2006). Single-walled carbon nanotubes synthesis using ferrocene and iron pentacarbonyl in a laminar flow reactor. *Chemical Engineering Science, 61,* 4393-4402.

Suraya, A.R., Vargis, C., Yunus, R. and Shamsudin, S. (2006). Evaluation of carbon vapour deposition technique for whiskerization treatment. *International Journal of Engineering and Technology, 3,* 85-90.

Thostenson, E.T., Ren, Z. and Chou, T-W. (2001). Advances in the science and technology of carbon nanotubes and their composites: A review. *Composites Science and Technology, 61,* 1899-1912.

Wang, S., Chen, Z-H., Ma, W-J. and Ma, Q-S. (2006). Influence of heat treatment on physical-chemical properties of PAN-based carbon fiber. *Ceramic International, 32,* 291-295.

Yang, K.L. and Yang, R.T. (1986). The accelerating and retarding effects of hydrogen on carbon deposition on metal surfaces. *Carbon, 24,* 687-693.

Zhao, Z-G., Ci, L-J., Cheng, H-M. and Bai, J-B. (2005). The growth of multi-walled carbon nanotubes with different morphologies on carbon fibers. *Letters to the Editor / Carbon, 43,* 651-673.

Pertanika

Our goal is to bring high quality research to the widest possible audience

Journal of Science & Technology

INSTRUCTIONS TO AUTHORS

(Manuscript Preparation & Submission Guidelines)

Revised January 2009

We aim for excellence, sustained by a responsible and professional approach to journal publishing.
We value and support our authors in the research community.

Please read the guidelines and follow these instructions carefully; doing so will ensure that the publication of your manuscript is as rapid and efficient as possible. The Editorial Board reserves the right to retum manuscripts that are not prepared in accordance with these guidelines.

About the Journal

Pertanika is an international peer-reviewed journal devoted to the publication of original papers, and it serves as a forum for practical approaches to improving quality in issues pertaining to tropical agriculture and its related fields. Pertanika Journal of Tropical Agricultural Science began publication in 1978. In 1992, a decision was made to streamline Pertanika into three journals to meet the need for specialised journals in areas of study aligned with the interdisciplinary strengths of the university. The revamped, Pertanika Journal of Science and Technology (JST) is now focusing on research in science and engineering, and its related fields. Other Pertanika series include Pertanika Journal of Tropical Agricultural Science (JTAS); and Pertanika Journal of Social Sciences and Humanities (JSSH).

JST is published in **English** and it is open to authors around the world regardless of the nationality. It is currently published two times a year i.e. in **January** and **July**.

Goal of Pertanika

Our goal is to bring the highest quality research to the widest possible audience.

Quality

We aim for excellence, sustained by a responsible and professional approach to journal publishing. JST is an international journal indexed in EBSCO.

Future vision

We are continuously improving access to our journal archives, content, and research services. We have the drive to realise exciting new horizons that will benefit not only the academic community, but society itself.

We also have views on the future of our journals. The emergence of the online medium as the predominant vehicle for the 'consumption' and distribution of much academic research will be the ultimate instrument in the dissemination of the research news to our scientists and readers.

Aims and scope

Pertanika Journal of Science and Technology aims to provide a forum for high quality research related to science and engineering research. Areas relevant to the scope of the journal include: *bioinformatics, bioscience, biotechnology and bio-molecular sciences, chemistry, computer science, ecology, engineering, engineering design, environmental control and management, mathematics and statistics, medicine and health sciences, nanotechnology, physics, safety and emergency management*, and related fields of study.

Editorial Statement

Pertanika is the official journal of Universiti Putra Malaysia. The abbreviation for Pertanika Journal of Science & Technology is *Pertanika J. Sci. Technol.*

Guidelines for Authors

Publication policies

Pertanika policy prohibits an author from submitting the same manuscript for concurrent consideration by two or more publications. It prohibits as well publication of any manuscript that has already been published either in whole or substantial part elsewhere.

Editorial process

Authors are notified on receipt of a manuscript and upon the editorial decision regarding publication.

Manuscript review: Manuscripts deemed suitable for publication are sent to the Editorial Advisory Board members and/or other reviewers. We encourage authors to suggest the names of possible reviewers. Notification of the editorial decision is usually provided within to eight to ten weeks from the receipt of manuscript. Publication of solicited manuscripts is not guaranteed. In most cases, manuscripts are accepted conditionally, pending an author's revision of the material.

Author approval: Authors are responsible for all statements in articles, including changes made by editors. The liaison author must be available for consultation with an editor of *The Journal* to answer questions during the editorial process and to approve the edited copy. Authors receive edited typescript (not galley proofs) for final approval. Changes **cannot** be made to the copy after the edited version has been approved.

Please direct all inquiries, manuscripts, and related correspondence to:

The Executive Editor
Pertanika Journals
Research Management Centre (RMC)
4th Floor, Administration Building
Universiti Putra Malaysia
43400 UPM, Serdang, Selangor
Malaysia
Phone: + (603) 8946 6192
Fax: + (603) 8947 2075
ndeeps@admin.upm.edu.my

or visit our website at http://rmc.upm.edu.my/pertanika for further information.

Manuscript preparation

Pertanika accepts submission of mainly four types of manuscripts. Each manuscript is classified as **regular** or **original** articles, **short communications**, **reviews**, and proposals for **special issues**. Articles must be in **English** and they must be competently written and argued in clear and concise grammatical English. Acceptable English usage and syntax are expected. Do not use slang, jargon, or obscure abbreviations or phrasing. Metric measurement is preferred; equivalent English measurement may be included in parentheses. Always provide the complete form of an acronym/abbreviation the first time it is presented in the text. Contributors are strongly recommended to have the manuscript checked by a colleague with ample experience in writing English manuscripts or an English language editor.

Linguistically hopeless manuscripts will be rejected straightaway (e.g., when the language is so poor that one cannot be sure of what the authors really mean). This process, taken by authors before submission, will greatly facilitate reviewing, and thus publication if the content is acceptable.

The instructions for authors must be followed. Manuscripts not adhering to the instructions will be returned for revision without review. Authors should prepare manuscripts according to the guidelines of Pertanika.

1. Regular article
Definition: Full-length original empirical investigations, consisting of introduction, materials and methods, results and discussion, conclusions. Original work must provide references and an explanation on research findings that contain new and significant findings.

Size: Should not exceed 5000 words or 8-10 printed pages (excluding the abstract, references, tables and/or figures). One printed page is roughly equivalent to 3 type-written pages.

2. Short communications
Definition: Significant new information to readers of the Journal in a short but complete form. It is suitable for the publication of technical advance, bioinformatics or insightful findings of plant and animal development and function.

Size: Should not exceed 2000 words or 4 printed pages, is intended for rapid publication. They are not intended for publishing preliminary results or to be a reduced version of Regular Papers or Rapid Papers.

3. Review article
Definition: Critical evaluation of materials about current research that had already been published by organizing, integrating, and evaluating previously published materials. Re-analyses as meta-analysis and systemic reviews are encouraged. Review articles should aim to provide systemic overviews, evaluations and interpretations of research in a given field.

Size: Should not exceed 4000 words or 7-8 printed pages.

4. Special issues
Definition: Usually papers from research presented at a conference, seminar, congress or a symposium.

Size: Should not exceed 5000 words or 8-10 printed pages.

5. Others
Definition: Brief reports, case studies, comments, Letters to the Editor, and replies on previously published articles may be considered.

Size: Should not exceed 2000 words or up to 4 printed pages.

With few exceptions, original manuscripts should not exceed the recommended length of 6 printed pages (about 18 typed pages, double-spaced and in 12-point font, tables and figures included). Printing is expensive, and, for the Journal, postage doubles when an issue exceeds 80 pages. You can understand then that there is little room for flexibility.

Long articles reduce the Journal's possibility to accept other high-quality contributions because of its 80-page restriction. We would like to publish as many good studies as possible, not only a few lengthy ones. (And, who reads overly long articles anyway?) Therefore, in our competition, short and concise manuscripts have a definite advantage.

Format

The paper should be formatted in one column format with the figures at the end. A maximum of eight keywords should be indicated below the abstract to describe the contents of the manuscript. Leave a blank line between each paragraph and between each entry in the list of bibliographic references. Tables should preferably be placed in the same electronic file as the text. Authors should consult a recent issue of the Journal for table layout.

There is no need to spend time formatting your article so that the printout is visually attractive (e.g. by making headings bold or creating a page layout with figures), as most formatting instructions will be removed upon processing.

Manuscripts should be typewritten, typed on one side of the ISO A4 paper with at least 4cm margins and double spacing throughout. Every page of the manuscript, including the title page, references, tables, etc. should be numbered. However, no reference should be made to page numbers in the text; if necessary, one may refer to sections. Underline words that should be in italics, and do not underline any other words.

Authors are advised to use Times New Roman 12-point font. Be especially careful when you are inserting special characters, as those inserted in different fonts may be replaced by different characters when converted to PDF files. It is well known that 'μ' will be replaced by other characters when fonts such as 'Symbol' or 'Mincho' are used.

We recommend that authors prepare the text as a **Microsoft Word** file.

1. Manuscripts in general should be organised in the following order:

    - **Page 1: Running title.** (Not to exceed 60 characters, counting letters and spaces). This page should **only** contain your running title/ full title of your paper. In addition, the **Subject areas** most relevant to the study must be indicated on this page. Select one or two subject areas (refer to the *Scope Form).*
      A **list** of number of **black and white / colour figures and tables** should also be indicated on this page**.** Figures submitted in color will be printed in colour. See "*5. Figures & Photographs"* for details.

    - **Page 2: Author(s) and Corresponding author information.** This page should **repeat** the title of your paper with name(s) of all the authors, institutions and corresponding author's name, institution and full address (Street address, telephone number (including extension), hand phone number, fax number and e-mail address) for editorial correspondence.

      Authors' addresses. Multiple authors with different addresses must indicate their respective addresses separately by superscript numbers:

      George Swan[1] and Nayan Kanwal[2]
      [1]Department of Biology, Faculty of Science, Duke University, Durham, North Carolina, USA.
      [2]Research Management Centre, Universiti Putra Malaysia, Serdang, Malaysia.

    - **Page 3**: This page should **repeat** the title of your paper with only the **Abstract** (the abstract should be less than 250 words for a Regular Paper and up to 100 words for a Short Communication). **Keywords** must also be provided on this page (Not more than eight keywords in alphabetical order).
    - **Page 4 and subsequent pages**: This page should begin with the **Introduction** of your article and the rest of your paper should follow from page 5 onwards.

    Abbreviations. Define alphabetically, other than abbreviations that can be used without definition. Words or phrases that are abbreviated in the introduction and following text should be written out in full the first time that they appear in the text, with each abbreviated form in parenthesis. Include the common name or scientific name, or both, of animal and plant materials.

    Footnotes. Current addresses of authors if different from heading.

2. **Text.** Regular Papers should be prepared with the headings **Introduction**, **Materials and Methods**, **Results and Discussion, Conclusions** in this order. Short Communications should be prepared according to "*8. Short Communications."* below.
3. **Tables.** All tables should be prepared in a form consistent with recent issues of Pertanika and should be numbered consecutively with Arabic numerals. Explanatory material should be given in the table legends and footnotes. Each table should be prepared on a separate page. (Note that when a manuscript is accepted for publication, tables must be submitted as data - .doc, .rtf, Excel or PowerPoint file- because tables submitted as image data cannot be edited for publication.)

4. **Equations and Formulae.** These must be set up clearly and should be typed triple spaced. Numbers identifying equations should be in square brackets and placed on the right margin of the text.

5. **Figures & Photographs.** Submit an original figure or photograph. Line drawings must be clear, with high black and white contrast. Each figure or photograph should be prepared on a separate sheet and numbered consecutively with Arabic numerals. Appropriate sized numbers, letters and symbols should be used, no smaller than 2 mm in size after reduction to single column width (85 mm), 1.5-column width (120 mm) or full 2-column width (175 mm). Failure to comply with these specifications will require new figures and delay in publication. For electronic figures, create your figures using applications that are capable of preparing high resolution TIFF files acceptable for publication. In general, we require **300 dpi or higher resolution for coloured and half-tone artwork** and **1200 dpi or higher for line drawings**. For review, you may attach low-resolution figures, which are still clear enough for reviewing, to keep the file of the manuscript under 5 MB. Illustrations may be produced at extra cost in colour at the discretion of the Publisher; the author could be charged Malaysian Ringgit 50 for each colour page.

6. **References.** Literature citations in the text should be made by name(s) of author(s) and year. For references with more than two authors, the name of the first author followed by 'et al.' should be used.

   Swan and Kanwal (2007) reported that …
   The results have been interpreted (Kanwal et al. 2009).

   - References should be listed in alphabetical order, by the authors' last names. For the same author, or for the same set of authors, references should be arranged chronologically. If there is more than one publication in the same year for the same author(s), the letters 'a', 'b', etc., should be added to the year.
   - When the authors are more than 11, list 5 authors and then et al.
   - Do not use indentations in typing References. Use one line of space to separate each reference. For example:
     - Jalaludin, S. (1997a). Metabolizable energy of some local feeding stuff. *Tumbuh, 1,* 21-24.
     - Jalaludin, S. (1997b). The use of different vegetable oil in chicken ration. *Mal. Agriculturist, 11,* 29-31.
     - Tan, S.G., Omar, M.Y., Mahani, K.W., Rahani, M., Selvaraj, O.S. (1994). Biochemical genetic studies on wild populations of three species of green leafhoppers *Nephotettix* from Peninsular Malaysia. *Biochemical Genetics*, *32,* 415 - 422.
   - In case of citing an author(s) who has published more than one paper in the same year, the papers should be distinguished by addition of a small letter as shown above, e.g. Jalaludin (1997a); Jalaludin (1997b).
   - Unpublished data and personal communications should not be cited as literature citations, but given in the text in parentheses. 'In press' articles that have been accepted for publication may be cited in References. Include in the citation the journal in which the 'in press' article will appear and the publication date, if a date is available.

7. **Examples of other reference citations**:
   Monographs: Turner, H.N. and Yong, S.S.Y. (2006). *Quantitative Genetics in Sheep Breeding*. Ithaca: Cornell University Press.

   Chapter in Book: Kanwal, N.D.S. (1992). Role of plantation crops in Papua New Guinea economy. In Angela R. McLean (Eds.), *Introduction of livestock in the Enga province PNG* (p. 221-250). United Kingdom: Oxford Press.

   Proceedings: Kanwal, N.D.S. (2001). Assessing the visual impact of degraded land management with landscape design software. In N.D.S. Kanwal and P. Lecoustre (Eds.), *International forum for Urban Landscape Technologies* (p. 117-127). Lullier, Geneva, Switzerland: CIRAD Press.

8. **Short Communications** should include **Introduction, Materials and Methods, Results and Discussion, Conclusions** in this order. Headings should only be inserted for Materials and Methods. The abstract should be up to 100 words, as stated above. Short Communications must be 5 printed pages or less, including all references, figures and tables. References should be less than 30. A 5 page paper is usually approximately 3000 words plus four figures or tables (if each figure or table is less than 1/4 page).

   *Authors should state the total number of words (including the Abstract) in the cover letter. Manuscripts that do not fulfill these criteria will be rejected as Short Communications without review.

STYLE OF THE MANUSCRIPT

Manuscripts should follow the style of the latest version of the Publication Manual of the American Psychological Association (APA). The journal uses British spelling and authors should therefore follow the latest edition of the Oxford Advanced Learner's Dictionary.

SUBMISSION OF MANUSCRIPTS

All articles submitted to the journal **must comply** with these instructions. Failure to do so will result in return of the manuscript and possible delay in publication.

The **four copies** of your original manuscript, four sets of photographic figures, as well as a CD with the **electronic copy in MS Word** (including text and figures) together with a **cover letter**, **declaration form**, **referral form A**, **scope form** need to be enclosed. They are available from the Pertanika's home page at http://rmc.upm.edu.my/pertanika or from the Executive Editor's office upon request.

Please do **not** submit manuscripts directly to the editor-in-chief or to the UPM Press. All manuscripts must be **submitted through the executive editor's office** to be properly acknowledged and rapidly processed:

Dr. Nayan KANWAL
Executive Editor
Research Management Centre (RMC)

4th Floor, Administration Building
Universiti Putra Malaysia
43400 UPM, Serdang, Selangor, Malaysia
email: ndeeps@admin.upm.edu.my; tel: + 603-8946 6192
fax: + 603 8947 2075

Authors should retain copies of submitted manuscripts and correspondence, as materials can not be returned.

Cover letter

All submissions must be accompanied by a cover letter detailing what you are submitting. Papers are accepted for publication in the journal on the understanding that the article is original and the content has not been published or submitted for publication elsewhere. This must be stated in the cover letter.

The cover letter must also contain an acknowledgement that all authors have contributed significantly, and that all authors are in agreement with the content of the manuscript.

The cover letter of the paper should contain (i) the title; (ii) the full names of the authors; (iii) the addresses of the institutions at which the work was carried out together with (iv) the full postal and email address, plus facsimile and telephone numbers of the author to whom correspondence about the manuscript should be sent. The present address of any author, if different from that where the work was carried out, should be supplied in a footnote.

As articles are double-blind reviewed, material that might identify authorship of the paper should be placed on a cover sheet.

Note When your manuscript is received at Pertanika, it is considered to be in its final form. Therefore, you need to check your manuscript carefully before submitting it to the executive editor (see also **English language editing** below).

Electronic copy

Preparation of manuscripts on a CD or DVD is preferable and articles should be prepared using MS Word. File name(s), the title of your article and authors of the article must be indicated on the CD. The CD must always be accompanied by four hard-copies of the article, and the content of the two must be identical. The CD text must be the same as that of the final refereed, revised manuscript. CDs formatted for IBM PC compatibles are preferred, as those formatted for Apple Macintosh are not acceptable. Please do not send ASCII files, as relevant data may be lost. Leave a blank line between each paragraph and between each entry in the list of bibliographic references. Tables should be placed in the same electronic file as the text. Authors should consult a recent issue of the Journal for table layout.

Peer review

In the peer-review process, three referees independently evaluate the scientific quality of the submitted manuscripts. The Journal uses a double-blind peer-review system. Authors are encouraged to indicate in **referral form A** the names of three potential reviewers, but the editors will make the final choice. The editors are not, however, bound by these suggestions.

Manuscripts should be written so that they are intelligible to the professional reader who is not a specialist in the particular field. They should be written in a clear, concise, direct style. Where contributions are judged as acceptable for publication on the basis of content, the Editor or the Publisher reserves the right to modify the typescripts to eliminate ambiguity and repetition and improve communication between author and reader. If extensive alterations are required, the manuscript will be returned to the author for revision.

The editorial review process

What happens to a manuscript once it is submitted to Pertanika? Typically, there are seven steps to the editorial review process:

1. The executive editor and the editorial board examine the paper to determine whether it is appropriate for the journal and should be reviewed. If not appropriate, the manuscript is rejected outright and the author is informed.
2. The executive editor sends the article-identifying information having been removed, to three reviewers. Typically, one of these is from the Journal's editorial board. Others are specialists in the subject matter represented by the article. The executive editor asks them to complete the review in three weeks and encloses two forms: (a) referral form B and (b) reviewer's comment form along with reviewer's guidelines. Comments to authors are about the appropriateness and adequacy of the theoretical or conceptual framework, literature review, method, results and discussion, and conclusions. Reviewers often include suggestions for strengthening of the manuscript. Comments to the editor are in the nature of the significance of the work and its potential contribution to the literature.
3. The executive editor, in consultation with the editor-in-chief, examines the reviews and decides whether to reject the manuscript, invite the author(s) to revise and resubmit the manuscript, or seek additional reviews. Final acceptance or rejection rests with the Editorial Board, who reserves the right to refuse any material for publication. In rare instances, the manuscript is accepted with almost no revision. Almost without exception, reviewers' comments (to the author) are forwarded to the author. If a revision is indicated, the editor provides guidelines for attending to the reviewers' suggestions and perhaps additional advice about revising the manuscript.
4. The authors decide whether and how to address the reviewers' comments and criticisms and the editor's concerns. The authors submit a revised version of the paper to the executive editor along with specific information describing how they have answered' the concerns of the reviewers and the editor.
5. The executive editor sends the revised paper out for review. Typically, at least one of the original reviewers will be asked to examine the article.
6. When the reviewers have completed their work, the executive editor in consultation with the editorial board and the editor-in-chief examine their comments and decide whether the paper is ready to be published, needs another round of revisions, or should be rejected.
7. If the decision is to accept, the paper is sent to that Press and the article should appear in print in approximately two to three months. The Publisher ensures that the paper adheres to the correct style (in-text citations, the reference list, and tables are typical areas of concern, clarity, and grammar). The authors are asked to respond to any queries by the Publisher. Following these corrections, page proofs are mailed to the corresponding authors for their final approval. At this point, only essential changes are accepted. Finally, the article appears in the pages of the Journal and is posted on-line.

English language editing
Authors are responsible for the linguistic accuracy of their manuscripts. Authors not fully conversant with the English language should seek advice from subject specialists with a sound knowledge of English. The cost will be borne by the author, and a copy of the certificate issued by the service should be attached to the cover letter.

Author material archive policy
Authors who require the return of any submitted material that is rejected for publication in the journal should indicate on the cover letter. If no indication is given, that author's material should be returned, the Editorial Office will dispose of all hardcopy and electronic material.

Copyright
Authors publishing the Journal will be asked to sign a declaration form. In signing the form, it is assumed that authors have obtained permission to use any copyrighted or previously published material. All authors must read and agree to the conditions outlined in the form, and must sign the form or agree that the corresponding author can sign on their behalf. Articles cannot be published until a signed form has been received.

Lag time
The elapsed time from submission to publication for the articles averages 5-6 months. A decision of acceptance of a manuscript is reached in 2 to 3 months (average 9 weeks).

Back issues
Single issues from current and recent volumes are available at the current single issue price from UPM Press. Earlier issues may also be obtained from UPM Press at a special discounted price. Please contact UPM Press at penerbit@putra.upm.edu.my or you may write for further details at the following address:

UPM Press
Universiti Putra Malaysia
43400 UPM, Serdang
Selangor Darul Ehsan
Malaysia.

Pertanika

Our goal is to bring high quality research to the widest possible audience

Pertanika is Indexed in Scopus & EBSCO

Pertanika is an international peer-reviewed leading journal in Malaysia which began publication in 1978. The journal publishes in three different areas — Journal of Tropical Agricultural Science (JTAS); Journal of Science and Technology (JST); and Journal of Social Sciences and Humanities (JSSH).

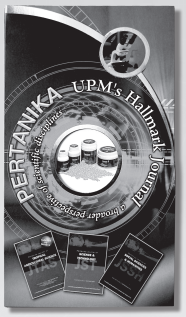

JTAS is devoted to the publication of original papers that serves as a forum for practical approaches to improving quality in issues pertaining to tropical agricultural research or related fields of study. It is published twice a year in **February** and **August**.

JST caters for science and engineering research or related fields of study. It is published twice a year in **January** and **July**.

JSSH deals in research or theories in social sciences and humanities research with a focus on emerging issues pertaining to the social and behavioural sciences as well as the humanities, particularly in the Asia Pacific region. It is published twice a year in **March** and **September**.

Why should you publish in Pertanika Journals?

Benefits to Authors

PROFILE: our journals are circulated in large numbers all over Malaysia, and beyond, in Southeast Asia. Recently, we have widened our circulation to other overseas countries as well. We will ensure that your work reaches the widest possible audience in print and online, through our wide publicity campaigns held frequently, and through our constantly developing electronic initiatives through e-pertanika and Pertanika Online.

QUALITY: Our double-blind peer refereeing procedures are fair and open, and we aim to help authors develop and improve their work. Pertanika JTAS is now over 30 years old; this accumulated knowledge has resulted in Pertanika JTAS being indexed by Scopus (Elsevier).

AUTHOR SERVICES: we provide a rapid response service to all our authors, with dedicated support staff for each journal, and a point of contact throughout the refereeing and production processes. Our aim is to ensure that the production process is as smooth as possible, is borne out by the high number of authors who publish with us again and again.

LAG TIME & REJECTION RATE: the elapsed time from submission to publication for the articles in Pertanika averages 6-8 months. A decision of acceptance of a manuscript is reached in 1 to 3 months (average 7 weeks).

Our journals have a 30% rejection rate of its submitted manuscripts, many of the papers fail on account of their substandard presentation and language (frustrating the peer reviewers).

Call for Papers

Pertanika invites you to explore frontiers from all fields of science and technology to social sciences and humanities. You may contribute your scientific work for publishing in UPM's hallmark journals either as a ***regular article***, ***short communications***, or a ***review article*** in our forthcoming issues. Papers submitted to this journal must contain original results and must not be submitted elsewhere while being evaluated for the Pertanika Journals.

Submissions in English should be accompanied by an abstract not exceeding 300 words. Your manuscript should be no more than 6,000 words or 10-12 printed pages, including notes and abstract. Submissions should conform to the Pertanika style, which is available at www.rmc.upm.edu.my/pertanika or by mail or email upon request.

Papers should be double-spaced 12 point type (Times New Roman fonts preferred). The first page should include the title of the article but no author information. Page 2 should repeat the title of the article together with the names and contact information of the corresponding author as well as all the other authors. Page 3 should contain the abstract only. Page 4 and subsequent pages to have the text - Acknowledgments - References - Tables - Legends to figures – Figures, etc.

Questions regarding submissions should only be directed to the Executive Editor, Pertanika Journals.

Remember, ***Pertanika is the resource to support you in strengthening research and research management capacity***.

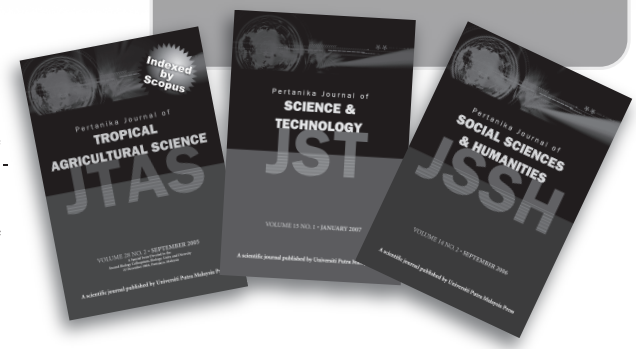

An Award Winning International-Malaysian Journal

FEB. 2008

Mail your submissions to:

The Executive Editor
Pertanika Journals
Research Management Centre (RMC)
Publication Division
4th Floor, Administration Building
Universiti Putra Malaysia
43400 UPM, Serdang, Selangor, Malaysia

Tel: +603-8946 6192
ndeeps@admin.upm.edu.my
www.rmc.upm.edu.my/pertanika

Pertanika Journal of Science & Technology
Volume 16 (1) Jan. 2008

Contents

Research Management Centre (RMC)
4th Floor, Administration Building
Universiti Putra Malaysia
43400 UPM Serdang
Selangor Darul Ehsan
Malaysia

http://www.rmc.upm.edu.my
E-mail : pertanika@rmc.upm.edu.my
Tel : +603 8946 6185/ 6192
Fax : +603 8947 2075

UPM Press
Universiti Putra Malaysia
43400 UPM Serdang
Selangor Darul Ehsan
Malaysia

http://penerbit.upm.edu.my
E-mail : penerbit@putra.upm.edu.my
Tel : +603 8946 8855/8854
Fax : +603 8941 6172

ISSN 0128-7680

9 770128 768083 01